

**SUBMISSION OF FINAL REPORT OF THE WORK DONE
FOR MINOR RESEARCH PROJECT**

Submitted to

**UGC SOUTH EASTERN REGIONAL OFFICE
HYDERABAD**



ज्ञान-विज्ञान विमुक्तये

**TAILORING THE SURFACE MORPHOLOGY OF
METAL OXIDE NANOPARTICLES AND ITS
INFLUENCE ON DYE EFFLUENT TREATMENT**

by

Dr. A. JEGATHA CHRISTY
Assistant Professor, Department of Physics
Principal Investigator- UGC MRP
No.F. MRP-6823/16 (SERO/UGC) dated 30 June 2107)



JAYARAJ ANNAPACKIAM COLLEGE FOR WOMEN
(Autonomous),
Periyakulam-625 601, Theni Dt, Tamil Nadu
2017-2019

JAYARAJ ANNAPACKIAM COLLEGE FOR WOMEN (AUTONOMOUS)



(A unit of the Sisters of St. Anne of Tiruchirapalli)

Re-accredited with 'A' Grade (Cycle – 3) by NAAC

Affiliated to Mother Teresa Women's University, Kodaikanal.

PERIYAKULAM – 625 601, THENI DISTRICT.

Phone : 04546-231482

Website : www.annejac.ac.in

Fax : 04546231482

e-mail : principal@annejac.ac.in

To

The Secretary
South Eastern Regional Office,
University Grants Commission
Hyderabad – 500 001.

Sir,

Sub: JAC- Submission of Final Report of the work done- forwarded- Reg.

Ref: Your Lr. F. MRP-6823/16 (SERO/UGC) dated 30 June 2017

* * * * *

I am glad to forward herewith the Final Report of the work done on the project in Physical Sciences of Dr. A. Jegatha Christy, Assistant Professor of Physics on the Minor Research Project (as referred above) entitled "**Tailoring the Surface Morphology of Metal oxide Nanoparticles and Its Influence on Dye Effluent Treatment**".

The amount allocated by UGC SERO for the project is Rs. 4,90,000/- which is fully utilized for the project and the amount sanctioned by the UGC is Rs. 3,70,000/-. Audited Utilization Certificate and Statement of Expenditure are enclosed. I request you to kindly sanction the balance amount of Rs. 1,20,000/- at your earliest.

We thank UGC SERO for the financial assistance to complete the Project. Thank You

Yours faithfully,


PRINCIPAL

Jayaraj Annapackiam College
for Women (Autonomous)
Thamiraparani, Periyakulam-625 601
Theni District Tamilnadu

Enclosures:

1. Copy of UGC- MRP Sanction Letter
2. Certificate from the principal
3. Accession Certificate
4. Asset Certificate
5. Annexure- III. Statement of Expenditure in respect of Minor Research Project
6. Annexure IV. Statement of expenditure incurred on field work.
7. Annexure V. Audited Utilization Certificate.
8. Annexure VI. Final Report of the work done on MRP
9. Annexure VII. Proforma for submission of information
10. Copies of research papers published in journals

JAYARAJ ANNAPACKIAM COLLEGE FOR WOMEN (AUTONOMOUS)



(A unit of the Sisters of St. Anne of Tiruchirapalli)

Re-accredited with 'A' Grade (Cycle – 3) by NAAC

Affiliated to Mother Teresa Women's University, Kodaikanal.

PERIYAKULAM – 625 601, THENI DISTRICT.

Phone : 04546-231482

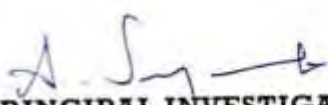
Website : www.annejac.ac.in

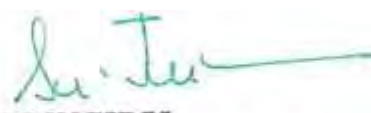
Fax : 04546231482

e-mail : principal@annejac.ac.in

CERTIFICATE FROM THE PRINCIPAL

Certified that the Executive summary of the report and papers published under the Minor research Project entitled "**Tailoring the Surface Morphology of Metal oxide Nanoparticles and its Influence on Dye Effluent Treatment**" vide UGC Letter **No.F. F. MRP-6823/16 (SERO/UGC) dated 30 June 2017** are posted on the website of the college www.annejac.ac.in and a copy of the report is kept in the library for reference by Dr. A. Jegatha Christy, Assistant Professor of Physics, Jayaraj Annapackiam College for Women (Autonomous), Periyakulam.


PRINCIPAL INVESTIGATOR
D. A. JEGATHA CHRISTY,
Assistant Professor of Physics
Department of Physics
College for Women,
(Autonomous)
PERIYAKULAM-625 601.


PRINCIPAL
Jayaraj Annapackiam College
for Women (Autonomous)
Thamarakulam, Periyakulam-625 601,
Theni District Tamilnadu.

JAYARAJ ANNAPACKIAM COLLEGE FOR WOMEN (AUTONOMOUS)



(A unit of the Sisters of St. Anne of Tiruchirapalli)

Re-accredited with 'A' Grade (Cycle – 3) by NAAC

Affiliated to Mother Teresa Women's University, Kodaikanal.

PERIYAKULAM – 625 601, THENI DISTRICT.

Phone : 04546-231482


Website : www.annejac.ac.in

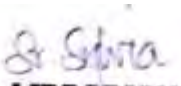
Fax : 04546231482


e-mail : principal@annejac.ac.in

ACCESSION CERTIFICATE

Certified that the books purchased for **Rs. 10,000/- (Rs. Ten Thousand Only)** out of the grant from UGC under the scheme of support for Minor research Project entitled **“Tailoring the Surface Morphology of Metal oxide Nanoparticles and Its Influence on Dye Effluent Treatment”** vide UGC Letter **No.F. F. MRP-6823/16 (SERO/UGC) dated 30 June 2017** have been transferred to the General Library by Dr. A. Jegatha Christy, Assistant Professor of Physics, Jayaraj Annapackiam College for Women (Autonomous), Periyakulam.


PRINCIPAL INVESTIGATOR
D. A. JEGATHA CHRISTY,
Assistant Professor of Physics
Jayaraj Annapackiam College
for Women (Autonomous)
PERIYAKULAM-625 601.


LIBRARIAN
LIBRARIAN
Jayaraj Annapackiam College
for Women (Autonomous)
PERIYAKULAM.


PRINCIPAL
Jayaraj Annapackiam College
for Women (Autonomous)
Thamarkulam, Periyakulam-625 601.
Theni District Tamilnadu.

JAYARAJ ANNAPACKIAM COLLEGE FOR WOMEN (AUTONOMOUS)



(A unit of the Sisters of St. Anne of Tiruchirapalli)

Re-accredited with 'A' Grade (Cycle – 3) by NAAC

Affiliated to Mother Teresa Women's University, Kodaikanal.

PERIYAKULAM – 625 601, THENI DISTRICT.

Phone : 04546-231482


Website : www.annejac.ac.in

Fax : 04546231482


e-mail : principal@annejac.ac.in

ASSET CERTIFICATE

Certified that equipment purchased for Rs.2,40,249 (**Rs. Two Lakhs forty thousand two hundred and forty nine only**) out of the grant from UGC under the scheme of support for Minor research Project entitled "**Tailoring the Surface Morphology of Metal oxide Nanoparticles and Its Influence on Dye Effluent Treatment**" vide UGC Letter **No.F. F. MRP-6823/16 (SERO/UGC) dated 30 June 2017** have been handed over to the Department of Physics by Dr. A. Jegatha Christy, Assistant Professor of Physics, Jayaraj Annapackiam College for Women (Autonomous), Periyakulam.


PRINCIPAL INVESTIGATOR
D. A. JEGATHA CHRISTY,
Assistant Professor of Physics
Department of Physics
College for Women,
(Autonomous)
PERIYAKULAM-625 601.


HEAD OF THE DEPARTMENT


PRINCIPAL
Jayaraj Annapackiam College
for Women (Autonomous)
Thamarakulam, Periyakulam-625 601.
Theni District Tamilnadu.

Dr.A.Jacquiline Regina Mary
Head and Associate Professor
Department of Physics
Jayaraj Annapackiam College
for women (Autonomous)
Periyakulam - 625601



UNIVERSITY GRANTS COMMISSION

BAHADUR SHAH ZAFAR MARG

NEW DELHI – 110 002

STATEMENT OF EXPENDITURE IN RESPECT OF MINOR RESEARCH PROJECT

- 1. Name of Principal Investigator : Dr. A. Jegatha Christy**
- 2. Deptt. of PI : Physics**
Name of College : Jayaraj Annapackiam College for Women, Periyakulam
- 3. UGC approval Letter No. and Date : F MRP-6823/16 (SERO/UGC) , 30 June 2107**
- 4. Title of the Research Project : Tailoring the surface morphology of metal oxide nanoparticles and its influence on dye effluent treatment**
- 5. Effective date of starting the project : 30 June 2017**
- 6. a. Period of Expenditure : From 30 June 2017 to 30 June 2019**

b. Details of Expenditure

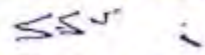
S.No.	Item	Amount Approved (Rs.)	Expenditure Incurred (Rs.)
i.	Books & Journals	10000	10000
ii.	Equipment	240000	240249
iii.	Contingency including special needs	10000	10375
iv.	Field Work/Travel	20000	20970
v.	Hiring Services	160000	164700
vi.	Chemicals & Glassware	50000	50270
	Total	4,90,000	4,96,564

It is certified that the grant of **Rs. 4,90,000 /-** (Rupees Four Lakh and Ninety Thousand Only) received from the UGC- SERO under the scheme of support for Minor Research Project entitled **Tailoring the surface morphology of metal oxide nanoparticles and its influence on dye effluent treatment vide UGC Letter No. F. MRP-6823/16 (SERO/UGC) , 30 June 2107** has been fully utilized for the purpose for which it was sanctioned and in accordance with the terms and conditions laid down by the UGC.


PRINCIPAL INVESTIGATOR



For S.S. & CO,
Chartered Accountants


S. Srinivasan, Partner
FRN: 003502S (Mem. No: 024142)

STATUTORY AUDITOR


PRINCIPAL

Jayalalitha Amirthapackiam College
for Women (Autonomous)
Thamarakulam, Periyakulam-625 60
Theni District Tamilnadu.

UGC MINOR RESEARCH PROJECT

Tailoring the surface morphology of metal oxide nanoparticles and its influence on dye effluent treatment

STATEMENT OF EXPENDITURE FOR BOOKS AND JOURNALS

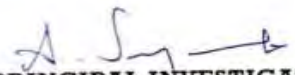
S.No	Bill Date	Bill Number	Name of the Book Dealer	Amount (Rs)
1	24.04.2018	41487	Maaya Book Centre	10,000/-


STATEMENT OF EXPENDITURE FOR EQUIPMENT

S.No	Bill Date	Bill Number	Name of the seller	Amount (Rs)
1	11.08.2017	BLR5-1252673	Amazon.in	43,114/-
2	11.08.2017	IN-625	Amazon.in	579/-
3	06.04.2018	001/18-19	HEBER scientific	112277
4	11.08.2017	AMD1-3729	Amazon.in	208
5	11.08.2017	AMD1-14075	Amazon.in	168
6	26.02.2018	3848	Modern Scientific Company	65,903/-
7	28.03.2018	S-218	J.K. Systems	18,000/-
			TOTAL	2,40,249

STATEMENT OF EXPENDITURE FOR FIELD WORK AND TRAVEL

S.No	Bill Date	Bill Number	agency	Amount (Rs)
1	13.11.2017&15.11.2017	6325	Private	4500
2	20.11.2017&21.11.2017	297	Radhaamani Saravanan Travels	6500
3	09.05.2018&10.05.2018	1403	RK Travels	3500
4	12.11.2018&14.11.2018	56028	Private	6470
			TOTAL	20,970/-


PRINCIPAL INVESTIGATOR
D. A. JECATHA CHRISTY,
Assistant Professor of Physics,
Jayaraj Annapackiam College,
Thamarakulam, Periyakulam,
(Autonomous)
PERIYAKULAM-625 601.

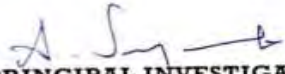

PRINCIPAL
Jayaraj Annapackiam College
for Women (Autonomous)
Thamarakulam, Periyakulam-625 601,
Theni District Tamilnadu.


STATEMENT OF EXPENDITURE FOR CHEMICAL AND GLASSWARES

S.No	Bill Date	Bill Number	Name of the seller	Amount (Rs)
1	12.12.2017	3513	Modern Scientific Company	8815
2	12.12.2017	3514	Modern Scientific Company	6436
3	12.12.2017	3505	Modern Scientific Company	2171
4	01.03.2018	3927	Modern Scientific Company	295
5	05.02.2018	3751	Modern Scientific Company	3161
6	29.01.2018	3715	Modern Scientific Company	1890
7	12.02.2018	3799	Modern Scientific Company	1035
8	02.02.2018	3733	Modern Scientific Company	5368
9	07.02.2019	2982	Modern Scientific Company	2113
10	03.10.2018	2456	Modern Scientific Company	8685
11	21.3.2019	3271	Modern Scientific Company	2301
12	28.03.2019	3327	Modern Scientific Company	8000
			TOTAL	50,270

STATEMENT OF EXPENDITURE FOR CONTIGENCY


S.No	Bill Date	Bill Number	Name of the seller	Amount (Rs)
1	04.09.2017	0047	Kovai Nehru & Co	6500
2	04.09.2017	---	stationary	360
3	04.09.17	----	stationary	10
4	06.01.18	----	India post	41
5	06.02.2018	1339544	courier	35
7	06.02.18	303	SARWODEEP	1010
8	26.6.18	----	stationary	25
9	26.6.18	531	stationary	34
10	20.01.18	----	stationary	45
11	16.02.2018	6220295	Courier	35
12	17.02.18	6221640	Courier	35
13	07.03.18	6227185	Courier	35
14	04.04.18	----	Stationary	10
15	20.07.18	----	Xerox and Stationary	2200
			Total	10,375/-

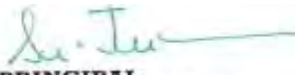

PRINCIPAL INVESTIGATOR
D. A. JECATHA CHRISTY,
Assistant Professor of Chemistry
Department of Chemistry,
Jayaraj Annapackiam College,
(Autonomous)
PERIYAKULAM-625 601.


PRINCIPAL
Jayaraj Annapackiam College
for Women (Autonomous)
Thamarakulam, Periyakulam-625 601.
Theni District Tamilnadu.

STATEMENT OF EXPENDITURE FOR HIRING SERVICES

S.No	Bill Date	Bill Number	Name of the seller	Amount (Rs)
1	4.08.17	--	MTWU, Kodaikanal	500
2	2.11.17	138	GRI	1500
3	07.12.17	6786	Alagappa University	5700
4	21.12.17	6813	Alagappa University	5700
5	23.1.18	---	Bharathidasan university	5380
6	17.02.18	---	TUCAS	1500
7	22.2.18	1	BSR LAB	300
8	18.3.18	9	BSR LAB	4000
9	15.03.2018	1490	PSG Centre for sponsored research and Consultancy	15340
10	15.03.2018	6912	Alagappa University	18340
11	18.03.18	1725	PSG Centre	15340
12	23.04.18	6936	Alagappa University	6000
13	25.04.18	3185	Bharathidasan university	5800
14	12.06.18	7001	Alagappa University	15380
15	17.07.18	7008	Alagappa University	15340
16	27.08.18	---	TUCAS	7500
17	27.08.18	3865	Bharathidasan university	15380
18	07.09.18	7011	AlagappaUniveristy	5600
19	13.11.18	7012	AlagappaUniveristy	5800
20	29.01.19	7015	Alagappa University	5800
21	18.03.19	5600	Bharathidasan university	5500
22	22.04.19	6033	Bharathidasan university	3000
Total				164700


PRINCIPAL INVESTIGATOR
 D. A. JAGATHA CHARI, IAS
 Additional Director of Higher Education
 Government of Tamil Nadu
 (Periyakulam)
 PERIYAKULAM-625 601.

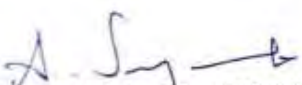

PRINCIPAL
 Jayaraj Annaspackiam College
 for Women (Autonomous)
 Thamerikulam, Periyakulam-625 601,
 Theni District Tamilnadu.


UGC MINOR RESEARCH PROJECT

STATEMENT OF EXPENDITURE INCURRED ON FIELD WORK

Principal Investigator: Dr. A. Jegatha Christy

Name of the Place visited	Duration of the Visit		Mode of Journey	Expendit ure Incurred (Rs.)
	From	To		
Visit to Tripur dye Sewage areas and collection of samples	13.11.2017	15.11.2017	Taxi	4500
Visit to Bharathidasan University for Research discussion	20.11.2017	21.11.2017	Taxi	6500
Visit to Madurai Kamaraj University for research discussion	09.05.2018	10.05.2018	Taxi	3500
Visit to Bharathidasan University for Research discussion and for experimentation	12.11.2018	14.11.2018	Taxi	6470
Total				20,970/-


PRINCIPAL INVESTIGATOR
D. A. JEGATHA CHRISTY,
 Department of Physics
 College for Women,
 Periyakulam
 (Autonomous)
 PERIYAKULAM-625 601.


PRINCIPAL
 Jayaraj Annapackiam College
 for Women (Autonomous)
 Thamarakulam, Periyakulam-625 601.
 Theni District Tamilnadu.



ज्ञान-विज्ञान विमुक्तये

UNIVERSITY GRANTS COMMISSION

BAHADUR SHAH ZAFAR MARG,

NEW DELHI – 110 002

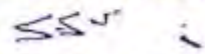
Utilization certificate

Certified that the grant of **Rs. 4,90,000/** (Rupees Four lakhs ninety thousand only) received from the University Grants Commission under the scheme of support for Minor Research Project entitled **Tailoring the surface morphology of metal oxide nanoparticles and its influence on dye effluent treatment vide UGC letter No. F. MRP-6823. (UGC/SERO) dated 30 June 2017** as been fully utilized for the purpose for which it was sanctioned and in accordance with the terms and conditions laid down by the University Grants Commission.


PRINCIPAL INVESTIGATOR



For S.S. & CO,
Chartered Accountants


S. Srinivasan, Partner
FRN: 003502S (Mem. No: 024142)

STATUTORY AUDITOR


PRINCIPAL

சாயல் தொழில்நுட்பக் கல்விக்கான
பெண்கள் (Autonomous)
தமரக்குளம், பெரியகுளம்-625 60
Theni District Tamilnadu.



ज्ञान-विज्ञान विमुक्तये

UNIVERSITY GRANTS COMMISSION

BAHADUR SHAH ZAFAR MARG

NEW DELHI – 110 002.

Final Report of the work done on the Minor Research Project.

1. Project report : **Final**
 2. UGC Reference No : **F. MRP-6823/16(SERO/UGC)**
 3. Period of report : **From 30 JUNE 2017to 30 JUNE 2019**
 4. Title of research project : **Tailoring the surface morphology of metal oxide nanoparticles and its Influence on dye effluent treatment**
 5. (a) Name of the Principal Investigator : **Dr. A. Jegatha Christy**
(b) Deptt. : **Physics**
(c) College where work has progressed : **Jayaraj Annapackiam College for Women, Periyakulam**
 6. Effective date of starting of the project : **30 June 2017**
 7. Grant approved and expenditure incurred during the period of the report:
 - a. Total amount approved **Rs. 4,90,000/-**
 - b. Total expenditure **Rs. 4,90,000/-**
 - c. Report of the work done: **Attached separately**
- i. Brief objective of the project:
The objectives of the projects are
- To synthesize photoactive and bioactive semiconductor nanoparticles like Iron oxide, Titanium oxide, Zinc oxide, Aluminium oxide etc of various shapes by combustion method.
 - To study the physico-chemical properties like UV- vis spectroscopy, XRD, BET,

HRTEM, FESEM, XPS, Laser Raman, Photoluminescence of the prepared nano powders.

- To study the photocatalytic and antimicrobial activity of the prepared nanoparticles.
- To apply the synthesized nanoparticles for dye effluent treatment by Advanced Oxidation Processes (AOP) - Photocatalytic Degradation MONPs/UV and to study in detail.
- To study effect of the surface morphology on dye effluent treatment.
- To collaborate with local companies that will support the study of effluent in reusable/drinkable water.

ii) Work done so far and results achieved and publications, if any, resulting from the work (Give details of the papers and names of the journals in which it has been published or accepted for publication

- ❖ Copper oxide nanoparticles (CuO NPs) were synthesized by solution combustion technique using copper nitrate as an oxidizer and malic acid, oxalic acid and starch as a fuel for fuel rich, stoichiometric, and fuel lean conditions. The band gap was calculated from UV-Vis spectra and it was in the range of 3.23 to 3.28 eV for all the samples. The average particle size calculated from XRD spectra was around in the range of 14 to 20 nm for all the samples. The SEM images revealed that the prepared CuO NPs exhibit different structural morphology for different fuel ratios. The change in fuel ratios plays a vital role in tailoring the surface morphology of CuO NPs and it is studied in detail.
- ❖ The Magnesium Oxide (MgO) nanoparticles synthesized via combustion method, characterized by spectroscopic and microscopic analysis. X-ray diffraction illustrated that the MgO nanoparticles were crystalline in nature with a face centred cubic structure. UV-Vis spectrums of the MgO nanoparticles have a sharp absorption peak around 260 nm. The presence of Magnesium and Oxygen is confirmed by EDX spectrum. FTIR analysis showed the presence of M-O stretching vibration for the synthesis of MgO nanoparticles. The aim of present study is to determine antibacterial activity of MgO nanoparticles against gram-negative and gram-positive bacteria. Escherichia coli (E. coli) – gram negative and

Staphylococcus aureus (*S. aureus*)-gram-positive were used as test organism. The effect of concentration on the antibacterial activity of MgO nanoparticles was studied using well diffusion agar methods for minimum bacterial concentration. The inhibitory concentration of MgO nanoparticles 20, 15, 10 and 5 $\mu\text{g}/\mu\text{l}$. The results showed that MgO nanoparticles have antibacterial inhibition average zone of 11 mm and 14 mm at the concentration of 10 $\mu\text{g}/\mu\text{l}$ against *E. coli* and *S. aureus* respectively. Photocatalytic activity of MgO nanoparticles witnessed by the quick degradation of the organic dye RhB exposure visible light irradiation. .

- ❖ Using nickel nitrate as an oxidizer and starch, oxalic acid and malic acid as fuel, the solution combustion method was used to synthesize nickel oxide (NiO) nanoparticles (NPs). The X-ray diffraction (XRD) has a cubic structure and confirmed the presence of NiO NPs (JCPDS: 78-0429). The average size of crystallite for S1, S2, and S3 are around 42,34 and 36 nm. FTIR spectra showed the band in the 400-550 cm^{-1} range, corresponding to stretching vibration mode, which confirms the presence of NiO NPs. The optical absorption spectra confirmed the presence NiO nanoparticles. The NiO NPs exhibit cubic structure and rod-like structure, inferred from FESEM and High-Resolution Electron Microscopy Transmission (HRTEM). The samples S1 and S3 are exhibiting effective bacterial resistance against gram-positive and gram-negative bacteria. S2 is not showing any antimicrobial activity and can be explained under the surface roughness factor. The NPs, which is having rough surface exhibit greater antimicrobial activity than the smooth surface one. photocatalytic activity of the prepared NiO NPs is evaluated using Methylene Orange and revealed effective degradation.
- ❖ $\alpha\text{-Fe}_2\text{O}_3$ nanoparticles have been prepared by combustion method by using urea. Completion of reaction was followed by Fourier transform infrared spectroscopy (FT-IR) and X-ray diffraction (XRD). The obtained powder was further characterized by energy dispersive spectroscopy (EDS), and scanning electron microscopy (SEM). Their magnetic properties were done by vibrating sample magnetometer (VSM). Urea fuel has reflected morphology of crystallites as well as on their magnetic properties. This results show the finest crystallite size and also high level of magnetic properties. The Fe_2O_3 nanoparticles showed very good antibacterial

activity. The Photocatalytic activity of Fe₂O₃ nanoparticles were also evaluated and were found that the prepared Fe₂O₃ nanoparticles enhance the photocatalytic degradation.

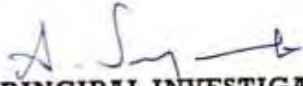
❖ The hexagonal Zinc Oxide Nanoparticles prepared by various methods. The ZnO were characterized by using XRD, FTIR, UV, FL, SEM, EDX, VSM, antibacterial & anticancer activity. The XRD results show hexagonal structure and the particle size of ZnO around 90 nm and lattice parameters $a=3.254\text{\AA}$, $c=5.122\text{\AA}$. With matches to JCPDS card number 76-0704. The functional groups were identified by using FTIR. The optical properties were studied using UV- Vis Spectrum & FL Spectrum. The band gap energy of the material found using UV-Vis Spectrum. The emission peak of Fluorescence Spectrum at room temperature. The prepared sample ZnO was found to have a ferromagnetic material using VSM. The morphology of the SEM images. The elemental spectroscopy found using EDX Spectroscopy. The Photocatalytic activity shows excitation wavelength at 554nm under the degradation of RhB. The anticancer activity (MTT- assay) shows ZnO has a good anticancer agent.


ii. Has the progress been according to original plan of work and towards achieving the objective? if not, state reasons

Yes. The work is completed as per plan the results are achieved

iii. please enclose a summary of the findings of the study. One bound copy of the final report of work done may also be sent to the concerned Regional Office of the UGC: **Enclosed**

iv. Any other information **Nil**


PRINCIPAL INVESTIGATOR
D. A. JECATHA CHRISTY,
Associate Professor of Chemistry
College for Women,
(Autonomous)
PERIYAKULAM-625 601.


PRINCIPAL
Jayaraj Annapackiam College
for Women (Autonomous)
Thamarakulam, Periyakulam-625 601.
Theni District Tamilnadu.

REPORT OF THE WORK DONE ON THE MINOR RESEARCH PROJECT

In this project Copper oxide, Nickel Oxide, Magnesium Oxide, Zinc Oxide, Ferrite oxide nanoparticles were synthesized. The photocatalytic and antimicrobial activities were studied.

EFFECT OF FUEL RATIOS IN TAILORING THE SURFACE MORPHOLOGY OF COPPER OXIDE NANOPARTICLES

Abstract

Copper oxide nanoparticles (CuO NPs) were synthesized by solution combustion technique using copper nitrate as an oxidizer and malic acid, oxalic acid and starch as a fuel for fuel rich, stoichiometric, and fuel lean conditions. The band gap was calculated from UV-Vis spectra and it was in the range of 3.23 to 3.28 eV for all the samples. The average particle size calculated from XRD spectra was around in the range of 14 to 20 nm for all the samples. The SEM images revealed that the prepared CuO NPs exhibit different structural morphology for different fuel ratios. The change in fuel ratios plays a vital role in tailoring the surface morphology of CuO NPs and it is studied in detail.

Keywords: CuO nanoparticles, Solution Combustion method, Malic acid, Oxalic acid, Starch.

1. Introduction

The metal oxide nanoparticles are an important class of semiconductors, which have applications in storage media, electronics, and solar energy. Due to its unique physical and chemical properties, CuO NPs has attracted considerable attention for its large number of applications as materials for catalysts, solar cells, optoelectronics devices, antibacterial materials, lithium batteries, and so on. They are used in the development of gas sensors because of its high specific surface area and good electrochemical activity [1]. They have been prepared by many methods such as the sol-

gel technique, combustion method, sonochemical method, electrochemical method, thermal decomposition method and so on. They were prepared by solution combustion method using different types of fuels such as glycine and citric acid which produces different shapes such as nano flowers and nano rods was reported [2]. Solution combustion synthesis is an exothermic redox reaction between metal nitrate (oxidizer agent) and an appropriate fuel (a reducing agent) and had been successfully used to synthesize nano-crystalline metal oxides. It is a versatile, simple and rapid process, which allows effective synthesis of a variety of nanosize materials [3]. In the present study, CuO NPs were synthesized by solution combustion method and its optical, structural, morphological and vibrational properties were studied in detail.

2. Experimental

2.1 Materials

Copper nitrate ($\text{Cu}(\text{NO}_3)_2$), Malic acid ($\text{C}_4\text{H}_6\text{O}_5$), Oxalic acid ($\text{C}_2\text{H}_2\text{O}_4$) and Starch ($\text{C}_6\text{H}_{10}\text{O}_5$) were used. All the reagents were of analytical grade, purchased from MERCK and were used without further purification.

2.2 Synthesis

The Copper Oxide nanoparticles were prepared by using solution combustion method. Copper Nitrate ($\text{Cu}(\text{NO}_3)_2$) was used as an oxidizer and malic acid, is used as a fuel. Copper Nitrate is dissolved in deionized water and then stoichiometric amount of malic acid is added into it. The solution was mixed vigorously until the homogenous solution was obtained. Then the solution was kept in the hot plate at 300°C . The solution boils, undergoes dehydration and reaches the point of combustion, it began to burn, released a lot of heat as fumes and vaporizing all the solution. The duration for the complete combustion reaction is 15 min. The fine black color powder CuO NPs were obtained. The same procedure is repeated for fuel rich and fuel lean conditions. The above synthesis is repeated by changing the fuels such as oxalic acid and starch respectively. The prepared CuO NPs were indicated as (M1, O1, S1) for fuel lean, (M2, O2, S2) for stoichiometric and (M3, O3, S3) for fuel rich conditions for malic acid, oxalic acid and starch respectively.

2.3 Characterization

Shimadzu 1700 UV–Visible spectrophotometer was used to carry out the optical measurements. The Shimadzu IR affinity-1 Fourier Transform Infrared spectrometer was used to carry out vibrational studies. The X-ray diffraction patterns were recorded using X-ray diffractometer (XPRT-PRO) using Cu-K α radiation ($\lambda=0.1542$ nm) operated at 40 kV and 30 mA. Energy Dispersive Spectroscopy was carried out by BRUKER instrument. Scanning Electron Microscopy images were obtained by an instrument VEGA3 LMU.

3. Results and Discussions

3.1 Optical studies

Ultraviolet-Visible spectroscopy (UV-Vis)

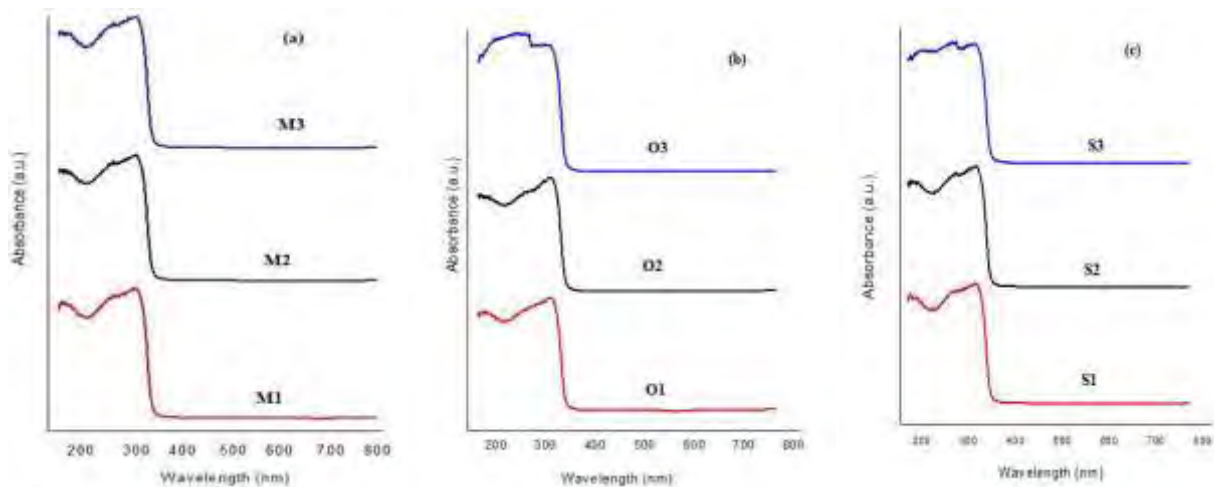


Fig. 1) Absorption spectra of (a) M3, M2, and M1 (b) O3, O2, and O1 (c) S3, S2 and S1.

Fig. 1(a, b, c) shows the UV-Visible absorption spectra of M3, M2, M1, O3, O2, O1, S3, S2, and S1. The peak maximum of the characteristic surface plasmon resonance (SPR) is given in the table 1 for all the samples. It was observed that they fall in the range of 343-348 nm. The optical direct band gap of the produced NPs is calculated using the Tauc's relation,

$$\alpha h\nu = A(h\nu - E_g)^n \dots\dots\dots (1)$$

where $\alpha=2.303A/t$ is called the absorption coefficient, A is the absorbance, E_g is the band gap, $h\nu$ is the photon energy (h is the planck's constant and ν is the frequency of the incident photon) and n is the exponent that determines the type of electronic transition causing the absorption having values $n = 1/2$ and 2 for direct and indirect band gap semiconductors respectively [4]. The optical energy band gap was calculated and the corresponding values are given in table 1.

3.2 Vibrational studies

Fourier Transform Infrared Spectroscopy (FTIR)

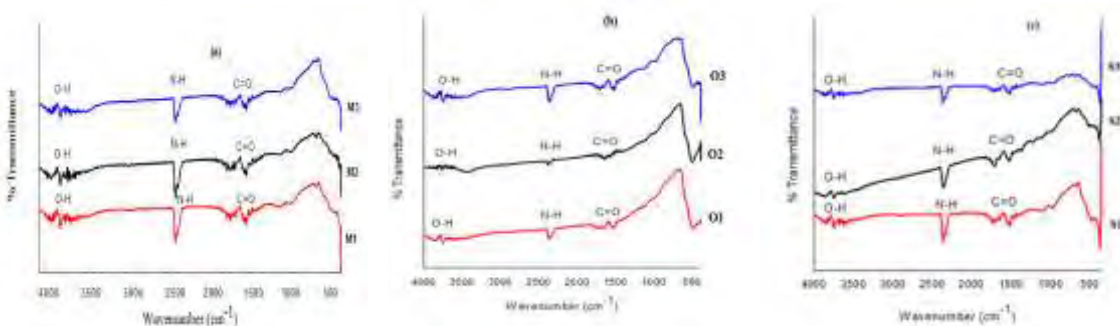


Fig. 2) FTIR spectra of (a) M3, M2, and M1 (b) O3, O2, and O1 (c) S3, S2 and S1.

Fig. 2 shows the FTIR spectra of M3, M2, M1, O3, O2, O1, S3, S2, and S1. FTIR Spectra were recorded in the range of 4000-400 cm^{-1} . The bands which are in the range of 3200-3800 cm^{-1} are attributed to O-H stretching vibration of water absorbed by the sample during pellet formation. The bands observed in the range of 2350-2360 cm^{-1} may be due to N-H stretching vibration. The bands observed in the range of 1700-1710 cm^{-1} may be due to C=O stretching vibration [5]. The band observed around 1500 cm^{-1} may be due to N-O asymmetric stretching. The bands observed around 450-550 cm^{-1} confirms the presence of CuO NPs [6].

3.3 Structural Studies

X-ray Diffraction (XRD)

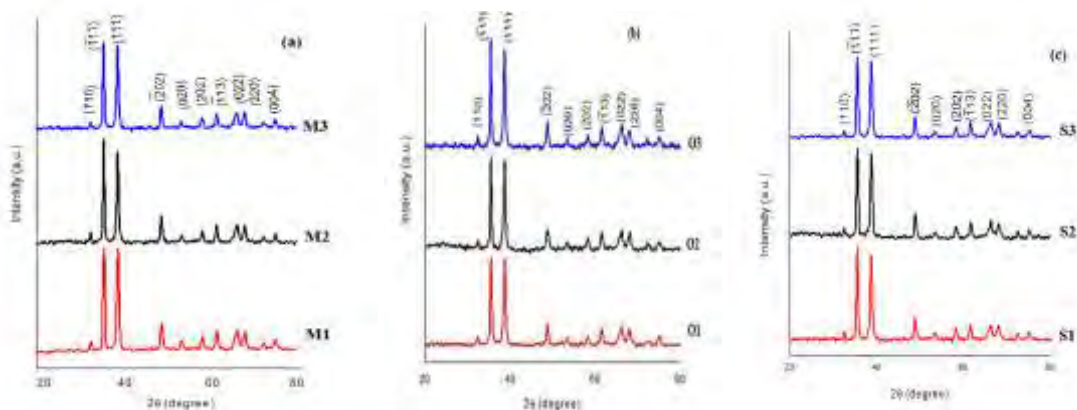


Fig. 3) XRD pattern of (a) M3, M2, and M1 (b) O3, O2, and O1 (c) S3, S2 and S1.

Fig. 3(a), 3(b) and 3(c) shows the XRD pattern of M3, M2, M1, O3, O2, O1, S3, S2, and S1. The peaks observed at 32.44°, 35.470°, 38.674°, 48.75°, 53.41°, 58.22°, 61.49°, 66.04°, 67.96°, 74.99° corresponding to (110), $\bar{1}11$, (111), $\bar{2}02$, (020), (202), $\bar{1}13$, (022), (220) and (004) diffraction planes respectively (JCPDS: 89-2529). They exhibit monoclinic structure and the lattice parameters of the unit cells are $a=4.683 \text{ \AA}$, $b=3.428 \text{ \AA}$, $c=5.129 \text{ \AA}$, having $\beta=99.30^\circ$. The volume of the cell for monoclinic structure was 81.29 (\AA)^3 for all the samples. The average particle size of CuO NPs were calculated using Debye-Scherrer equation,

$$D = K\lambda / \beta \cos\theta \dots\dots\dots (2)$$

Where D is the crystallite size (nm), k is a constant (0.94), λ is the wavelength of X-ray radiation (1.5406 \AA), β is the full-width at half-maximum (FWHM) of the peak (in radians) and 2θ is the Bragg angle (degree) [7]. The average crystallite size for all the samples is given in table 1.

Table 1: Specific data of all the samples

Samples	Average Particle size (XRD) (nm)	SPR (nm)	Band gap (ev)
M3	18	345	3.25
M2	20	344	3.24
M1	17	343	3.23
O3	17	348	3.28
O2	14	347	3.27
O1	18	346	3.26
S3	17	346	3.26
S2	18	346	3.26
S1	16	345	3.25

Energy- Dispersive X-ray Spectroscopy (EDS)

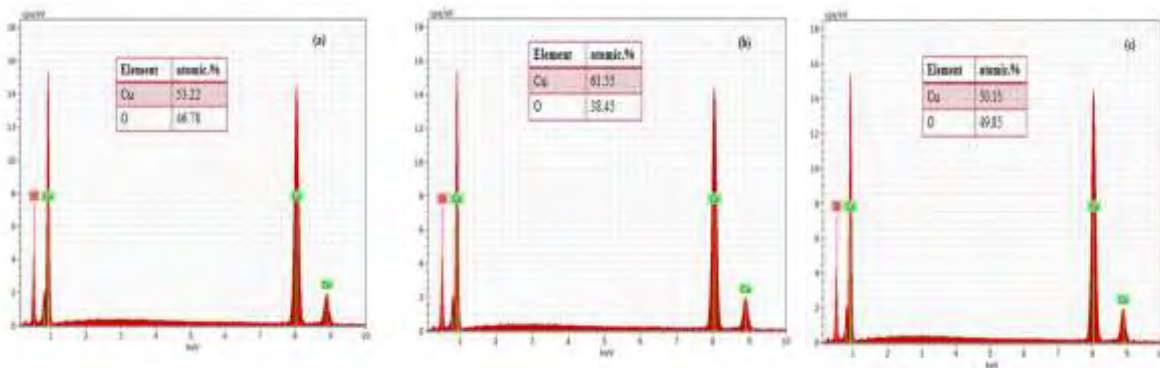


Fig. 4) EDS spectrum of (a) M3, M2, and M1 (b) O3, O2, and O1 (c) S3, S2 and S1.

Fig. 4 shows the EDS spectra of M3, M2, M1, O3, O2, O1, S3, S2, and S1. The elemental analysis of copper oxide nanoparticles were confirmed by Energy dispersive X-ray analysis (EDX or EDS). From the spectrum, an oxygen peak found at 0.53 keV and a copper peak observed at 1, 8 and 9 keV. EDX analysis confirms the formation of CuO nanoparticles [8].

3.4 Morphological Studies

Scanning Electron Microscopy (SEM)

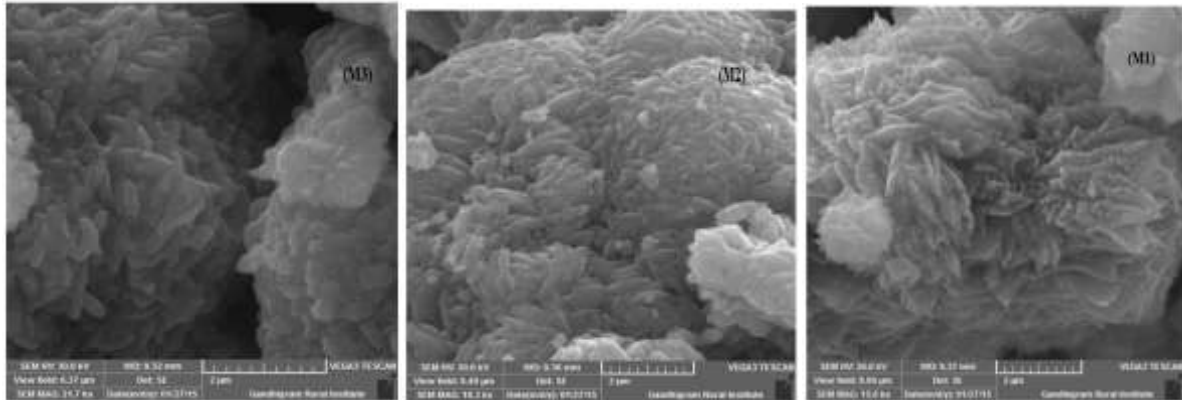


Fig. 5) SEM images for (a) M3 (fuel rich), (b) M2 (stoichiometric) and (c) M1 (fuel lean).

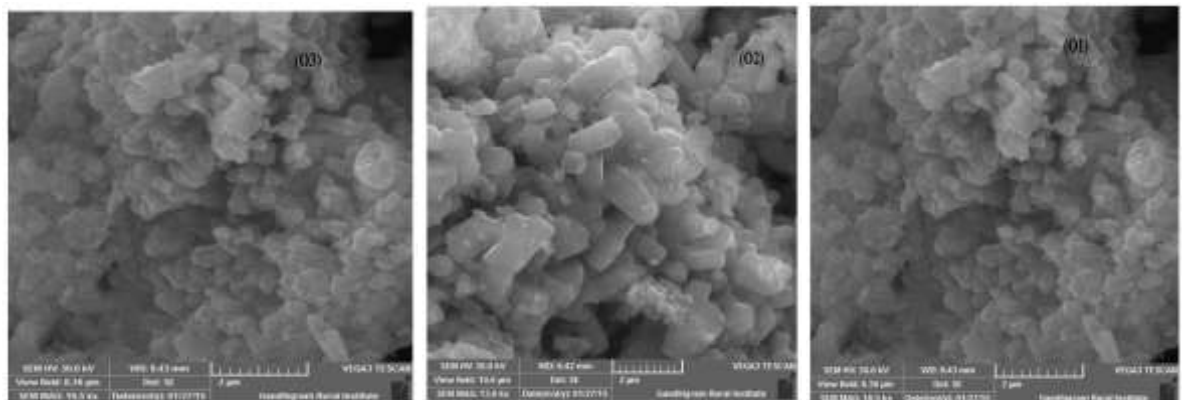


Fig. 6) SEM images for (a) O3 (fuel rich), (b) O2 (stoichiometric) and (c) O1 (fuel lean).

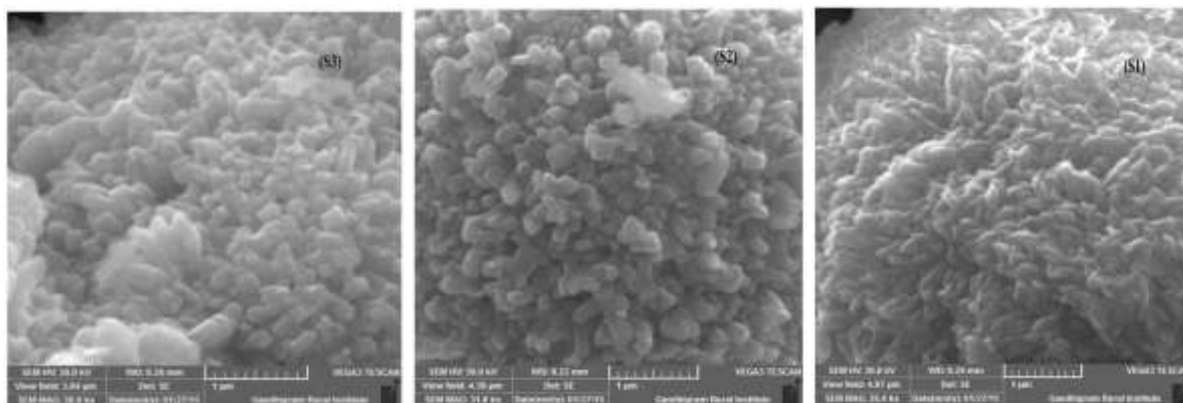


Fig. 7) SEM images for (a) S3 (fuel rich), (b) S2 (stoichiometric) and (c) S1 (fuel lean).

Fig. 5 shows the SEM images of M3, M2 and M1. The CuO NPs exhibit initial stage of the rice like structure in M3. In M2, the formation became clear and exhibits exact rice like one. Finally, the rice like structure began to compress and deformed in the corners and changed in to rice flake like structure for M1.

Fig. 6 shows the SEM images of O3, O2, and O1. The CuO NPs exhibit initial formation of rod like structure in O3. Then it is elongated and shows the uniform rod like structure in O2 and it is completely agglomerated in O1 [9].

Fig. 7 shows the SEM images of S3, S2, and S1. The CuO NPs exhibit initial formation of cuboid like structure in S3. Then it shows the even formation of cuboid like structure in S2. The edges of cuboid are broken and it is completely transformed in to wheat like structure in S1 [10].

It is clearly understood from the SEM images that, the amount of fuel used plays a vital role in tailoring the surface morphology of the prepared CuO nanoparticles. When malic acid, oxalic acid and starch is employed as a fuel, the heat released in combustion is more and as a result the combustion enthalpy is more which is responsible for the growth of the sample and complete combustion reaction with more crystalline phase. So the result indicates that the presence of fuels has a significant effect on the morphology of the sample [11]. The stoichiometric ratio produced uniform structure patterns where Fuel low and fuel high conditions failed to do so.

4. Conclusion

The CuO NPs with various morphologies were synthesized by using solution combustion method by changing fuel ratios. The UV-Vis analysis shows the SPR peak in the range of 343-348 nm for all the samples. The FTIR spectra show the band in the range of 450-550 cm^{-1} for all the samples. The average size was calculated from XRD spectra in the range of 14-20 nm for all the samples. From the SEM analysis, CuO NPs exhibit different shapes such as rice, rod and cuboid like structures. The EDS spectra confirm the presence of CuO NPs for all the samples.

Acknowledgement

One of the author Dr. A. Jegatha Christy is grateful to UGC SERO for the financial assistance.

[1] Y Zou, Y Li, X Lian, and An Dongmin Preparation and Characterization of Flower-shaped CuO Nanostructures by Complex Precipitation Method Res. Mater. Sci. Vol 3, p 44-1 (2014)

[2] M Umadevi, and A Jegatha Christy Synthesis, characterization and photocatalytic activity of CuO nanoflowers Spectrochimica Acta Vol 109, p133-7 (2013)

[3] T Singanahally Aruna, and S Alexander Mukasyan Combustion synthesis and nanomaterials Curr. Opin.Solid State Mater. Sci. Vol 12, p 44-0 (2008)

[4] P Mallick, and S Sahu Structure, Microstructure and Optical Absorption Analysis of CuO Nanoparticles Synthesized by Sol-Gel Route Nano.Sci. Nano.Tech. Vol 2(3), p 71-4 (2012)

[5] S Sankar, M R Manikandan, S D GopalRam, T Mahalingam, and G Ravi J. Cryst.

Growth Vol 312, p 2729-3 (2010)

[6] Y Liu, Y Chu, M Li, L Lia, and L Dong J. Mater. Chem Vol 16, p 192-8 (2006)

[7] S Thakur, N Sharma, A Varkia, and J Kumar Structural and optical properties of copper doped ZnO nanoparticles and thin films Adv. App. Sci. Res. Vol 5(4), p 18-4 (2014)

[8] J Mayekar, V Dhar, and S Radha Synthesis of Copper Oxide Nanoparticles Using Simple Chemical Route Int. Journal of Sci. & Eng. Res. Vol 5, p 928-0 (2014)

[9] A Jegatha Christy, L C Nehru, and M Umadevi A novel combustion method to prepare CuO nanorods and its antimicrobial and photocatalytic activities Powder Technology Vol 235, p 783-6 (2013)

[10] H Siddiqui, M S Qureshi, and F Z Haque Structural and Optical Properties of CuO Nanocubes Prepared Through Simple Hydrothermal Route Int. Journal of Sci. & Eng. Res. Vol 5, p 173-7 (2014)

[11] A Jegatha Christy, and M Umadevi Novel combustion method to prepare octahedral NiO nanoparticles and its photocatalytic activity Mater. Res. Bulletin Vol 48, p 4248-4 (2013)

PROPERTIES OF MAGNESIUM OXIDE NANOPARTICLES AND THEIR ACTIVITY ON GRAM-POSITIVE AND GRAM-NEGATIVE BACTERIA VIA COMBUSTION METHOD

Abstract:

The Magnesium Oxide (MgO) nanoparticles synthesized via combustion method, characterized by spectroscopic and microscopic analysis. X-ray diffraction illustrated that the MgO nanoparticles were crystalline in nature with a face centred cubic structure. UV-Vis spectrums of the MgO nanoparticles have a sharp absorption peak around 260 nm. The presence of Magnesium and Oxygen is confirmed by EDX spectrum. FTIR analysis showed the presence of M-O stretching vibration for the synthesis of MgO nanoparticles. The aim of present study is to determine antibacterial activity of MgO nanoparticles against gram-negative and gram-positive bacteria. Escherichia coli (E. coli) – gram negative and Staphylococcus aureus (S. aureus)-gram-positive were used as test organism. The effect of concentration on the antibacterial activity of MgO nanoparticles was studied using well diffusion agar methods for minimum bacterial concentration. The inhibitory concentration of MgO nanoparticles 20, 15, 10 and 5µg/µl. The results showed that MgO nanoparticles have antibacterial inhibition average zone of 11 mm and 14 mm at the concentration of 10µg/µl against E. coli and S. aureus respectively. Photocatalytic activity of MgO nanoparticles witnessed by the quick degradation of the organic dye RhB exposure visible light irradiation. .

Key words: MgO; XRD; FTIR; SEM; EDX; Antibacterial activity; S. aureus; E. coli

1. Introduction

Nanoparticles is a special group of materials with unique features and extensive applications in diverse fields (Matie et al., 2008) [1]. Studying the particular features has always been of great interest to many scientists. In fact, nanoparticles display completely unique properties in comparison with their bulk size counterparts (Priyanka et al., 2009) [2]. A large number of Nanomaterials which were considered to be safe develop toxicity due to specific surface area and high reactivity of nanosize materials.

In particular, magnesium oxide (MgO), is one of the versatile oxide material with assorted properties finds extensive applications in catalysis, ceramics, toxic waste remediation and as an additive in paint and super conductor product [2]. Due to application of large band gap (7.8 eV), excellent thermodynamically stability, low dielectric constant and refractive index, biology, medicine [3, 4]. Therefore many synthesis method have been developed to prepare nanosized of MgO nanoparticles [5-15]. These method involve complex procedures, sophisticated apparatus/equipments rigorous experimental conditions, high temperature annealing. In the work a simple route of synthesis of MgO Nanoparticles has been used under mild reaction conditions without any surfactants or organic solvents. A synthetic study of the structural, morphological and optical properties of the calcinated and as synthesized MgO nanoparticles.

The considerable antimicrobial activities of inorganic metal oxide nanoparticles such as ZnO, MgO, TiO₂, SiO₂ and their selective toxicity to biological systems suggest their potential application as therapeutics, diagnostics, surgical devices and nanomedicine based antimicrobial agents. The advantages of antimicrobial agents are their greater effectiveness on resistant strain of microbial pathogens, less toxicity and heat resistance. In addition, they provide mineral elements essential to human cells and even small amounts of them exhibit strong activity [16].

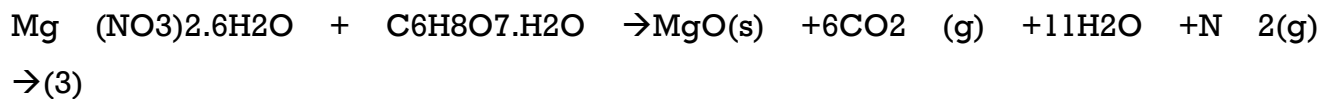
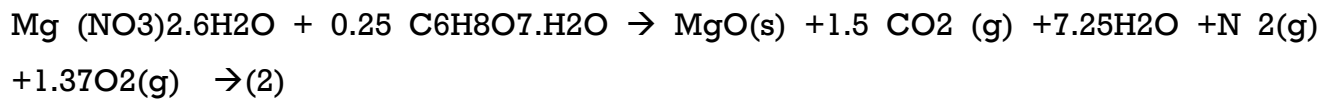
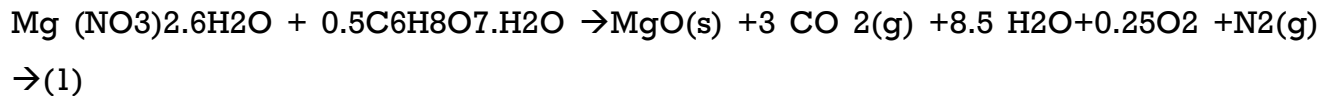
In the present work, Mg (NO₃)₂.6H₂O is used as oxidizer and C₆H₈O₇.H₂O is used as fuel. Similar to the oxidation number concept, the valency of the oxidizing elements is considered as negative and the reducing element is the positive, in solution combustion calculation [17]. Accordingly the elemental valency of C,H and Mg is +4, +1 and +2 respectively, and the oxidizing valency of magnesium nitrate and the reducing valency of citric acid can be calculated as Mg(NO₃)₂.6H₂O = -[2-24+12+0]=10 and C₆H₈O₇.H₂O = [24+10-16]=18. According to the equivalence ratio theory, for the combustion of Magnesium nitrate and Citric acid molar ratio becomes 10/18=0.55. C₆H₈O₇.H₂O

That is, $\phi_e = \frac{\sum \text{Coefficient of oxidizing elements is specific formula} * \text{valency} (-1)}{\sum \text{Coefficient of reducing elements is specific formula} * \text{valency}} = \frac{10}{18} = 0.55$. in order to the variation of fuel to oxidant ratio is 2:1/2 oxidant to fuel ratio is taken for fuel-lean , 2:1 for stoichiometry and 2:2 molar ratio of Mg(NO₃)₂.6H₂O and C₆H₈O₇.H₂O was taken in fuel-rich condition.

2. Experimental procedure

2.1 Synthesis of MgO nanopowders

The nanocrystalline MgO particles were prepared by combustion method using Magnesium nitrate and Citric acid (fuel). The composition of oxidizer and fuel are calculated by on the following chemical equations



Here, equation (1) represent Stoichiometry conditions, equation (2) is the Fuel-lean, and equation (3) is the Fuel-rich conditions. The commercially available Mg (NO₃)₂·6H₂O was first dissolved in minimum quantity of deionized water. Then, this solution was stirred at 70rpm for a few minutes. After that the Citric acid (C₆H₈O₇·H₂O) was dissolved in minimum quantity of deionised water was mixed to the magnesium nitrate solution and stirred well. Then, the solution combustion mixture was heated slowly in heating mantle until it gets ignited. When the temperature reached at 1000c, completely water molecule evaporated combustion flame appeared. The obtained MgO powder was annealed at 3000c for 2 hours in groove rolled muffle furnace was cooled at room temperature by switching off the powder. After completion of combustion the crude white color powder was appeared in fuel-lean condition, light brown color appeared stoichiometry; brown color was appeared in fuel-rich condition.

2.2 Characterization

The identification and purity of the materials were tested powder XRD and FTIR Spectroscopy by using Powder X-ray diffraction (Bruker Advanced D8) with Cu-K α radiation. Infrared spectra were acquired with a Nicolet 760ESP FT-IR spectrometer that

was purged with boil-off from liquid N₂. The spectrometer was equipped with a liquid nitrogen-cooled HgCdTe detector. The nanoparticle powder sample was mixed with KBr powder and ground into fine powders. The powders were pressed into pellets at 15000psi. The solution sample was measured using a thin-layer (0.5mm) IR cell. The IR spectra were collected over the range of 400-4000cm⁻¹. Ultraviolet visible-near infrared (UV-Vis) studies were carried out in the range of 200–1000 nm using Perkin Elmer UV-Vis (Model-lambda35) Spectrophotometer. The surface morphology of the sample was analyzed using a Scanning Electron Microscope (SEM) (Hitachi 3000 H). The Fluorescence emission and excitation spectra were recorded at room temperature by use of a Shimadzu RF-5301 PC spectro fluometer. The chemical composition of the powders was analyzed by energy-dispersive X-ray spectroscopy (EDX).

Antibacterial Activity of MgO NPs

Anti-bacterial activity of MgO NPs was assessed against Gram positive (*Staphylococcus aureus* (MTCC2412) and Gram negative *Escherichia coli* (MTCC 2412) bought from Microbial Type Culture Collection IMTEC, India. Oxytetracyclin was used as positive control based on Kirby–Bauer disk diffusion method [13]. Sterile discs (6 mm diameter) loaded with various concentrations of MgONPs (5–20 µg/ml) were placed on the culture plates and incubated at 37 °C overnight and the zone of inhibition were measured and recorded in mm.

Catalytic Activity of MgO NPs

The catalytic activity of MgONPs was assessed based on their ability to degrade the dye Rhodamine B (RhB) in presence of visible radiations. Tungsten lamp (300 W) was used as the visible lamp source. Stock solution (10 mg/l) of Rhodamine B was prepared. About 10 mg of MgONPs was added to 100 ml of dye solution and subjected to constant stirring in dark for half an hour to promote the equilibrium between RhB and photocatalyst before exposure to sunlight and UV irradiation. The reaction mixture was exposed to light source and about 2 ml of the suspensions were withdrawn at selected time intervals (every 30 min) and suspended particles were removed by ultracentrifugation. The rate of dye degradation was determined using the absorbance measured in a UV–visible spectrophotometer (U-2800, Hitachi, Japan) at 552 nm. The dye degradation percentage

was assessed based on the formula % of degradation = $\frac{C_i - C_f}{C_i} \times 100$ Where, C_i and C_f were the initial and final concentrations of dye at time interval "t" respectively.

3. Result and discussion

3.1. XRD characterization of MgO nano powders

The XRD pattern of MgO nanoparticles obtained from combustion synthesis were as shown in Figure 1. The result showed that the structure was in cubic structure and these results were matched with JCPDS card number 75-1525. Peaks were absorbed at 12° , 42° and 62° along with miller indices values (1 0 0), (2 0 0) and (2 2 0) respectively. The lattice parameters were obtained $a=b=c= 0.4195$ nm. The crystallite size was measured by Debye Scherer's equation as mentioned below.

$$D = \frac{0.94 \lambda}{\beta^{1/2} \cos \theta} \quad \text{_____} \quad (4)$$

Where D is the average crystallite size of the particles, K is Debye scherrer's constant (=0.94), λ is the wavelength of the Cu $K\alpha$ - radiation (=0.154 nm), β is the full width half maximum (FWHM) of the peak, θ -is the Bragg's angle. The particle size for fuel-lean (35), Stoichiometry (25) and fuel-rich (20nm) respectively.

3.2 FTIR Spectroscopy

The typical FTIR Spectrum for the annealed MgO NPs is depicted in fig (2). From FTIR analysis the stretching vibration mode for the Mg-O-Mg compound is present in the range of 400-900 cm^{-1} broad band. Two distinct broad band at 1420-1425 cm^{-1} and 1560-1700 cm^{-1} and are attributed to the bending vibration of absorbed water molecule and surface hydroxyl group (O-H) respectively. A broad vibration band is seen in the wave number range 3325-3650 cm^{-1} due to O-H stretching vibration of absorbed water molecule and surface hydroxyl group.

3.3 UV Spectrum of MgO

The UV- Vis Spectra of Magnesium Oxide nanoparticle is as shown in fig (3). In UV- Spectrum the scale range will take 190-1000 nm. The maximum excitation wavelength MgO nanoparticle was 200- 265nm. Generally optical properties of the material depend

on band gap energy of the material. The band gap energy of the MgO nanoparticle was found to have a linear relation. The band gap energy of the prepared compound 5.3, 5.5 & 5.9 which is corresponding to fuel-lean, stoichiometry and fuel-rich condition.

3.4 FL-emission & excitation Spectra

The Fluorescence spectrum of MgO nanopowder is as shown in fig (4). The fluorescence spectrum was recorded in the range between 200 to 400nm. For fluorescence spectrum the emission wavelength is fixed at 465nm. The excitation wavelength was observed 230-240nm. is as shown in fig (4).

The Fluorescence emission spectrum of MgO nanopowder is as shown in fig (4b). The fluorescence emission spectrum was recorded in the range between from 400 - 900nm. The, excitation wavelength is fixed at 380nm. The emission wavelength of spectrum is given as 735, 743 and 764nm for fuel-lean, Stoichiometric and fuel-rich condition.

3.5 SEM with EDX Spectrum of MgO nanopowder

Fig (5) shows SEM with EDX spectrum of MgO nanopowder by using fuel citric acid under the three different conditions for Fuel-lean, Stoichiometry, Fuel-rich conditions. The SEM image results reveal that the annealed MgO nanomaterials are seemingly highly agglomerated.

Fig (6a) shows Fuel-lean condition of prepared MgO Nanoparticles. From EDX Spectrum Oxygen have a 60.10%, Carbon has 5.72%, Magnesium has 29.97%, and Nitrogen has 4.21 weight percentages present in the prepared MgO Nanoparticles by using Citric acid fuel under the condition of Fuel-lean condition.

Fig (6b) shows Oxygen has 54.49%, Carbon has 24.27%, Magnesium has 18.74%, and Nitrogen has 2.50% containing weight percentage of the prepared MgO Nanoparticles by using Citric acid fuel under the condition of Stoichiometry condition.

From Fig (6c) shows a EDX Spectrum of MgO Nanopowder by using citric acid fuel. This is the Fuel-rich conditions. The prepared sample containing weight percentage of Oxygen has 43.38%, Carbon has 32.51% and Magnesium has 24.12 percentage of the prepared MgO Nanoparticles by using Citric acid fuel under the condition of Stoichiometry condition. Here, Nitrogen absent to this condition. For above two conditions N is present.

3.6 Antibacterial Activity of MgO NPs

The bactericidal activity of MgONPs was assessed by Kirby–Bauer test. Results illustrated that the MgONPs synthesized from brown algae showed potent bactericidal activity against gram positive and negative bacterial strains in a dose dependent manner (Fig.6 and Table 1). MgONPs showed potent antibacterial activity against gram positive bacterial strains such as *Staphylococcus aureus* (MTCC2412) and Gram negative *Escherichia coli* (MTCC 2412) compared to positive control. Among the microbial strains tested, MgONPs exhibited the highest inhibitory activity against Gram positive (*Staphylococcus aureus* (MTCC2412) and Gram negative *Escherichia coli* (MTCC 2412) for 20 µg/ml. The antibacterial efficacy of MgONPs might be due to their smaller sizes, which was consistent with the report that MgONPs with smaller sizes would exhibit potent bactericidal efficiency [18].

3.7 Photocatalytic activity of MgO NPs

Catalytic activity of MgONPs was evaluated based on the rate of degradation of organic dye pollutant (Rhodamine B -RhB) widely used in dye industry. Rate of RhB degradation was calculated as the percentage of decolorization with respect to time based on the absorbance at the optimum wavelength of 552 nm.

Conclusion:

In this paper MgO nanoparticles were prepared by a combustion method. The synthesized Nanoparticles calcinated at 4000c for 2 hours under these three conditions Fuel-lean, Stoichiometry, Fuel-rich conditions. From XRD spectrum the prepared sample was conformation by using JCPDS file no-75-1525, the particle size of the nano powder 35, 25 and 20nm which is corresponding to fuel-lean, Stoichiometry and fuel-rich condition. The optical properties studied by using UV and Fluorescence Spectra. The band gap energy was calculated by using UV-Vis Spectroscopy 4.7eV for Fuel-lean, Stoichiometry and 5.2eV for Fuel-rich condition. The functional group was identification by using FTIR Spectrum Mg-O-Mg, O-H groups and water molecules identifications. SEM images show the morphology of the nanoparticles. The percentage of the chemical composition was find out EDX spectroscopy. The prepared MgO nanoparticles have good antibacterial & photocatalytic activity.

Acknowledgment

The author Dr. A. Jegatha Christy is grateful to SERO/UGC for financial support.

References:

- [1] T. Jintakosol, P.Singjai, *Curr. Appl.Phys.*9, 2009, 1288- 1292
- [2] G. Duan, X. Yang, J. Chen, A. Huang, L. Lu, X. Wang, *Powder Technol.*172, 2007, 27-29.
- [3] T. Qiu, X.L. Wu, F.Y. Jin, A.P. Huang, Paul K. Chu, *Appl. Surf. Sci. Eng.*, C26, 2006, 1097- 1101.
- [4] Xie Yi, L. Wang, J. Wang, D. Yang, *Mater. Sci.Eng.*, C26, 2006, 1097-1101.
- [5] T. Selvamani, T. Yagyu, S. Kawasaki, I. Mukhopadhyay, Easy and effective synthesis of micrometer-sized rectangular MgO sheets with very high catalytic activity, *Catal. Commun.* 11 (2011) 537 - 541.
- [6] N. Sutradhar, A. Sinhamahapatra, B. Roy, H.C. Bajaj, I. Mukhopadhyay, A.B. Panda, Preparation of MgO nano-rods with strong catalytic activity via hydrated basic magnesium carbonates, *Mater. Res. Bull.* 46 (2011) 2163 - 2167.

- [7] E. Esmaeili, A. Khodadadi, Y. Mortazavi, Microwave-induced combustion process variables for MgO nanoparticles synthesis using polyethylene glycol and sorbitol, *J. Eur. Ceram. Soc.* 29 (2009) 1061 - 1068.
- [8] M.A. Shah, A. Qurashi, Novel surfactant-free synthesis of MgO nanoflakes, *J. Alloys Compd.* 482 (2009) 548 - 551.
- [9] T.X. Phuoc, B.H. Howard, D.V. Martello, Y. Soong, M.K. Chyu, Synthesis of Mg(OH)₂, MgO and Mg nanoparticles using laser ablation of magnesium in water and solvents *Opt. Laser Eng.* 46 (2008) 829 - 834.
- [10] L. Sun, H. He, C. Liu, Z. Ye, Local super-saturation dependent synthesis of MgO nanosheets, *Appl. Surf. Sci.* 257 (2011) 3607 - 3611. [14] Y. Su, H. Wei, Z. Zhou, Z. Yang, L. Wei, Y. Zhang, Rapid synthesis and characterization of magnesium oxide nanocubes via DC arc discharge, *Mater. Lett.* 65 (2011) 100 - 103.
- [11] Y. Su, H. Wei, Z. Zhou, Z. Yang, L. Wei, Y. Zhang, Rapid synthesis and characterization of magnesium oxide nanocubes via DC arc discharge, *Mater. Lett.* 65 (2011) 100 - 103.
- [12] T. Lopez, I. Garcia-Cruz, R. Gomez, Synthesis of magnesium oxide by the sol-gel method: Effect of the pH on the surface hydroxylation, *J. Catal.* 127 (1991) 75 - 85.
- [13] Bokhimi., A. Morales, Crystalline structure of MgO prepared by the sol-gel technique with different hydrolysis catalysts *J. Solid State Chem.* 115 (1995) 411 - 415.
- [14] R. Portillo, T. Lopez, R. Gomez, Magnesia synthesis via sol-gel: Structure and reactivity, *Langmuir* 12 (1996) 40 - 44.
- [15] Danith Kumar¹, L. S. Reddy Yadav², K. Lingaraju³, K. Manjunath⁴, D. Suresh⁵, Daruka Prasad⁶, H. Nagabhushana⁷, S. C. Sharma⁸, H. Raja Naika³, Chikkahanumantharayappa¹, and G. Nagaraju^{2*}, Combustion synthesis of MgO nanoparticles using plant extract: Structural characterization and photoluminescence studies", *Journal of Applied Physics Letters*, 1665(Volume), 25-06-2015.

- [16] Mohammad Moslem Imani¹ and Mohsen Safaei² , “Optimized Synthesis of Magnesium Oxide Nanoparticles as Bactericidal Agents”, Journal of Nanotechnology, (2019).
- [17] N. C. S. Selvam, R. T. Kumar, L. J. Kennedy, and J. J. Vijaya, “Comparative study of microwave and conventional methods for the preparation and optical properties of novel MgO-micro and nano-structures,” Journal of Alloys and Compounds, vol. 509, no. 41, pp. 9809–9815, 2011.
- [18] Yiping He^{1*}, Shakuntala Ingudam² , Sue Reed¹ , Andrew Gehring¹ , Terence P. Strobaugh Jr.¹ and Peter Irwin¹, “ Study on the mechanism of antibacterial action of magnesium oxide nanoparticles against forborne pathogens”, Journal of Nano biotechnology (2016).

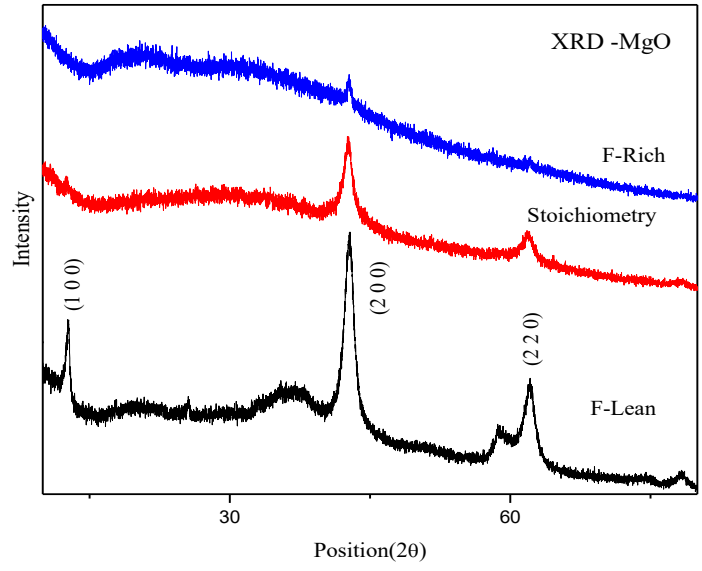


Fig (1) XRD Spectrum of MgO nanopowders by using Citric acid

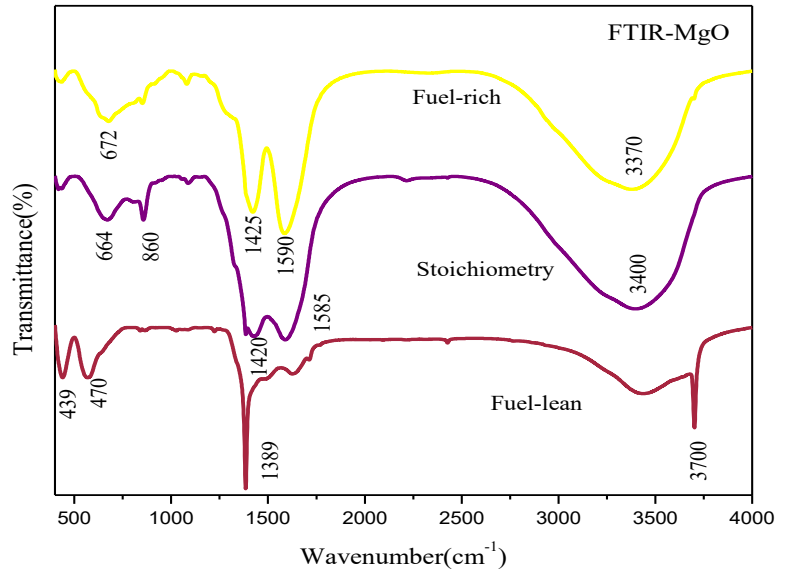
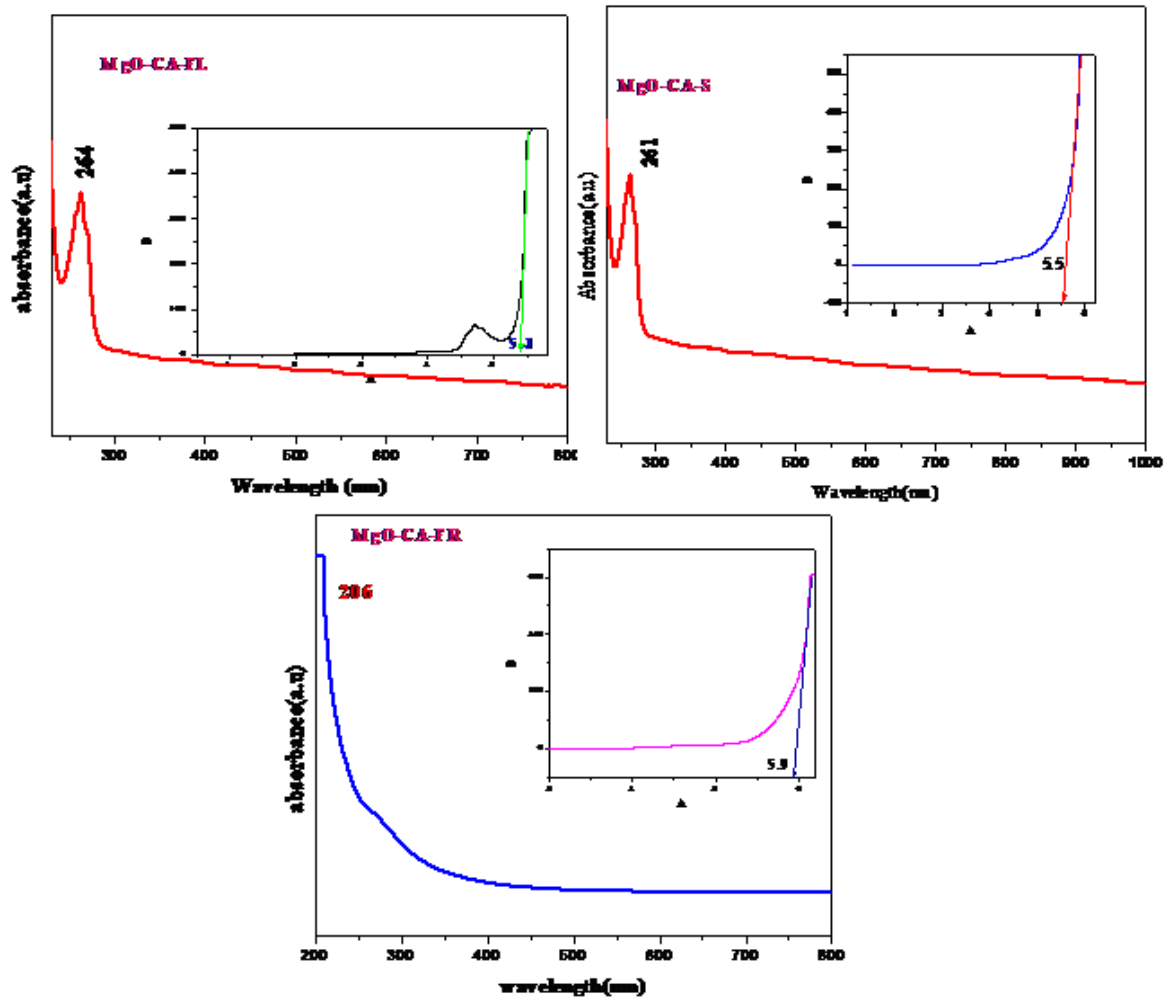


Fig (2) FTIR Spectrum of MgO nanopowders



Fig(3) UV-Spectrum of MgO nanopowder

S

Fig(4a) Shows FL-excitation Spectrum of MgO nanopowder

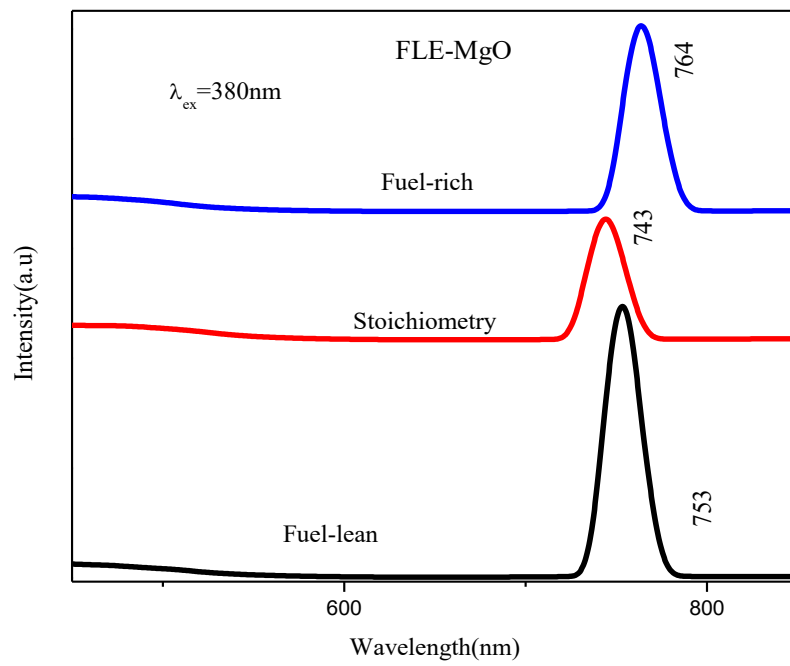
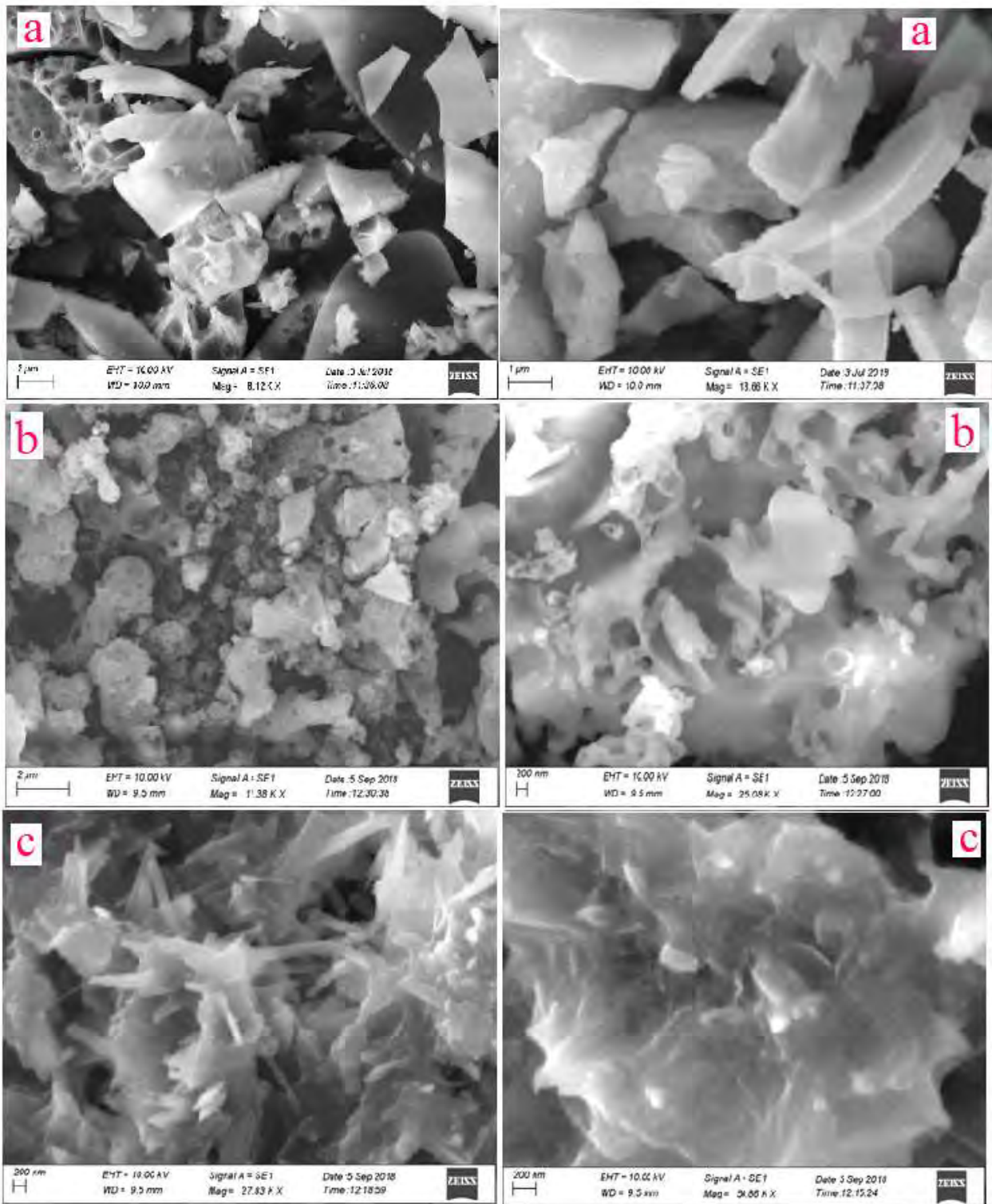
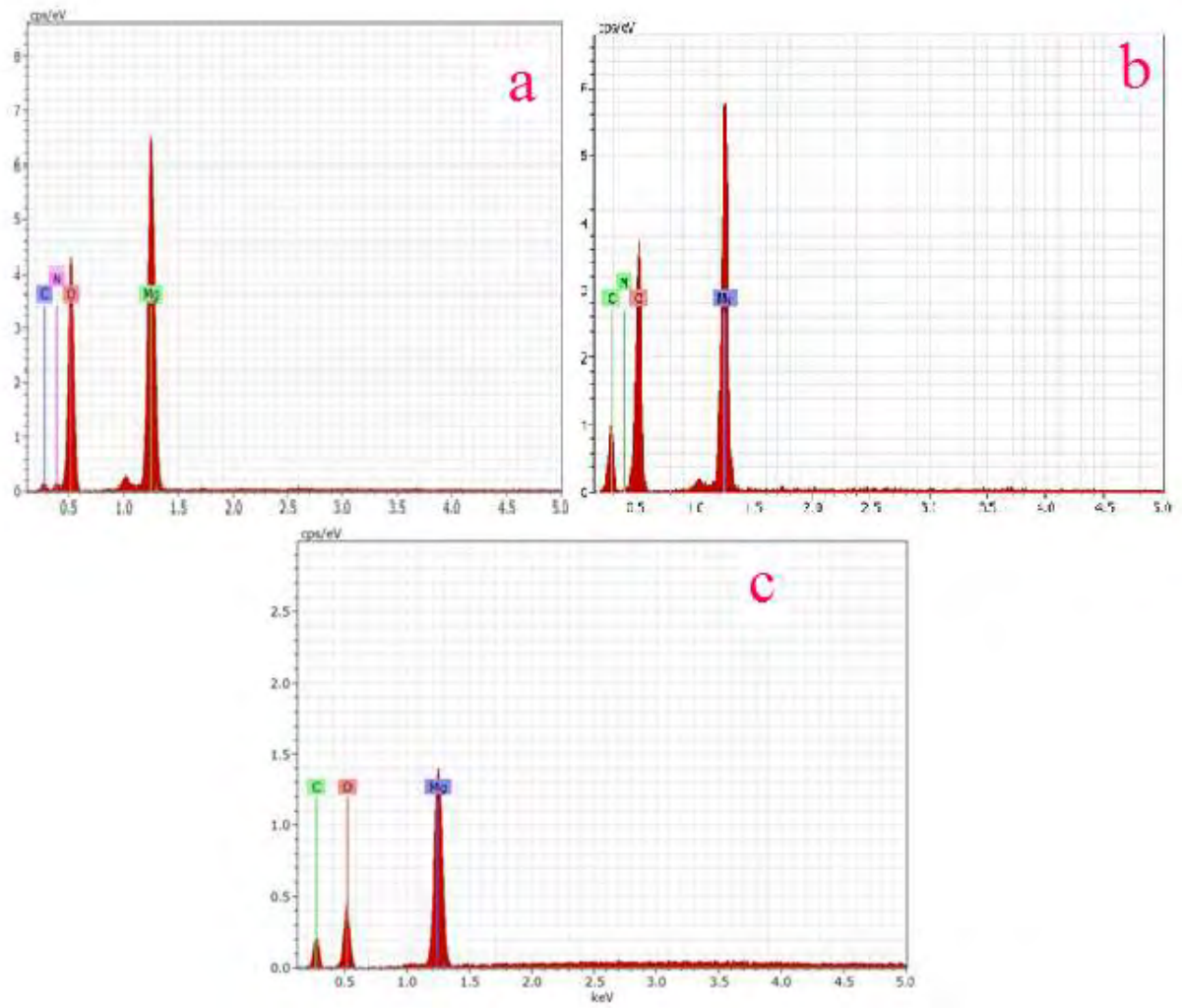


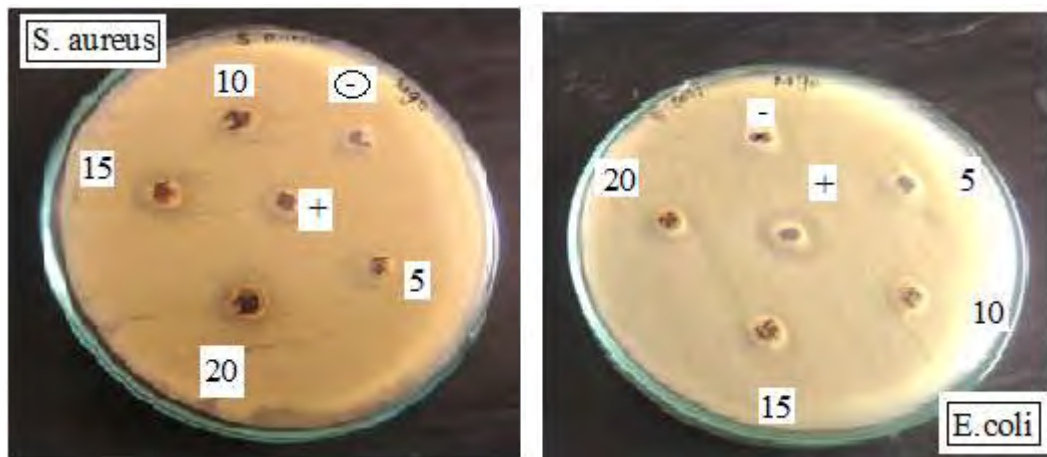
Fig (4b) FL-emission Spectrum of MgO nanopowder



Fig(5) shows SEM Spectrum of MgO nanopowder (a) FR, (b) S, (c) FL



Fig(6) shows SEM Spectrum of MgO nanopowder (a) FR, (b) S, (c) FL



Fig(7) Shows Anti-bacterial activity of MgO nanoparticles

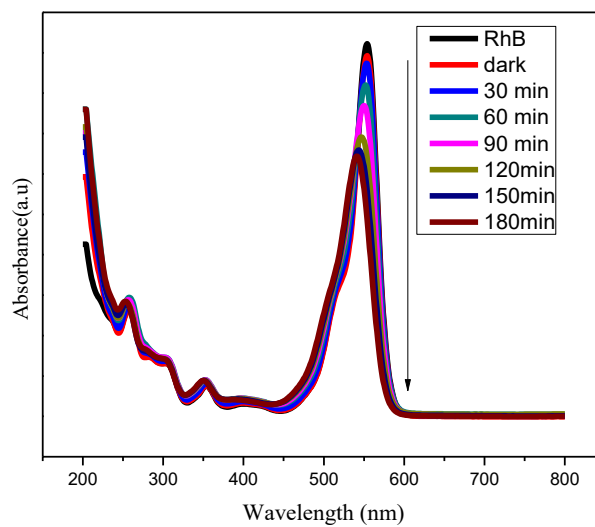


Fig (8) Photocatalytic activity of MgO nanoparticles

TAILORING THE MORPHOLOGICAL CHARACTERISTICS OF THE NICKEL OXIDE NANOPARTICLES FOR ANTIMICROBIAL AND PHOTOCATALYTIC ACTIVITY

Abstract

Using nickel nitrate as an oxidizer and starch, oxalic acid and malic acid as fuel, the solution combustion method was used to synthesize nickel oxide (NiO) nanoparticles (NPs). The X-ray diffraction (XRD) has a cubic structure and confirmed the presence of NiO NPs (JCPDS: 78-0429). The average size of crystallite for S1, S2, and S3 are around 42, 34 and 36 nm. FTIR spectra showed the band in the 400-550 cm^{-1} range, corresponding to stretching vibration mode, which confirms the presence of NiO NPs. The optical absorption spectra confirmed the presence NiO nanoparticles. The NiO NPs exhibit cubic structure and rod-like structure, inferred from FESEM and High-Resolution Electron Microscopy Transmission (HRTEM). The samples S1 and S3 are exhibiting effective bacterial resistance against gram-positive and gram-negative bacteria. S2 is not showing any antimicrobial activity and can be explained under the surface roughness factor. The NPs, which is having rough surface exhibit greater antimicrobial activity than the smooth surface one. photocatalytic activity of the prepared NiO NPs is evaluated using Methylene Orange and revealed effective degradation.

Keywords: Nanostructure, NiO, Antimicrobial activity, Photocatalytic Activity, HRTEM

1. Introduction

In recent years, synthesis processes to grow dispersed nanoparticles in a matrix have attracted the attention of several researchers. However, the growth of dispersed nanoparticles with homogenous sizes is not easy. With the manufacture and engineering of nanoscale materials, structures, and systems, nanotechnology is a known field of research and technology actions. The idea of plans from chemistry, physics, biology combined to develop a new material with intended properties [1]. Metal Oxides nanomaterials have attracted considerable interest in several areas of technology. NiO NPs can have several applications, for example in the manufacture of electrochromic films, films, magnetic materials, p-type transparent films, gas sensors, catalysts, cathode alkaline batteries, and anode solid oxide fuel cells [2]. Several methods have been reported to synthesize NiO NPs by various expensive and/or difficult methods. The NiO

NPs prepared by a different method such as sol-gel [3], thermal decomposition [4], solid state reaction [5], precipitation, sonochemical [6] have been reported earlier. Solution combustion synthesis is a fast and easy process among these methods, with the main benefits of saving time and energy. This process is directly used to produce high purity, homogeneous powders of ceramic oxide. Solution Combustion Synthesis (SCS) is a versatile process reported for synthesizing a wide range of particles including nanometer size powder[7]. NiO NPs ' surfactant-free synthesis using the combustion method with different sizes and studied their thermal conductivity[8]. As an oxidizing agent, it uses a metal nitrate and an organic fuel as a reduction agent in oxidation/reduction reactions that occur as the catalyst is synthesized. While the heat obtained can help to decompose metal nitrate and salts, the initiation of the reactions requires primary heat so that they can continue the process without additional energy[9]. The SCS may occur as either volume or layer-by-layer propagating combustion modes, depending on the type of precursors as well as the conditions used for the process organization. This result is not surprising from a chemical point of view because it is well known that the decomposition of metal nitrates leads to the formation of corresponding oxides. During this auto-ignition process, large volumes of gases are generated, making fine powder the resulting product. Developing methods for the synthesis of nickel oxide nanoparticles in which the particle size and the product crystal structure can be controlled is very important[10]. Materials such as nickel, copper, silver, zinc have high antibacterial activity, low toxicity, chemical stability, thermal resistance in comparison with organic antibacterial agents[11]. In the present study, NiO NPs were synthesized with Starch, Oxalic acid and Malic acid as fuel by solution combustion method and investigated the optical, structural, morphological, antibacterial and photocatalytic properties.

2. Materials and Method

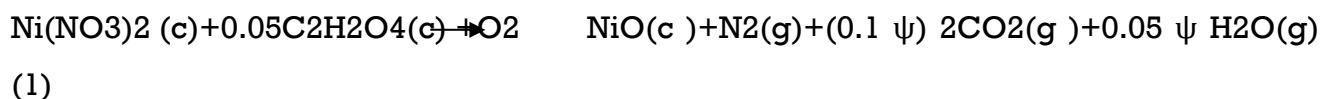
2.1 Materials

Nickel nitrate, Starch, Oxalic acid and Malic acid of analytical grade, were used without further purifications.

2.2 Synthesis of NiO NPs

For the preparation of NiO NPs, Stoichiometric ratio of Nickel Nitrate and Starch were taken as starting materials, keeping the oxidizer (metal nitrate) to the fuel(starch) ratio as

unity. Stoichiometric amount of nickel (II) nitrate was dissolved in deionized water and then starch was added into it. The solution has been kept at 400°C in the furnace. With enormous fumes, the combustion reaction was completed in 15 minutes. Finally, NiO NPs were obtained as black color powder. The same procedure is repeated for Oxalic acid and malic acid fuels respectively. In the combustion reaction, fuel is oxidized by the metal nitrate and the expected reaction to form NiO NPs can be written as:



The molar ratio of oxalic acid to nickel nitrate $\psi = 0.05$ here corresponds to the oxygen content of nickel nitrate which can be fully reacted to completely oxidize the oxalic acid. In the equation, c and g refers to compound and gas.

For the Nickel nitrate and Malic acid combination of combustion, the expected reaction can be written as:



Here the molar ratio of malic acid to nickel nitrate is $\psi = 0.0083$. As a result, NiO product and CO₂, H₂O, and N₂ gasses can be formed directly from the fuel-oxidizer reaction without the need for oxygen from outside.

2.3 Characterizations

The patterns of X-ray diffraction (XRD) were recorded on the PANalytical X-ray diffractometer using the 50KV and 100 mA operated Cu K α radiation ($\lambda = 0.1542$ nm). The experiments were conducted in the range of diffraction angles $2\theta = 20-80^\circ$. The optical measurements were performed using Shimadzu 1700 UV-Visible spectrophotometer. The vibrational studies were performed using the Shimadzu IRAffinity-1 Fourier Transform Infrared spectrometer. Field Emission Scanning Electron Microscope (FESEM) (Carl Zeiss sigma) High-Resolution Transmission Electron Microscopy (HRTEM) (200KeV JEOLJEM2100) analyzed the size, composition and atomic structure of the NiO NPs.

2.4 Assay for antimicrobial activity of NiO NPs against microorganism

NiO NPs' antimicrobial activity was evaluated with their agar disc diffusion method against gram-negative, *Klebsiella pneumonia*, *Acinetobacter baumannii*, *Pseudomonas aeruginosa*, *Citrobacter freundii*, *Escherichia coli*, *Vibrio cholera*. With 100 μ L of actively grown broth cultures of the respective test bacteria, Mueller Hinton agar plates were spread and allowed to dry for 10 minutes. The plates have been incubated at 37 $^{\circ}$ C for 48 hours.

The inhibition zone development around the extract loaded disks has been recorded.

2.5 Photocatalytic Activity

The photocatalytic activity of the samples was evaluated by the degradation of Methyl Orange (MO) at an initial concentration of 0.1 mM. 0.0125 mM of NiO NPs with MO Solution is fully diluted and added. The prepared solution was irradiated under visible light and the reaction solution was taken in regular interval of time and the absorption change was observed.

3. Results and Discussion

3.1 X-ray diffraction (XRD) analysis

XRD pattern of NiO NPs as shown in Fig.1. and confirmed the presence and phase of the synthesized NiO NPs. The XRD diffraction peaks were observed at 37.34 $^{\circ}$, 43.37 $^{\circ}$, 62.91 $^{\circ}$, 75.42 $^{\circ}$, 79.38 $^{\circ}$ for S1, 37.34 $^{\circ}$, 43.40 $^{\circ}$, 62.95 $^{\circ}$, 75.49 $^{\circ}$, 79.51 $^{\circ}$ for S2, 37.37 $^{\circ}$, 43.41 $^{\circ}$, 62.96 $^{\circ}$, 75.43 $^{\circ}$, 79.54 $^{\circ}$ for S3 corresponding to (111), (200), (220), (311), and (222) diffraction plans respectively (JCPDS: 78-0429). All NiO diffraction peaks correspond to the cubic structure. The volume of the unit cell was 72.84 (Å)³, 72.82(Å)³ and 72.85(Å)³ for S1, S2, and S3. The average NiO NPs crystallite size was calculated using the Debye Scherrer equation,

$$D = K \lambda / \beta \cos \theta \quad (3)$$

Where D is the size of the crystallite (nm), where λ is the wavelength of the X-ray source (0.15406 Å), where β is the full width at half the maximum diffraction peak (FWHM) in radians, K is the Scherrer constant with a value of 0.9 to 1. The constant value of the lattice

is also calculated and the standard data is very close to 4.177 Å. The average grain size was approximately 42, 34 and 36 nm [12].

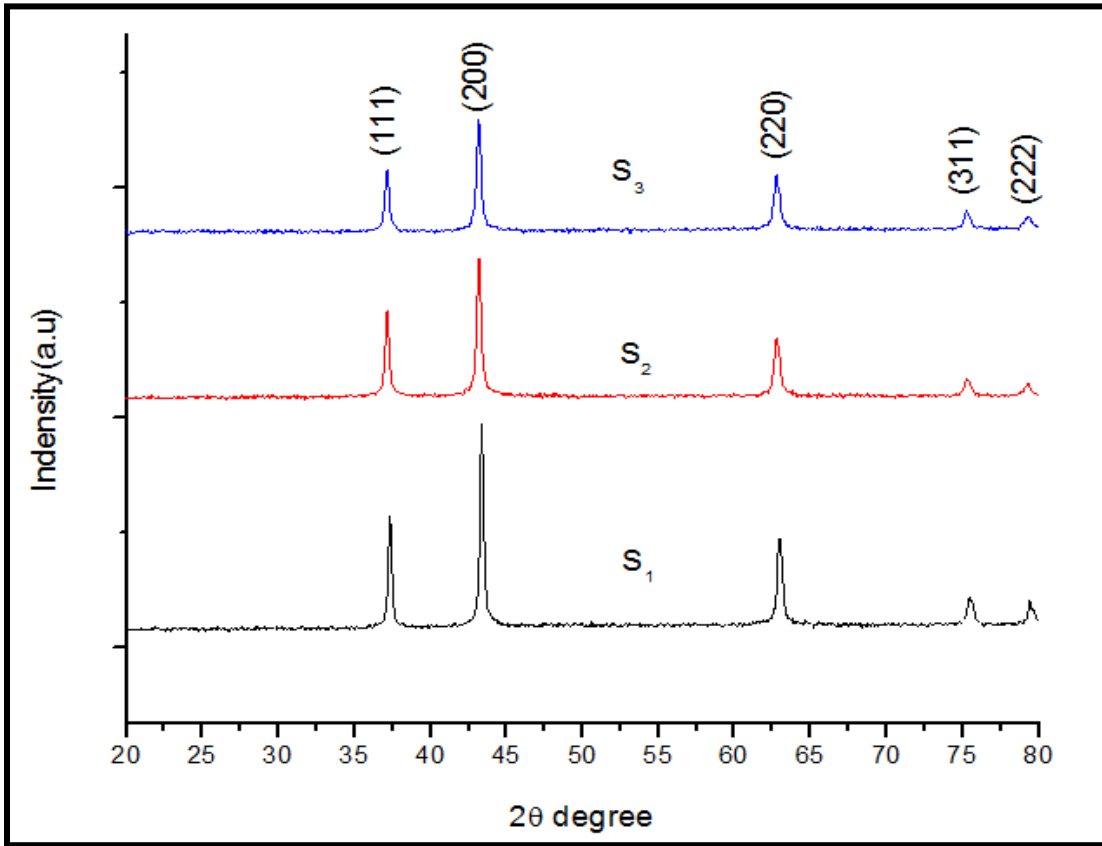


Fig.1. XRD pattern for NiO NPs

3.1.1 Williamson-Hall method

Numerous experiments have shown that a special logarithmic series expansion of the Bragg reflection peak profiles. Fourier coefficients can well describe strain expansion caused by dislocations.

W-H equation may be expressed in the form,

$$\beta h k l \cos \theta = (k \lambda / D) + 4 \varepsilon \tan \theta \quad (4)$$

Rearranging this Eq. (4)

$$\beta h k l \cos \theta = (k \lambda / D) + (4 \varepsilon \sin \theta) \quad (5)$$

A plot drawn between $\beta \cos\theta$, and $4 \sin\theta$, and the line slope gives grain size (D) to the strain (ϵ) and intercept (k/D). The term $\beta \cos\theta$ was plotted for the prepared orientation peaks of NiO NPs with respect to $4 \sin\theta$. Fig.2 shows the results of the W-H analysis plot of S1, S2 and S3 having positive strain and is found to have the value 0.001. Due to the small size of crystallite and lattice strain, the line extension of cubic NiO. The strain from the W-H model, however, is very small and has a negligible effect on peak expansion.

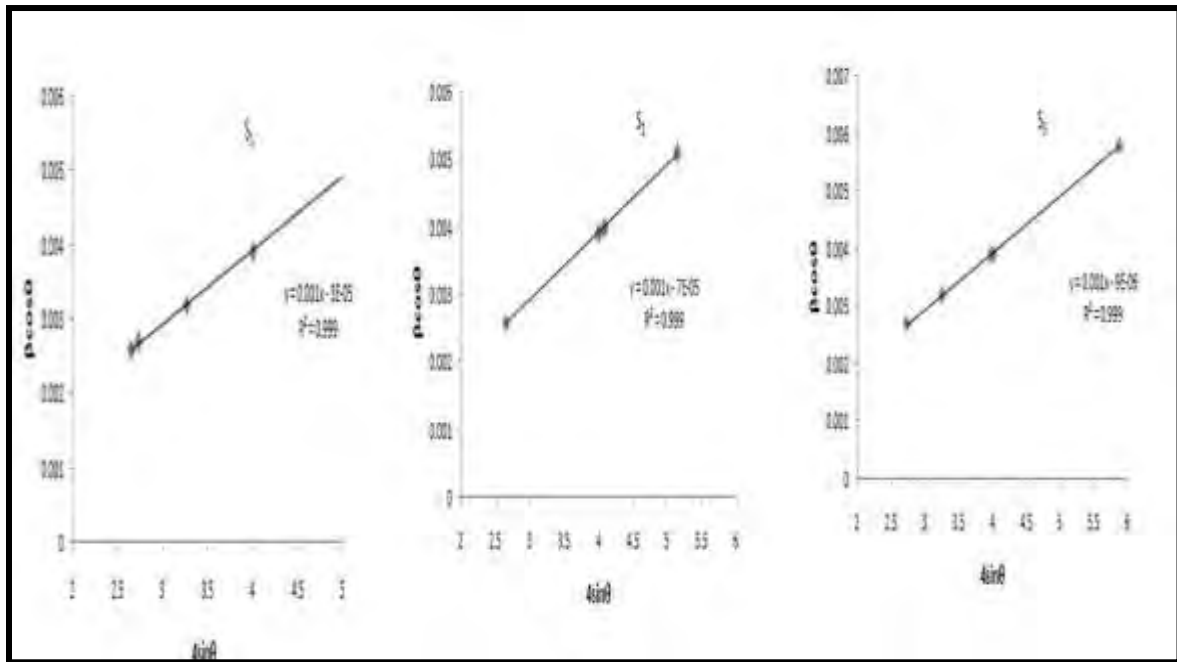


Fig 2. W-H plot analysis of NiO NPs (S1, S2, and S3)

3.2 Fourier transforms infrared spectroscopy (FT-IR)

The FTIR spectra were observed in the 500-4000 cm^{-1} frequency range for NiO NPs as shown in Fig.3. Ni-O stretching vibration mode is assigned to the broadband in the 400-550 cm^{-1} region. The prepared NiO NPs shows the characteristic band of 3474 cm^{-1} which attributable to O-H stretching and the band at 1635 cm^{-1} is assigned to the mode of H-O-H bending vibrations presented due to water adsorption in the air during the preparation of FTIR sample disks in an open-air environment. O-C=O symmetric and asymmetric stretching vibrations are attributed to the band at 1382 cm^{-1} [13]. The band in the 400-550 cm^{-1} range, corresponding to stretching vibration mode, confirms the presence of NiO NPs.

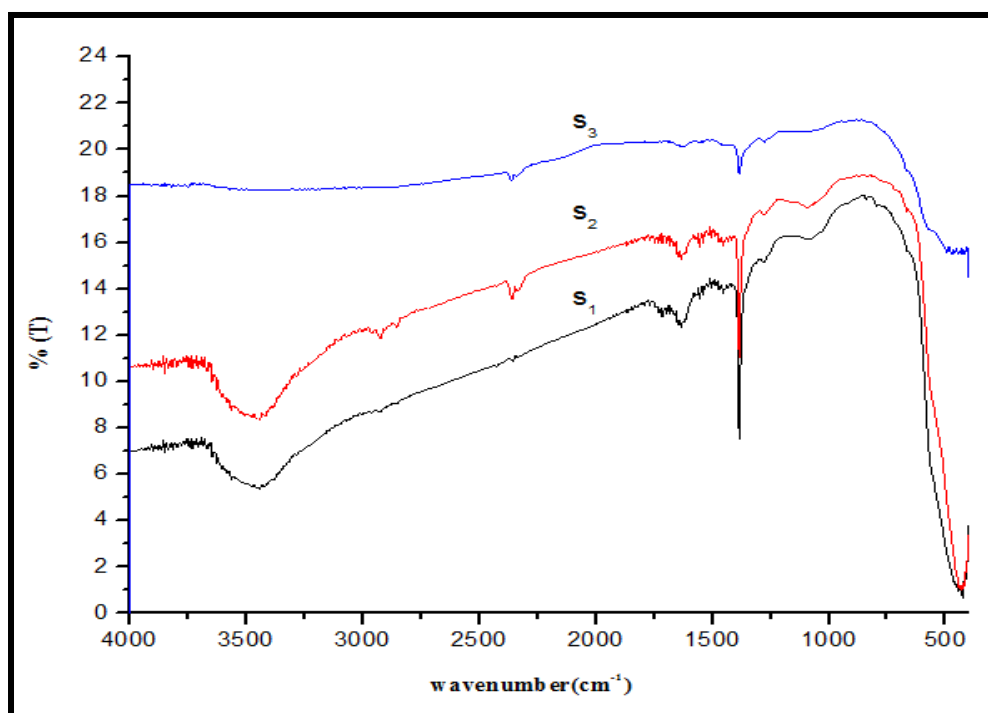


Fig 3. FTIR spectra of NiO NPs

3.3 UV-Vis spectroscopy (UV-Vis)

Fig.4 shows the UV-Vis absorption spectra for the S1, S2 and S3. NiO NPs showed strong absorption peaks in the UV region which is blue shifted from the absorption edge of bulk NiO [14]. This lower wavelength shifts or blue shift in the latter case is attributed to the Burstein – Moss effect, which confirms the quantum confinement effect. The absorption peaks in the UV region appeared at wavelengths of about 244, 245 and 246 nm respectively for S1, S2, and S3. The absorption edge is observed in the range of 240-250 nm. This blue shift of the absorption edges for different sized nanocrystals is related to the size decrease of particles due to the quantum confinement effect of nanoparticles. The lower band gap value of NiO nanoparticles exhibits the nature of blue shift due to quantum confinement effect in the nanoscale region [15].

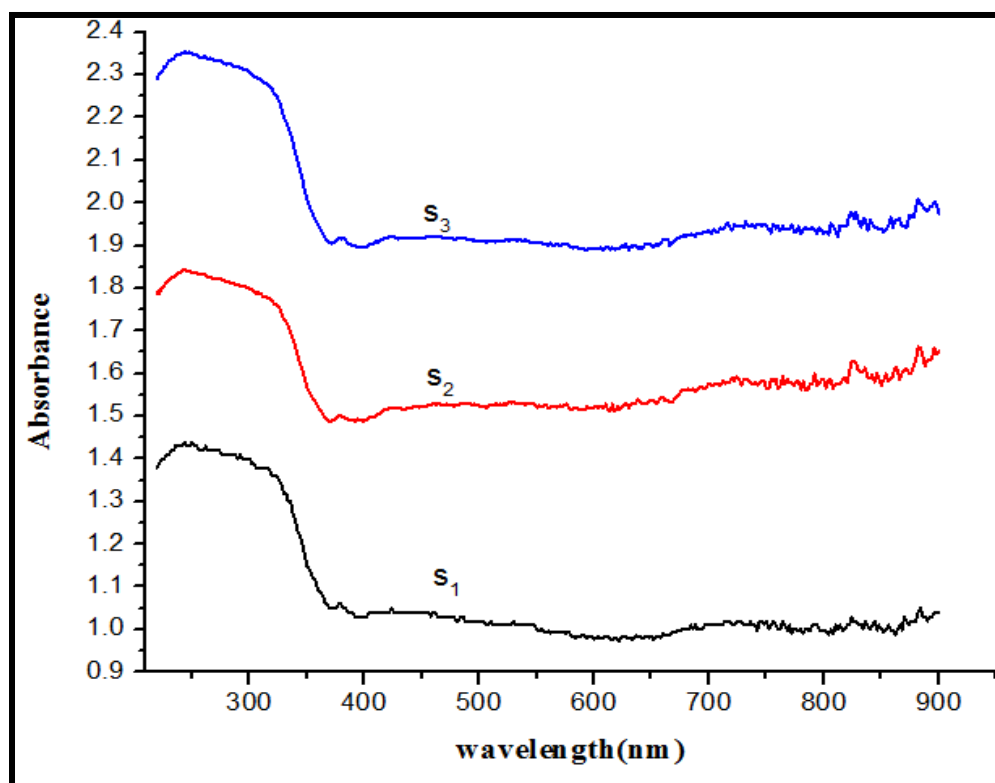


Fig.4 optical absorption spectra of NiO NPs

3.4 Field Emission Scanning Electron Microscope (FESEM) and Energy Dispersive Spectroscopy (EDS)

Fig 5 shows the FESEM images of S1, S2 & S3. NiO NPs are observed to be almost cubic and rod-like structure. During adsorption on these surfaces, the introduction of selective fuel can control the growth rates of different metal oxide nanoparticles faces. Studying the growth mechanism of NiO NPs, it can be suggested that the fuel is responsible for different morphologies of S1, S2 and S3. When growth occurred in the atmosphere, vapor concentration and oxygen atmospheric pressure resulted in low vapor supersaturation and this could be the main reason for nanorod formation [16]. It shows the presence of several small particles. This was thought to be related to the non-uniform distribution in the combustion flame of temperature and mass flow. From the FESEM images, it is clearly understood that the Starch, Oxalic acid and Malic acid ratio plays a vital role in tailoring the morphology of the surface. Fig.6 shows the EDAX spectra of the prepared NiO NPs. The characteristic NiO peak is observed at 1, 7 and 8keV for S1, S2 and S3. The presence of nickel oxide is confirmed. The signal of Cu originated from the carbon-coated Cu grid. From the obtained spectra the presence of Ni and O were detected.

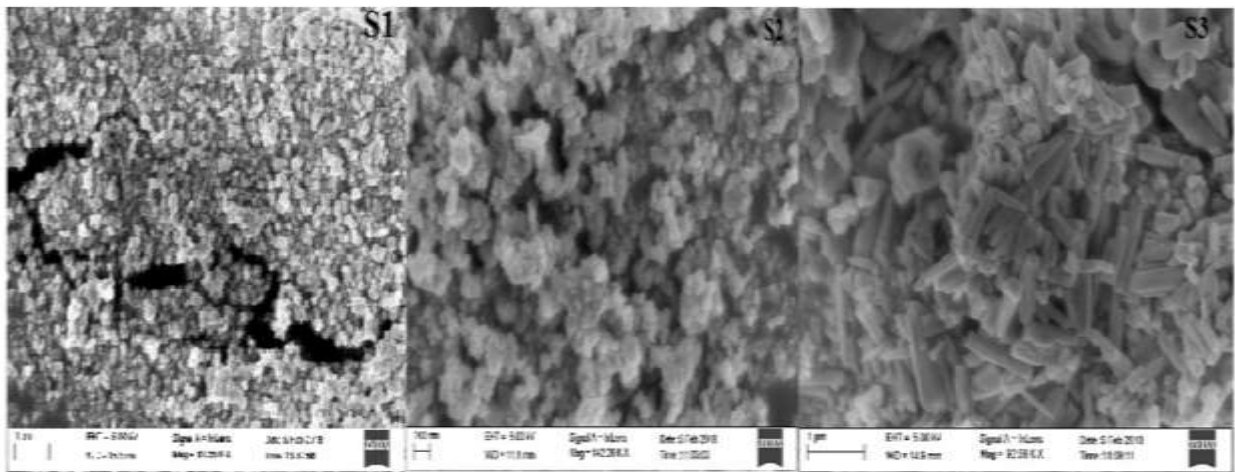


Fig 5. FESEM image of S1, S2, and S3

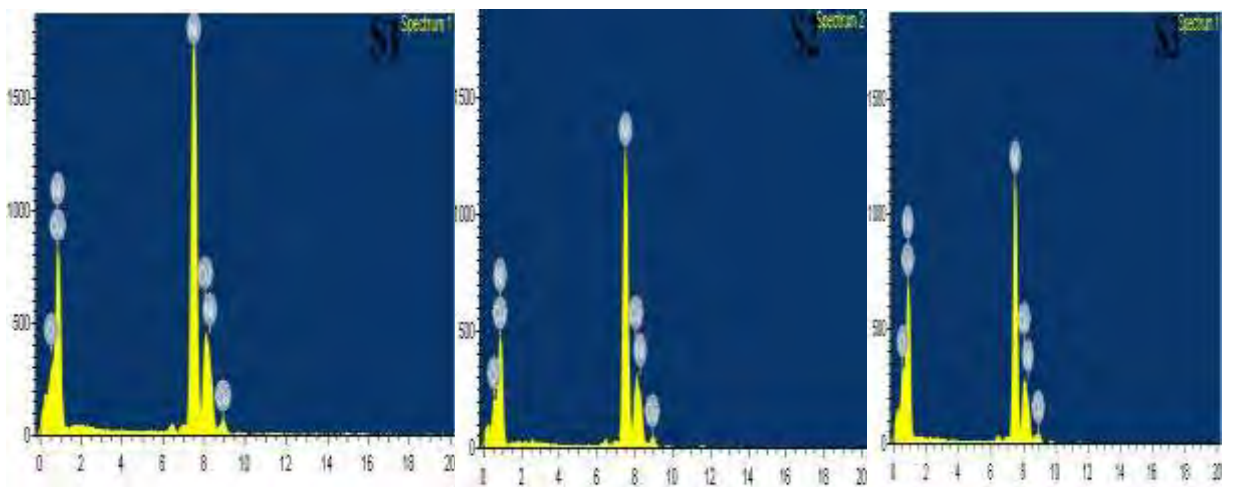


Fig 6. Energy dispersion spectra of S1, S2, and S3

3.5 High-Resolution Transmission Electron Microscopy (HR-TEM)

Figs 7 (a,b,c) shows the HRTEM image of S1, S2 & S3 at the different magnification of NiO NPs. The prepared NiO NPs exhibit cubic structure of approximately 100-200 nm in width. It was found that the lattice spacing is 0.147 nm, which corresponds to (220) NiO NPs cubic structure planes for S1, S2 and S3 and the interplanar distance between the (220) planes corresponds to the atomic fringe spacing. S2 is revealing smooth surface than S1 and S2 and it is mainly governed by the enthalpy and flame temperature generated during the combustion process, which in turn depends on the type of fuel and oxidizer used in the reaction [17]. As a result, the presence of Starch, Oxalic acid & Malic acid has a significant role in deciding the shape, size, crystallinity and surface roughness of the NiO NPs. In the

present study, Oxalic acid played its role very well and helped the Nickel nitrate to oxidize better than Starch and Malic acid and the resultant NPs S2 seems to have clear, smooth and well defined structure.

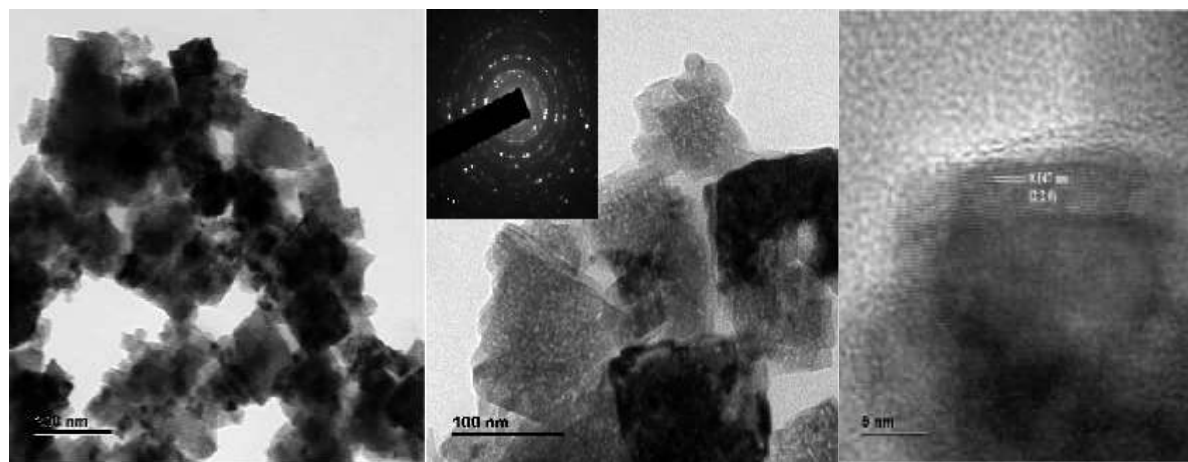


Fig.7 (a) HRTEM images NiO NPs in different magnification of S1.

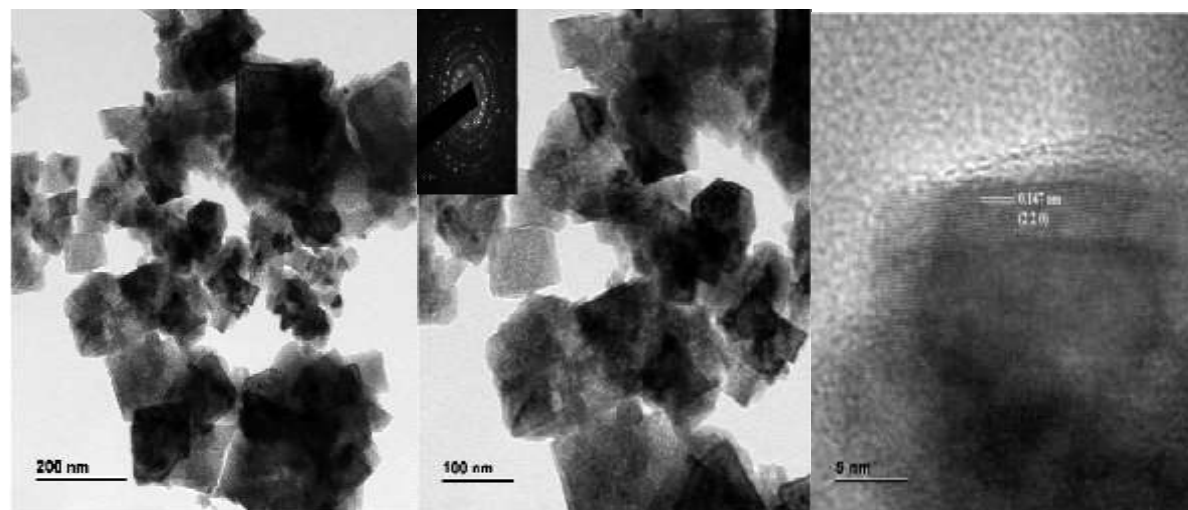


Fig.7 (b) HRTEM images NiO NPs in different magnification of S2.

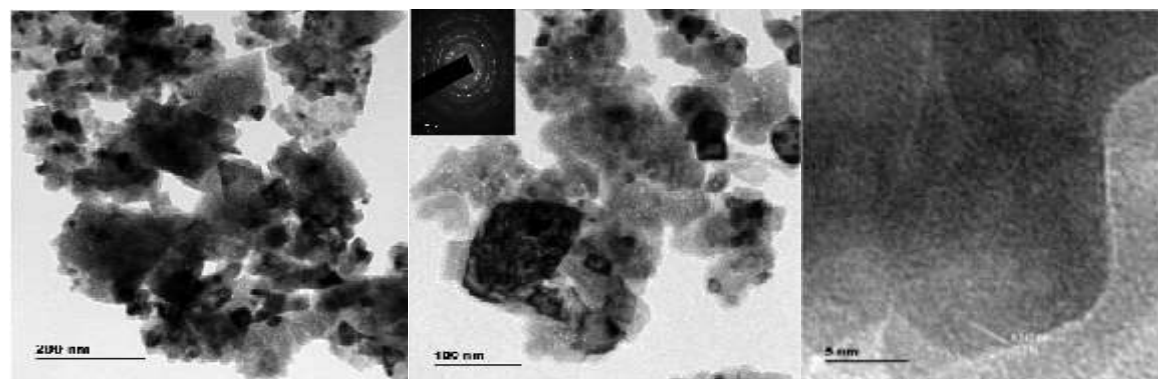


Fig.7 (c) HRTEM images NiO NPs in different magnification of S3

3.6 Antibacterial and Photocatalytic activity

The antimicrobial activity against various microorganisms (gram-negative), *Klebsiella pneumonia*, *Acinetobacterbaumannii*, *Pseudomonas aeruginosa*, *Citrobacter freundii*, *Escherichia coli*, *Vibrio cholerae* were evaluated in this study as shown in Fig.8. Based on the inhibition zone, the antibacterial activity of NiO NPs was quantitatively evaluated and compared to a standard antibiotic. The increased inhibition of bacterial cells may be caused by the distraction of cell membranes by NiO NPs resulting in cell enzyme breakdown.

Table 1 shows the antibacterial activity of S1, S2, and S3 against various strains. The samples S1 and S3 are exhibiting effective bacterial resistance against gram-negative bacteria and S2 is not effective against them. It can be explained under the surface roughness factor. The NPs, which is having high rough surface exhibit greater antimicrobial activity than the smooth surface one. Even though the particle size of S3 is smaller than that of S1, S1 is highly active than S3. Again, this can be explained based on the surface roughness. This unique property influences the transport of NPs into the bacteria. The surface roughening produces cavities on the external surface for air entrapment and eased improved interaction with bacteria resulting high antibacterial activity.

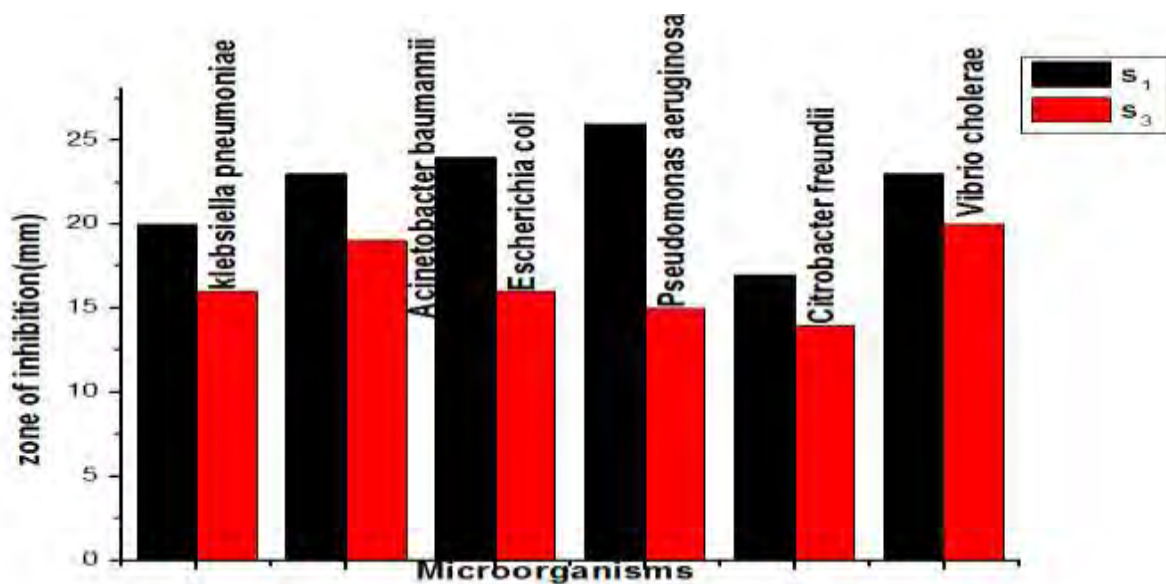


Fig 8. The plot represents the antibacterial effect of NiO NPs on various microorganisms

Table 1. Antibacterial efficacy results of NiO NPs

Microorganisms	S1 (mm)	S2 (mm)	S3 (mm)
Klebsiella pneumoniae	20	-	16
Acinetobacter baumannii	23	-	19
Escherichia coli	24	-	16
Pseudomonas aeruginosa	26	-	15
Citrobacter freundii	17	-	14
Vibrio cholera	23	-	20

Figure 9 shows the photo degradation absorption spectra of MO in the presence of S, S2 and S3. The reduction kinetic equation may be written as [9];

$$\frac{dC_t}{dt} = \ln \frac{C_t}{C_o} = -k_{app} C_t \quad (7)$$

where C_t is the concentration of MO at time t and K_{app} is the apparent rate constant, which can be obtained from the decrease of the peak intensity at 467 nm with time.

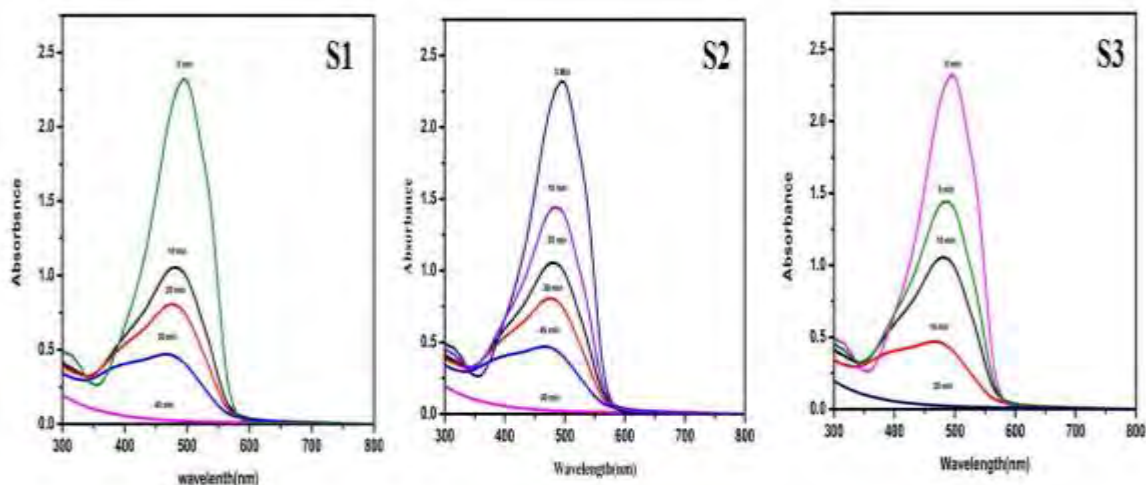
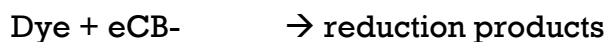
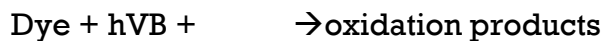
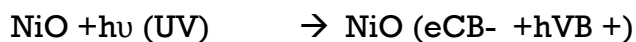


Fig. 9 Absorbance Spectra of MO degradation in the presence of S1, S2, and S3.

The appropriate reactions at the NiO surface initiating the degradation of dyes can be stated as follows:



where h is photon energy essential to excite the semiconductor electron from the valence band (VB) region to the conduction band (CB) region.

The apparent rate constants of this catalytic reaction are found to be 0.0165/ min, 0.0239/ min and 0.0214/min for S1, S2 and S3 respectively as measured from the plot. The surface roughness also played important role in enhancing the photocatalytic activity. The NPs of smooth surfaces ionizes fast than the rough surface NPs. As discussed earlier, S2, due to its smooth surface exhibiting high catalytic activity than S3 and S1. S1, which is considered to have high surface roughness is having low photocatalytic activity

4. Conclusion

Using Starch, Oxalic Acid & Malic Acid as fuels, the NiO NPs were synthesized by solution combustion method. The synthesized NiO were characterized by optical, structural, functional, and morphological characterizations. The results of XRD confirmed NiO NPs cubic structure. It was found that the average crystallite size for S1, S2, and S3 are around 42,34 and 36 nm. FESEM& HRTEM confirms the cubic and rod-like morphology of NiO NPs. Using FTIR spectra, the different functional groups were studied. UV-Visible absorption spectroscopy showed a blue shift due to quantum confinement effect in NiO NPs. The NiO NPs have been studied for antibacterial and photocatalytic activity. It was elucidated that due of their efficient antimicrobial efficacy, NiO NPs can be used in the Bio medical field. Photodegradation of NiO NPs was assessed and explained using surface roughness.

Acknowledgment

The author Dr. A. Jegatha Christy is grateful to SERO/UGC for financial support.

References

- [1] Shreyash Hadke, Madhu Telugu Kalimila, Shashwat Rathkanthiwar, Shivani Gour, Reshma Sonkusare, Atul Ballal, Role of fuel and fuel-to-oxidizer ratio in combustion synthesis of nano-crystalline nickel oxide powders, *Ceramics International*, 41(2015) 14949-14957
- [2] A. Manikandan, J. Vijaya, Judith, L. Kennedy, J. Joh, Structural, Optical and Magnetic Properties of Porous α -Fe₂O₃ Nanostructures Prepared by Rapid Combustion Method *Nanosci. Nanotechol.* 13 (2013) 2986–2992

- [3] Manas Kumar Rath, Susant Kumar Acharya, Bok-Hee Kim, Ki Tae Lee, Byung Guk Ahn, Photoluminescence properties of sesquioxide doped ceria synthesized by modified sol-gel route, *Materials Letters*, 65(6) (2011) 955-958
- [4] Xiaojun Zhang, Dongen Zhang, Xiaomin Ni, Jimei Song, Huagui Zhen, Synthesis and electrochemical properties of different sizes of the CuO particles, *J Nanopart Res* 10(2008) 839-844
- [5] C. C. Vidyasagar, Y. Arthoba Naik, T. G. Venkatesha, R. Viswanatha, Solid-State Synthesis and Effect of Temperature on Optical Properties of CuO Nanoparticles, *Nano-Micro Letters*, 4 (2012) 73-77
- [6] R. Vijaya Kumar, Y. Diamant, and A. Gedanken, Sonochemical Synthesis and Characterization of Nanometer-Size Transition Metal Oxides from Metal Acetates, *Chem. Mater.*, 12(2000) 2301-2305
- [7] Poonam Sharma, Gurmeet Singh Lotey, Sukhpreet Singh, N. K. Verma, Solution-combustion: the versatile route to synthesize silver nanoparticles, *J Nanopart Res*, 13 (2011) 2553-256
- [8] Pranati Sahoo, Dinesh K. Misra, Jim Salvador, Julien P.A. Makongoa, Girija S. Chaubey, Nathan J. Takas, John B. Wiley, Pierre F.P. Poudeu, Microstructure and thermal conductivity of surfactant-free NiO nanostructures, *Journal of Solid State Chemistry*, 190(2012) 29-35
- [9] C.T. Alves, A. Oliveira, S.A.V. Carneiro, A.G. Silva, H.M.C. Andrade, S.A.B. Vieira de Melo, E.A. Torres, Transesterification of waste frying oil using a zinc aluminate catalyst, *Fuel Processing Technology*, 106(2013) 102-107
- [10] Masoud Salavati Niasari, Fatemeh Mohandes, Fatemeh Davar, Mehdi Mazaheri, Majid Monemzadeh, Nooshin Yavarinia, Preparation of NiO nanoparticles from metal-organic frameworks via a solid-state decomposition route, *Inorganica Chimica Acta*, 362(2009) 3691-3697
- [11] M. Hasanpoor, M. Aliofkhaeaei, H. Delavari, Microwave-assisted synthesis of zinc oxide nanoparticles, *Procedia Materials Science* 11 (2015) 320 - 325

- [12] M. Umadevi, A. Jegatha Christy, Optical, structural and morphological properties of silver nanoparticles and its influence on the photocatalytic activity of TiO₂, *Spectrochimica Acta Part A: Molecular and Biomolecular Spectroscopy*, 111(2013)80-85
- [13] S. Mohseni Meybodi, S.A. Hosseini, M. Rezaee, S.K. Sadrnezhad, and D. Mohammadyani, Synthesis of wide band gap nanocrystalline NiO powder via a sonochemical method, *Ultrasonics Sonochemistry*, 19 (2012)841–845
- [14] A. Barakat, M. Al-Noaimi, M. Suleiman, A.S. Aldwayyan, B. Hammouti, T.B. Hadda, S.F. Haddad, A. Boshala, I. Warad, Effect of calcination temperature on Cu doped NiO nanoparticles prepared via wet-chemical method: Structural, optical and morphological studies, *Int. J. Mol. Sci.* 14 (2013) 23941–23954.
- [15] AbulKalam, Abdullah G.Al-Sehemi, Ayed S.Al-Shihri, GaohuiDu, TokeerAhmad, Synthesis and characterization of NiO nanoparticles by thermal decomposition of nickel linoleate and their optical properties, *Materials Characterization*, 68(2012)77-81
- [16] Da-Peng Chen, Xiao-Lin Wang, Yi Du, Song Ni, Zi-Bin Chen, and Xiaozhou Liao, Growth Mechanism and Magnetic Properties of Highly Crystalline NiO Nanocubes and Nanorods Fabricated by Evaporation, *Cryst. Growth Des.*, 12 (2012) 2842–2849
- [17] A. Jegatha Christy, M. Umadevi, Novel combustion method to prepare octahedral NiO nanoparticles and its photocatalytic activity, *Materials Research Bulletin*, 48(2013)4248-4254
- [18] Ratiram Gomaji Chaudhary, Jay A. Tanna, Nilesh V. Gandhare, Alok R. Rai, Harjeet D. Juneja, Synthesis of Nickel Nanoparticles: Microscopic Investigation, An Efficient Catalyst and Effective Antibacterial Activity, *Advanced Materials Letters*, 6 (2015)990-998

EFFECT OF UREA ON THE STRUCTURAL AND MAGNETIC PROPERTIES OF Fe₂O₃ AND ITS ANTIMICROBIAL AND PHOTO CATALYTIC ACTIVITIES

Abstract:

α -Fe₂O₃ nanoparticles have been prepared by combustion method by using urea. Completion of reaction was followed by Fourier transform infrared spectroscopy (FT-IR) and X-ray diffraction (XRD). The obtained powder was further characterized by energy dispersive spectroscopy (EDS), and scanning electron microscopy (SEM). Their magnetic properties were done by vibrating sample magnetometer (VSM). Urea fuel has reflected morphology of crystallites as well as on their magnetic properties. This results show the finest crystallite size and also high level of magnetic properties. The Fe₂O₃ nanoparticles showed very good antibacterial activity. The Photocatalytic activity of Fe₂O₃ nanoparticles were also evaluated and were found that the prepared Fe₂O₃ nanoparticles enhance the photocatalytic degradation.

Keywords: α -Fe₂O₃, XRD, FTIR, SEM, EDX, Photocatalytic

Introduction:

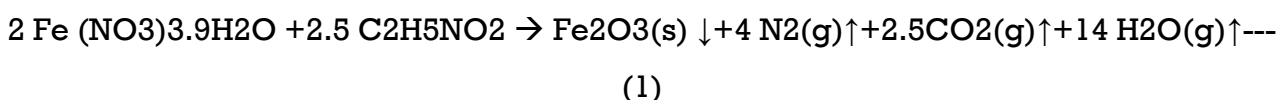
Nanoscience is one of the most important research area and development frontiers in modern science. Nanotechnology is now widely used throughout the pharmaceutical industry, medicine, electronics, robotics, etc.,. In the few decade, magnetic nanomaterials have attracted much attention due to their physical properties [1-3].The use of nanoparticle offers many advantages due to their unique size and physical properties. Nano sized iron oxide particles have emerged as versatile materials for different applications due to their, magnetic, electronic and optical properties. The structure-function relationship of these nano particles have been intensively studied because of the applications in magnetic storage, gas sensing, biomedical, and catalysis applications [4-8].

Iron oxides nano particles have been prepared by a variety of methods such as co-precipitation [9], hydrothermal [10], solvothermal [11], microemulsion [12], auto combustion [13], sonochemical and chemical route techniques available [15]. In this article, Iron Oxide nanoparticles prepared by solution combustion method. Solution

combustion method is an effective method for the synthesis of nanoscale materials. Iron Oxide exists in many forms magnetite (Fe₃O₄) maghemite (γ-Fe₂O₃) and hematite (α-Fe₂O₃) being probably the most common. An effect of Urea it have good antibacterial activity. Hematite is the oldest known of the iron oxides and is widespread in rock and soils. It is also known as ferric oxide, iron sesquioxide, red ochre, specular iron ore, kidney ore or martite. Hematite is blood-red in color if finely divided, and black or gray if coarsely crystalline. It is extremely stable at ambient conditions, and often it is the end product of the transformation of other iron oxides. The prepared Iron Oxide nanoparticles have good antibacterial activity due to the effect of urea.

Materials & Methods:

Iron (III) nitrate nonhydrate (98%) was purchased from MERCK and Urea was purchased from Merk. All the chemicals were used directly without further purification. The following chemical equation (1) used in this synthesis procedure.



α-Fe₂O₃ nanoparticles have been prepared by a combustion method, which have been used and C₂H₅NO₂. The composition of the mixture can be calculated by the ratio of sum of fuel to oxidizing reducing agent. For φ=1 is stoichiometric ratio. 0.2 mole concentration of Fe (NO₃)₃·9H₂O) was dissolved in a required amount of distilled water. The prepared solution was heated at 500°C for 15 minutes by using muffle furnace. Finally we will get a Iron Oxide Nanopowders.

The photo catalytic activity of α-Fe₂O₃ was evaluated through photo degradation of Rhodamine B under UV- irradiation. This experiment was conducted at room temperature in air. In this experiment, 15 mg of the catalyst was suspended in 50 mL of aqueous solution contains (10 mg/ L) of RhB dye. Prior to irradiation, the suspension was held for 30 min in the dark to achieve adsorption–desorption equilibrium by aeration. Photocatalytic activity was investigated under visible and UV light irradiation by 300W tungsten halogen lamp (8500 lumen). The solution was illuminated with a light source at the centre of the solution reservoir, covered and separated by cylindrical quartz glass housing. Air was bubbled through the reaction solution to ensure a constant supply of oxygen and to give agitation

effect to achieve equilibrium state of dye and the photocatalyst. The reaction mixture was aerated continuously under irradiation until the reaction mixture was thorough mix. At the given time interval 3.0 mL of the sample was withdrawn and centrifuged to separate the catalyst in different time intervals. The dye degradation was carried out for 180 mins. The degradation was determined by measuring the maximum absorbance at 554 nm on a UV-VIS Spectrophotometer.

XRD Spectrum:

Fig (1a) shows the XRD pattern of the Iron Oxide will match JCPDS # 89-8104. The lattice constant was calculated using d- value and with their respective (h k l) parameters. The XRD pattern showing $2\theta=24.140, 33.360, 35.850, 40.690, 49.500, 54.150, 62.470$ and 64.140 . The peaks found in angle are labeled as (0 1 2), (1 0 4), (1 1 0), (1 1 3), (0 2 4), (1 1 6), (2 1 4) and (3 0 0). All the planes are well match with the standard JCPDS 89-8104. The geometry of the Iron Oxide nanoparticles found as per this XRD data corresponds to rhombohedra geometry. Using Scherrer formula [12] average crystallite size was estimated. It was found that the size of nanoparticles around 30nm from the X-ray line broadening value.

FTIR Spectrum:

Fig (1b) represented FT-IR spectrum between $4000-400\text{cm}^{-1}$ of $\alpha\text{-Fe}_2\text{O}_3$ nanoparticles. The finger print of $\alpha\text{-Fe}_2\text{O}_3$ occurs mainly at 560 and 467cm^{-1} , where a strong sharp peak at 560cm^{-1} corresponds to Fe-O-Fe stretch of magnetic nanoparticles [16]. The peak 1389cm^{-1} indicates -C-O stretching [16]. The beak 1630 cm^{-1} indicates C=O bond [16]. The peak 3420 cm^{-1} represented the OH group is present [16].

SEM with EDX Spectrum:

Fig (1c) shows the SEM image of the as-prepared Fe_2O_3 nanoparticles. The Iron Oxide nanoparticles have a spherical shape, size range between around 50nm [17]. From EDX Spectrum Iron is 65% and Oxygen is 35% is present.

VSM Spectrum:

Fig(2) shows magnetic hysteresis loop of Iron Oxide nanoparticles at room temperature in the applied magnetic field sweeping from -60 to +60 H[Oe]. The hysteresis loop indicate that these hematite nanoparticles have diamagnetic material behavior and the magnetization at the maximum applied magnetic field was (saturation magnetization of magnetic field) 0.504 emu/g respectively.

Photocatalytic activity:

The photocatalytic activity of Iron Oxide nanoparticles under UV light irradiation as shown in fig(3a). The time dependent absorption spectrum for the degradation of RhB is as shown in fig (3b). This fig shows UV light decomposed by RhB with various time interval from 0 to 180 min and the maximum absorbance wavelength occurred at 540 nm. A decrease in RhB dye concentration by increasing concentration of the Iron Oxide nanoparticles. Because the absorbance intensities of RhB are gradually decreased in the presence of iron oxide nanoparticles with the increase of exposed time. Interestingly, the RhB dye is significantly degraded by RhB 95% within relatively short exposed time (210 min) as shown in fig(3a).

Antibacterial activity:

Fig (4) antibacterial activity shows gram positive (*Staphylococcus aureus*) and gram negative (*Escherichia coli*) bacteria. The bacterial inhibition depends on concentration[18]. Iron Oxide nanoparticles do not negatively impact all cells but with an appropriate magnetic field of Iron Oxide, nanoparticles may be engaged to destroy bacteria. Antibacterial activity are very important in the textile industry, water disinfection, medicine and food packing. The gram-positive inhibit 16mm and gram-negative bacteria inhibit 14mm.

Conclusion:

The Iron Oxide nanoparticle was prepared by combustion method. A average particle is around 30 nm by using XRD. The functional group was found out using FT-IR. The morphology and size of the particle was studied using SEM analysis, it will be mirror like shape and particle size is around 40nm. And also EDX spectrum indicates Iron 64.96% and Oxygen 35.04% elemental composition is present in the sample. The magnetization

of nanoparticle at room temperature was measured maximum applied magnetic field is 0.504 emu/g and the hysteresis loop indicate hematite magnetic nanoparticle have a diamagnetic behavior. From the photocatalytic the rate constant (k) is 0.00074. The α -Fe₂O₃ nanoparticles have outstanding anti-bacterial activity in gram-positive (*Staphylococcus aureus*) and gram-negative (*Escherichia coli*) bacteria.

Acknowledgment

The author Dr. A. Jegatha Christy is grateful to SERO/UGC for financial support.

References:

- [1] Faraji, M.; Yamini, Y.; Rezaee, M. Magnetic Nanoparticles: Synthesis, Stabilization, Functionalization, Characterization, and Applications. *J. Iran. Chem. Soc.* 2010, 7, 1–37.
- [2] Prijic.S, Sersa, G. Magnetic nanoparticles as targeted delivery systems in oncology. *Radiol. Oncol.* 2011, 45, 1–16.
- [3] Hong, R.Y.Pan, T.T.Han, Y.P. Li, H.Z.Ding, J. Sijin, H. Magnetic field synthesis of Fe₃O₄ nanoparticles used as a precursor of ferrofluids.*J.Magn.Mater.* 2007, 310, 3747.
- [4] Nidhin, M. Indumathy, R.; Sreeram, K.J.Nair, B.U. Synthesis of iron oxide nanoparticles of narrow size distribution on polysaccharide templates.*Bull.Mater.Sci.* 2008, 31, 93–96.
- [5] Hong, R.Y. Feng B.; Chen L.L. Liu G.H. Li H.Z. Zheng Y.; We D.G. Synthesis, Characterization and MRI application of dextran-coated Fe₃O₄ magnetic nanoparticles. *Biochem.Eng.J.* 2008, 42, 290–300.
- [6]. Avilés, M.O. Ebner, A.D.Ritter, J.A. In vitro study of magnetic particle seeding for implants assisted-magnetic drug targeting. *J.Magn.Mater.* 2008, 320, 2640–2646.

- [7] Q. Liu, Z. Cui, Z. Ma, S. Bian, W. Song and L. Wan, *Nanotechnology* 18 (2007) 385605 (5pp)
- [8] Teja, A.S.; Koh, P.Y. Synthesis, properties, and applications of magnetic iron oxide nanoparticles. *Prog. Cryst. Growth. Character.* 2009, 55, 22–45.
- [9] X.T. Wen, J.X. Yang, B. He, Z.W. Gu, *Curr. Appl. Phys.* 8 (2008) 535.
- [10] X. Yang, W. Jiang, L. Liu, B. Chen, S. Wu, D. Sun F & Li, One step hydrothermal synthesis of highly water soluble secondary structured Fe₃O₄ nanoparticles, *J. Magn. Mater.* (2012) 324.(14) 2249.
- [11] Lu, J.; Jiao, X.; Chen, D.; Li, W. Solvothermal synthesis and characterization of Fe₃O₄ and γ -Fe₂O₃ nanoplates. *J. Phys. Chem. C.* 2009, 113, 4012-4017.
- [12] D. E. Zhang, Z. W. Tong, S. Z. Li, X. B. Zhang, and A. L. Ying, *Mater Lett* 62, (2008)4053.
- [13] G. V. Kurlyandskaya, S. M. Bhagat, S. E. Jacobo, J. C. Apesteguy, and N. N. Schegoleva, *J. Phys. Chem. Sol.* (2011) 72, 276 .
- [14] N. Islam, L.V. Phong, J.R. Jeong, C.G. Kim, A facile route to sonochemical synthesis of magnetic iron oxide (Fe₃O₄) nanoparticles, *Thin Solid Films* (2011) 519 8277–8279.
- [15]. I. Deneva, I. Nedkov . Raman spectroscopy investigation of magnetite nanoparticles in ferro fluids. *Journal of Magnetism and Magnetic materials* (2010).
- [16] Dhanajayan Sivakumar^{1,2}, Mehboob Mohamed Rafi², Balaraman Sathyaseelan³; Kulam Mohammed Prem Nazeer^{2*}, Ahmed Meeran, Ayisha Begam , *Synthesis*

and characterization of Super Paramagnetic Iron Oxide nanoparticles (SPIONs) stabilized by Glucose, Fructose and Sucrose, *Dimens Int.J.Nano.*, 8(3): 257-264 (2017).

- [17]. Shao-Wen Cao, Ying – Jie Zhu*, Iron Oxide hollow spheres: Microwave-hydrothermal ionic liquid preparation, formation mechanism, crystal phase and morphology control and properties. *Journal of Acta MATERIALIA* 57 (2009) 2154-2165.
- [18]. Taylor EN., Webster TJ. The use of super paramagnetic nanoparticles for prosthetic biofilm. *International Journal of Nanomedicine*. 2009. 4(1), 145–152.

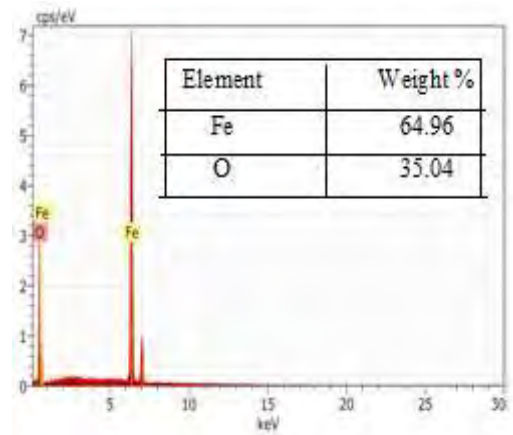
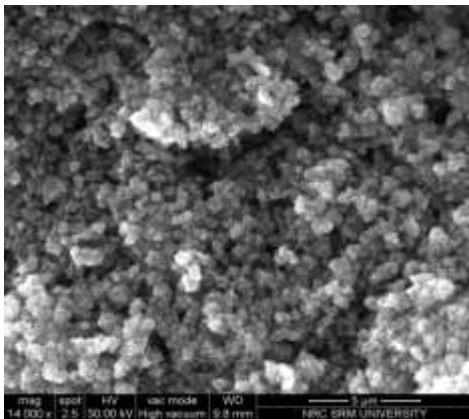
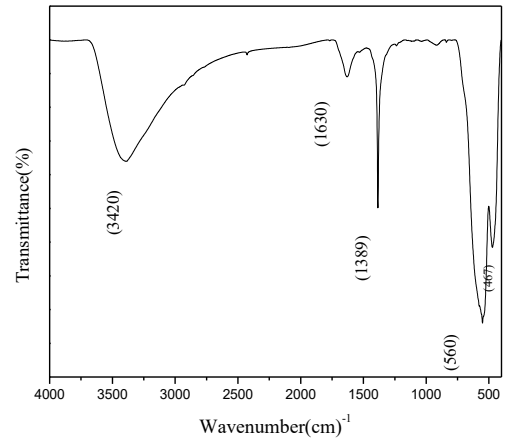
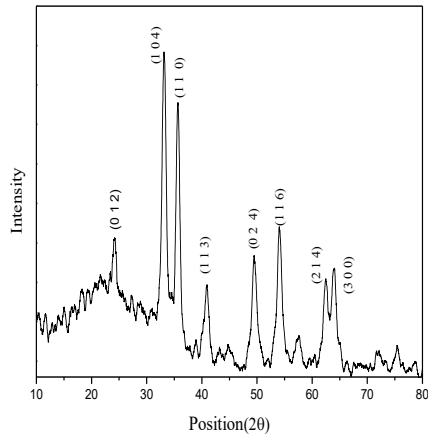


Fig- (1a) XRD Spectrum of Iron Oxide Nanoparticles

(1b) FTIR Spectrum of Iron Oxide Nanoparticles

(1c) SEM Spectrum of Iron Oxide Nanoparticles

(1d) EDX Spectrum of Iron Oxide Nanoparticles

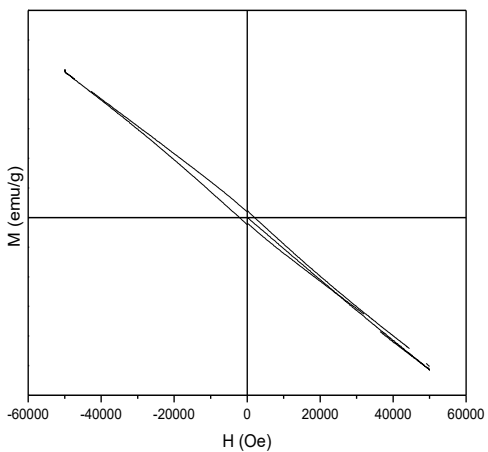


Fig-(2) VSM Spectrum of Iron Oxide Nanoparticles

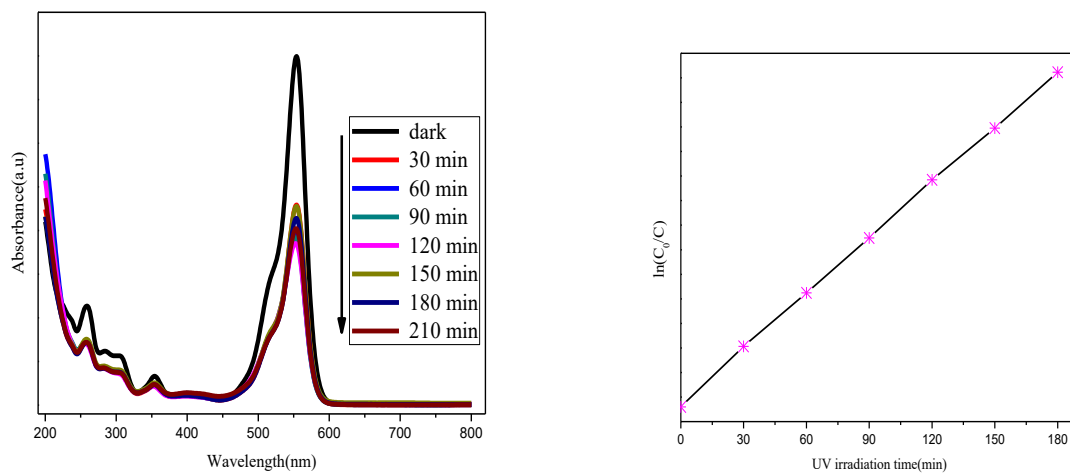


Fig (3a) Photo catalytic activity of Iron Oxide Nanoparticles

Fig(3b) First-order rate law

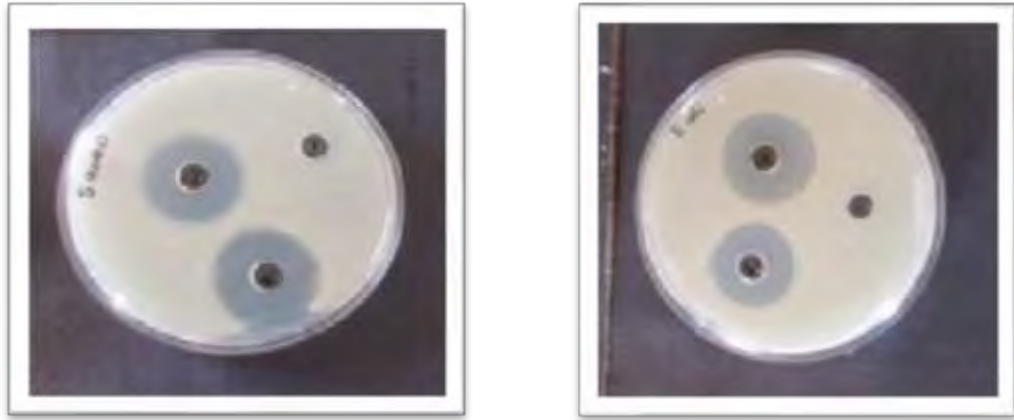


Fig (4) Antibacterial activity of Iron Oxide Nanoparticles

PHOTOCATALYTIC ,ANTIMICROBIAL AND ANTICANCER ACTIVITIES OF ZnO NANOPARTICLES

Abstract

In this article, ZnO nanoparticles have been prepared by various methods. The synthesized ZnO nanoparticles was characterized by X-Ray Diffraction, Fourier Transform Infrared Spectroscopy, Scanning Electron Microscopy, Energy Dispersive Spectroscopy, UV-Vis Spectroscopy, Florescence emission and excitation Spectroscopy. From XRD the particle size of ZnO ~90 nm. The band gap energy of ZnO have 3.2 eV. Further discuss about photo catalytic, anti-bacterial and activity was studied. The cytotoxic activity of ZnO nanoparticles was evaluated by 3 (4, 5-dimethylthiazol-.2-yl) -2, 5- diphenyltetrazolium bromide (MTT) assay by using A549 (lung cancer cell line).

Keywords: ZnO, XRD, FTIR, UV, SEM, Antimicrobial and Anticancer activity.

Introduction

Zinc Oxide Nanoparticles as one of the multifunctional inorganic nanoparticles has many significant features such as peculiar physical and chemical properties, high catalytic activity, such as good chemical stability, strong electrochemical coupling and broad range of radiation absorption and good photo stability, effective antibacterial activity as well as intensive ultraviolet and infrared adsorption with broad range of application in semiconductors, sensors, transparent electrodes, cosmetics, pigments, biomedical applications, cell imaging, first aid taps, polymers, textile industries, anti diabetic, anti cancer drug delivery systems, rubber industry, concrete manufacture, solar cells.

Advances of medical applications of ZnO widely applicable in cancer drug delivery system. The human body made up of atoms. Zinc compound important role in over all functions such as enzymes, proteins, nucleic acid synthesis, nurogenesis, tissues, bones, muscles, brain and skin. It will have good naturally blocking of sun radiation UVA (400-320nm) & UVB (320-260nm). It has

excellent photo catalytic activity in electronics. Various techniques used for the preparation of ZnO nanoparticles such as sol-gel method, vapor transport process, spray pyrolysis, thermal decomposition, hydrothermal synthesis, direct precipitation, chemical route technique, combustion and co-precipitation etc.,[1-6]. In this articles the nanoparticles synthesized by precipitation, combustion and sol-gel method of preparation. Some of the most important advantages of the combustion method are: easiness of the synthesis, large amount of product, self propagating and control of the chemical composition. The advantages make the combustion technique a very attractive preparation method, especially in the case of photo catalytically active ZnO powders. In this work, a simple sol gel method was used to prepare ZnO nanoparticles. The advantages of Sol-gel technique (i) It give very fine power, (ii) low temperature (iii) large quantity of powder. Among these synthetic routes, precipitation approach compared with other methods provided a facile way for low cost, large-scale production, simple & productions of nanoparticles. The n-type semiconductor behavior is due to the ionization of excess Zinc atoms in interstitial positions and the Oxygen vacancies. Surface defects play an important role in the photocatalytic activities of metal oxides as they increase the number of the active sites. The synthesized ZnO nanoparticles have been confirmed using XRD, UV-Vis, SEM and EDX analysis.

Materials & methods:

The ZnO nanoparticles prepared by different techniques by using the following chemicals. Zinc Nitrate ($\text{Zn}(\text{NO}_3)_2 \cdot 6\text{H}_2\text{O}$) $\geq 99\%$ (Merk), Zinc Chloride (ZnCl_2) $\geq 99\%$ (Merk), Citric acid ($\text{C}_6\text{H}_8\text{O}_7 \cdot \text{H}_2\text{O}$) $\geq 99\%$ (Merk), Glycine ($\text{C}_2\text{H}_5\text{NO}_2$) $\geq 99\%$ (Merk), Urea ($\text{CH}_4\text{N}_2\text{O}$) $\geq 99\%$ (Merk), Sodium hydroxide (NaOH) $\geq 98\%$ (Merk), Ammonia $\geq 98\%$ (NH_3) (Merk). All chemicals used in the experiment are of analytic reagent grade.

Preparation of ZnO:

Precipitation technique:

Method I:

ZnO nanoparticles were synthesized by precipitation method using Zinc nitrate and NH_3 precursors. In this work the aqueous solution (0.1M) of Zinc nitrate ($\text{Zn}(\text{NO}_3)_2 \cdot 6\text{H}_2\text{O}$) added to 100ml of distilled water, continuously stirrer at room temperature and then few drops added to

the ammonia solution. The pH value of the solution measured at pH meter 7. The prepared solution heated 1000c by using hot plate. Finally ZnO nanopowders were collected.

Method II:

Zinc Chloride ($ZnCl_2$) and Sodium hydroxide (NaOH) were the starting material for the synthesis of ZnO nanoparticles. In this study, 1:2 molar concentrations of $ZnCl_2$ & NaOH dissolved in 100ml deionized water. After 30 minutes the compound heated with hotplate 1000c or 1 hour. Finally, collect ZnO nanopowder.

Method III:

In this method Zinc Oxide nanoparticles were prepared by sol-gel method by using 1M concentration of $ZnCl_2$ and 0.1 molar concentration of Sodium hydroxide (NaOH) was dissolved in 100 ml of distilled water. A solution of NH_3 was added till pH value of the solution reached 7. After 2 hour the settled white precipitate was washed three times in double distilled water. Finally, the solution filtrate was obtained by passing through whatman filter paper to remove the chlorine groups. The obtained sample dried in a hotplate at 1000c for 2 hours and subsequently the product was crushed into fine powder.

Method IV:

In this experiment, discuss combustion method of preparation. Here, Zinc nitrate ($Zn(NO_3)_2 \cdot 6H_2O$) was oxidizer. We will choose three different fuels such as Glycine ($C_2H_5NO_2$), Citric acid ($C_6H_8O_7 \cdot H_2O$) and Urea (CH_4N_2O).

And also this experiment discusses three different conditions such as (i) Fuel-lean, (ii) Stoichiometry & (iii) Fuel-rich condition.

First, 1 molar concentration of Zinc Nitrate was dissolved in 100 ml deionized water. This starting solution stirred 1 hour at room temperature, then added desired amount of fuel (X, Y, Z). This quantity will be choose balance chemical eqns (Appendix-1). After, 1 hour this solution heated with muffle furnace at 3000c. Finally, collect ZnO nanopowder.

Analysis of ZnO nanoparticles:

The synthesized powder was characterized by powder X-ray diffraction (Bruker Advanced D8) with Cu-K α radiation. Ultraviolet visible-near infrared (UV-Vis) studies were carried out in the range of 300–450 nm using Perkin Elmer UV-Vis (Model-lambda35) Spectrophotometer. The surface morphology of the sample was analyzed using a Scanning Electron Microscope (SEM) (Hitachi 3000 H). The magnetic properties of the investigated solids were measured at room temperature using a Vibrating Sample Magnetometer (VSM; 9600-1 LDJ). The test organisms, Escherichia coli (MTCC2412) and Staphylococcus aureus (MTCC2412) bought from Microbial Type Culture Collection IMTEC, India.

Animal Cell Culture:

The A549 human lung cancer cell line was obtained from National Center for Cell Science (NCCS), Pune, India. The cells were cultured in DMEM high glucose medium (Sigma-Aldrich, USA), supplemented with 10% fetal bovine serum (Gibco), and 20 mL of penicillin/streptomycin as antibiotics (Gibco), in 96 well culture plates, at 37°C in a humidified atmosphere of 5% CO₂ in a CO₂ incubator (Thermo scientific, USA). All experiments were performed using cells from passage 15 or less.

Cell Viability Assay:

The cell viability was measured using a standard MTT-assay. The complex, ZnO was dissolved in dimethyl sulfoxide (DMSO) to make a stock. These stock solutions were diluted separately with media to get various concentrations of the complex. Two hundred micro liters of these samples were added to wells containing 5 X 10³ A549 cells per well. DMSO solution was used as the solvent control. After 24 h, 20 μ L of MTT solution (5mg/mL in PBS) was added to each well and the plate was wrapped with aluminum foil and incubated for 4 h at 37 °C. The purple formazan product was dissolved by addition of 100 μ L of DMSO to each well. The absorbance was monitored at 570 nm (measurement) and 630 nm (reference) using a 96-well plate reader (Bio-Rad, i Mark, USA). Data were collected for three replicates each and used to calculate the respective mean. The percentage inhibition was calculated, from this data, using the formula:

$$\frac{\text{Mean absorbance of untreated cells (Control)} - \text{Mean absorbance of treated cells}}{\text{Mean absorbance of untreated cells (Control)}} * 100$$

Acridine orange (AO) and ethidium bromide (EB) staining

Apoptotic morphology was investigated by AO/EB double staining method as described by Spector et al with some modifications. Briefly, the cells treated with IC50 Concentration of compound for 24 h. After incubation, the cells were harvested and washed with cold PBS. Cell pellets were resuspended and diluted with PBS to a concentration of 5X10⁵ cells/mL and mixed with 25 µL of AO/EB solution (3.8 µM of AO and 2.5 µM of EB in PBS) on clean microscope slide and immediately examined under fluorescent microscope (Carl Zeiss, Axioscope2plus) with UV filter (450–490 nm). Three hundred cells for each sample were scored for viable, apoptotic or necrotic by staining the nucleus structure and membrane integrity and the percentage of apoptotic and necrotic cells were calculated.

Result & discussion:

XRD Spectrum of ZnO nanopowder:

The different techniques of synthesized ZnO nanopowders were as show in fig (1). All the samples will matches to the JCPDS-data (card number 76-0704) which is confirm the formation of ZnO having hexagonal crystal structure with diffraction peaks (1 0 0), (0 0 2), (1 0 1), (1 0 2), (1 1 0), (1 0 3), (2 0 0), (1 0 2) and (0 0 4) planes at 31.770, 34.120, 36.140, 47.420, 56.580, 62.930, 67.860, 69.130 and 72.360 (2θ) degree respectively. The peaks intensity is sharp and narrow, confirming that the sample is of high quality with good crystallinity and fine grain size. Using Scherrer formula average crystallite size was estimated.

$$D = \frac{0.94 \lambda}{\beta \cos \theta} \quad \text{----- (1)}$$

Where, 0.94 is the dimension constant of the equipment, λ is the wavelength of radiation corresponding to the Cu-Kα, β1/2 is the full width half maximum and θ is the Bragg angle. It was found that the size of nanoparticles around 85 nm from the X-ray line broadening value. It crystallizes in a hexagonal wurtzite structure (zincite) with lattice parameters as c = 5.205 Å, a = 3.249 Å.

FTIR Spectrum of ZnO nanopowder:

Fig (2) represented FT-IR spectrum between 4000-400cm⁻¹ of ZnO nanoparticles. The finger print of ZnO occurs mainly at 472cm⁻¹, where a strong sharp peak corresponds to Zn-O-Zn stretch

of metallic group is present in the sample. The peak 720 cm⁻¹ aromatic C-H bending is present. The peak 920 cm⁻¹ OH group is present. The peak 1041 cm⁻¹ represents polysaccharide. The peaks 1410 & 1579 cm⁻¹ C-O stretching are present. The peaks 2970 cm⁻¹ represent to the alkane (C-H) stretching. Amines (doublet for NH₂) stretching is present in the peak of 3491.

UV Spectrum of ZnO nanopowder:

The UV-VIS Spectrum of ZnO nanoparticles are as shown in fig (3). Figure (3) shows the variations of the absorption coefficient with the energy of the incident photons. The absorption coefficient increases slowly with increasing the wavelength of the incident photons up to a certain value after which it increased very rapidly showing a peak shows in fig.

$$\alpha = C / h\nu (h\nu - E_0)^{1/2} \text{ ----- (3)}$$

$$(\alpha h\nu)^2 = C(h\nu - E_0) \text{ -----(4)}$$

Where, C is a constant of proportionality and E₀ is optical energy gap of the investigated solution. The experimental points fit with the above equation only if the direct electronic transitions are responsible for the photon absorption inside the nanoparticles. Intercept of the straight line with the photon energy axis at $(\alpha h\nu)^2 = 0$ is as shown in fig(tauc plot) yields the optical energy gap (=3.3eV). Band gap energy increases with decreasing particle size due to quantum size effects.

SEM SPECTRUM:

Fig (4) represents SEM spectrum of ZnO nanopowder. The ZnO nanoparticle have rice like structure particle size of ZnO around 90nm. The elemental composition of the ZnO nanopowder measured using EDX spectrum. The presence of Zinc element is 78.35 percentage and Oxygen element 21.65 percentage as shown in below (fig 4b).

FL Spectrum of ZnO nanopowder:

Fluorescence (FL) spectrum of ZnO nanoparticle, taken at room temperature, as shown in fig (5). The excitation wavelength of ZnO is selected at 370nm. The emission peaks at 765 nm (1.62 eV).

VSM spectrum of ZnO nanopowder:

Fig (6) shows a typical magnetization curve of ZnO nanoparticles at room temperature in the applied magnetic field sweeping from -20 to +20 kOe. The hysteresis loop indicates that ZnO have a weak ferromagnetic behavior in which the coercivity value has a 334 Oe.

Antibacterial activity:

ZnO nanoparticles one of the multifunctional inorganic nanoparticles. So it has effective antibacterial activity. Fig (7) shows antibacterial activity of both gram positive (*Staphylococcus aureus*), gram negative (*Escherichia coli*) of ZnO. Here 10($\mu\text{g}/\mu\text{l}$) concentration of ZnO was taken. From the fig (7) shows the prepared ZnO is denoted A. The *Staphylococcus Aureus* (gram positive) is zone of inhibition of growth 29mm and *Escherichia Coli* (gram negative) bacteria contains the zone of inhibition 27 mm. The diameter of zone of inhibition of ZnO is as shown in table (2).

Cell Viability Assay:

The cytotoxic activities of all the complexes have been investigated against the A549 human lung cancer cell line by using MTT assay (Mosmann T, 1983). The cytotoxic activity was determined according to the dose values of the exposure of the complex required to reduce survival to 50% (IC₅₀), compared to untreated cells. The observed IC₅₀ values for 24 h reveal that all the complexes exhibit different ranges of cytotoxicity (Figure 8). The ability of the complexes to kill the cancer cells at 24 hour incubation vary as ZnO. The results from this MTT assay indicate that the ZnO samples are toxic to the A549 cells.

Acridine orange (AO) and ethidium bromide (EB) staining

The most important characteristics of apoptosis are morphological changes during cell death. Figure (9) represents that AO/EB double-stained A549 human lung cancer cell line treated with test substances 24 hr underwent both early apoptosis (cells with red arrows) and late apoptosis. The control or viable cells shows green fluorescence and normal cell features of uniform chromatin with an intact cell membrane, whereas, the early apoptosis cells showed bright green region with yellowish green nuclear fragmentation and membrane bubbles and apoptotic bodies outside. The late apoptosis cells exhibited orange-yellow or red nuclei with condensed or fragmented chromatin. The results demonstrate that all substances induce majority of cell death through apoptosis mode and very fewer in necrosis for 24 hr treatment. Chromatin condensation and fragmentation were majorly observed in ZnO treated cells.

Conclusion:

The hexagonal Zinc Oxide Nanoparticles prepared by various methods. The ZnO were characterized by using XRD, FTIR, UV, FL, SEM, EDX, VSM, antibacterial & anticancer activity. The XRD results show hexagonal structure and the particle size of ZnO around 90 nm and lattice parameters $a=3.254\text{\AA}$, $c=5.122\text{\AA}$. With matches to JCPDS card number 76-0704. The functional groups were identified by using FTIR. The optical properties were studied using UV-Vis Spectrum & FL Spectrum. The band gap energy of the material found using UV-Vis Spectrum. The emission peak of Fluorescence Spectrum at room temperature. The prepared sample ZnO was found to have a ferromagnetic material using VSM. The morphology of the SEM images. The elemental spectroscopy found using EDX Spectroscopy. The Photocatalytic activity shows excitation wavelength at 554nm under the degradation of RhB. The anticancer activity (MTT- assay) shows ZnO has a good anticancer agent.

Acknowledgment

The author Dr. A. Jegatha Christy is grateful to SERO/UGC for financial support.

References:

1. J.-H. Lee, K.-H. Ko, and B.-O. Park, "Electrical and optical properties of ZnO transparent conducting films by the sol-gel method," *Journal of Crystal Growth*, vol. 247, no. 1-2, pp. 119–125, 2003.
2. C. Wang, W. X. Zhang, X. F. Qian, X. M. Zhang, Y. Xie, and Y. T. Qian, "Room temperature chemical route to nanocrystalline PbS semiconductor," *Materials Letters*, vol. 40, no. 6, pp. 255–258, 1999.
3. Lee SD, Nam S-H, Kim M-H, Boo J-H. Synthesis and photocatalytic property of ZnO nanoparticles prepared by spray-pyrolysis method. *Physics Procedia*, vol. 32, 2012, pp. 320-326.
4. Yang Y, Chen H, Zhao B, Bao XJ. Size control of ZnO nanoparticles via thermal decomposition of zinc acetate coated on organic additives. *Journal of Crystal Growth*, vol. 263, 2004, pp. 447-453.

5. Liu B, Zeng HC. Hydrothermal synthesis of ZnO nanorods in the diameter regime of 50 nm. *Journal of the American Chemical Society*, vol. 125, 2003, pp.4430-4431.
6. Raoufi D. Synthesis and microstructural properties of ZnO nanoparticles prepared by precipitation method. *Renewable Energy*, vol. 50, 2013, pp. 932-937.
7. M. S. Samuel, L. Bose, and K. C. George, "Optical properties of ZnO nanoparticles," *Academic Review*, vol. 16, no. 1-2, pp. 57–65, 2009.

Method of Preparation	Particle Size
Precipitation technique	50, 60
Sol-gel	80
Combustion-Urea	70,60,75
Combustion-Glycine	75, 45,50
Combustion-Citric acid	70,40,45

Table (1) Shows grain size of ZnO nanopowder by using De-bye Scherrer formula

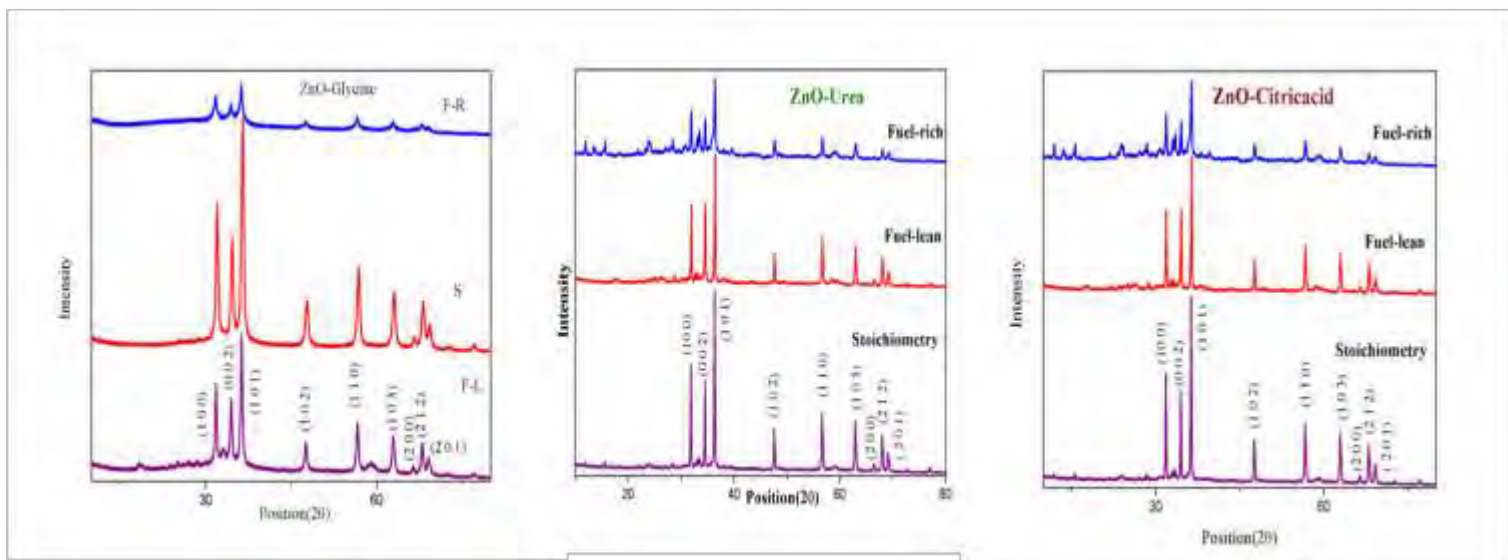
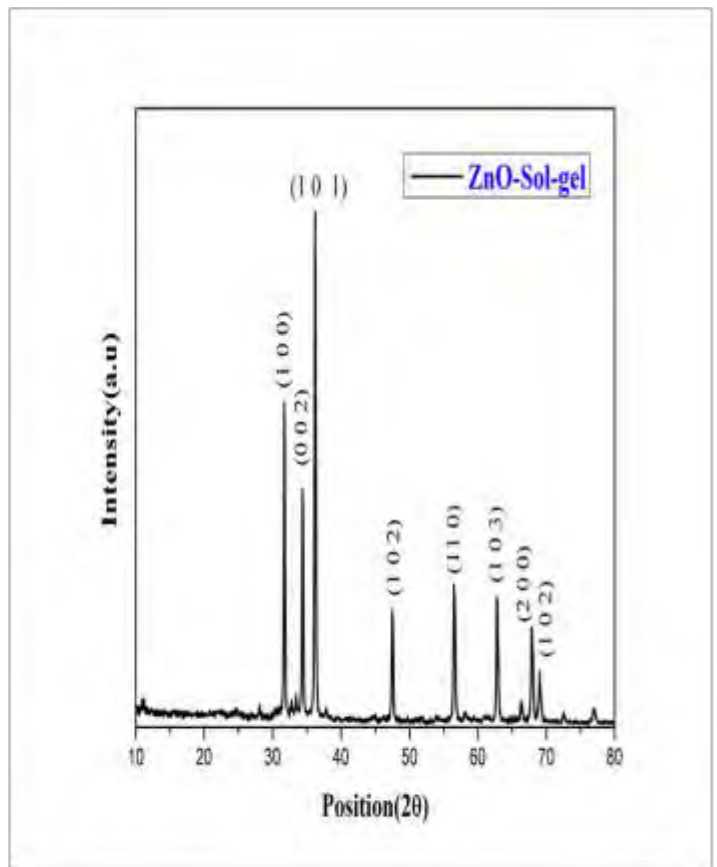
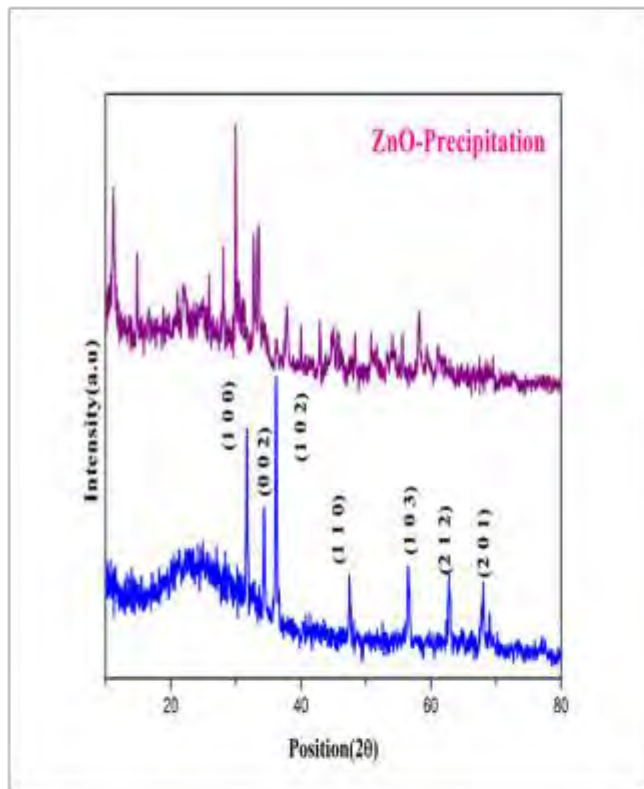


Fig (1) Shows XRD pattern of ZnO –different techniques

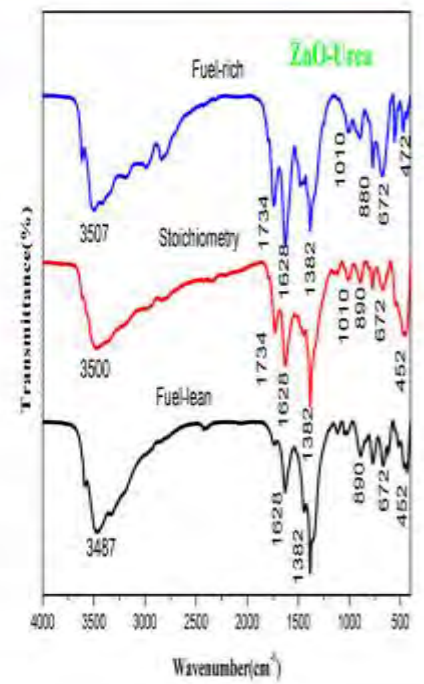
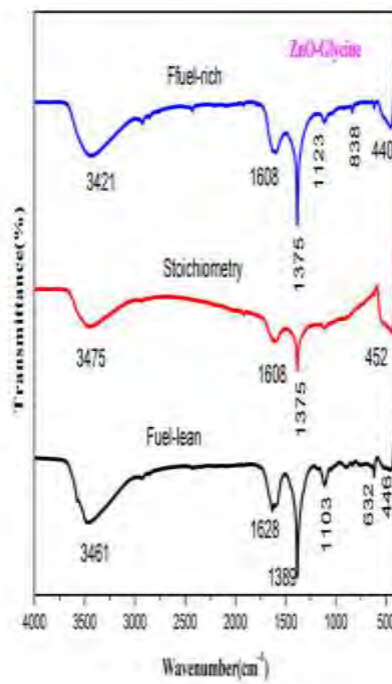
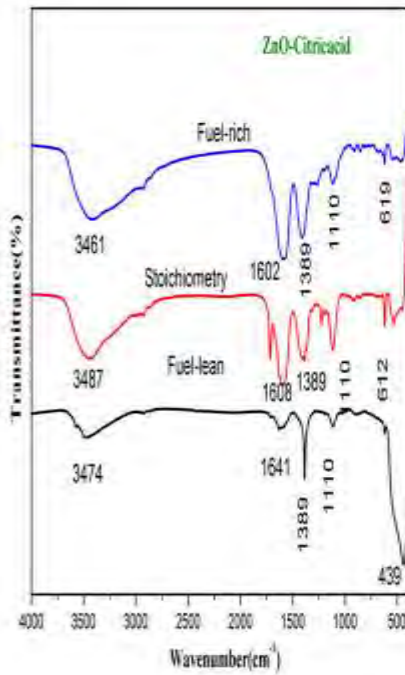
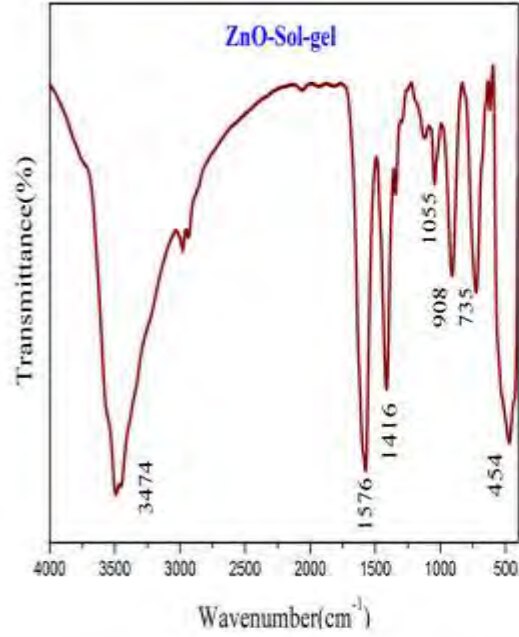
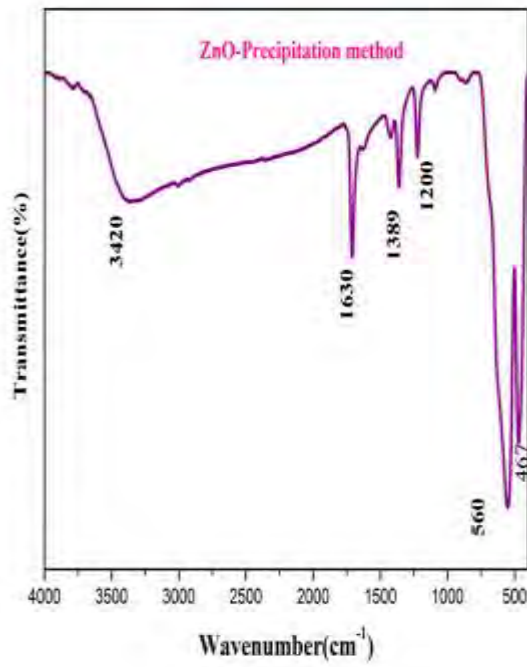


Fig (2) shows FTIR Spectrum of ZnO nanoparticles

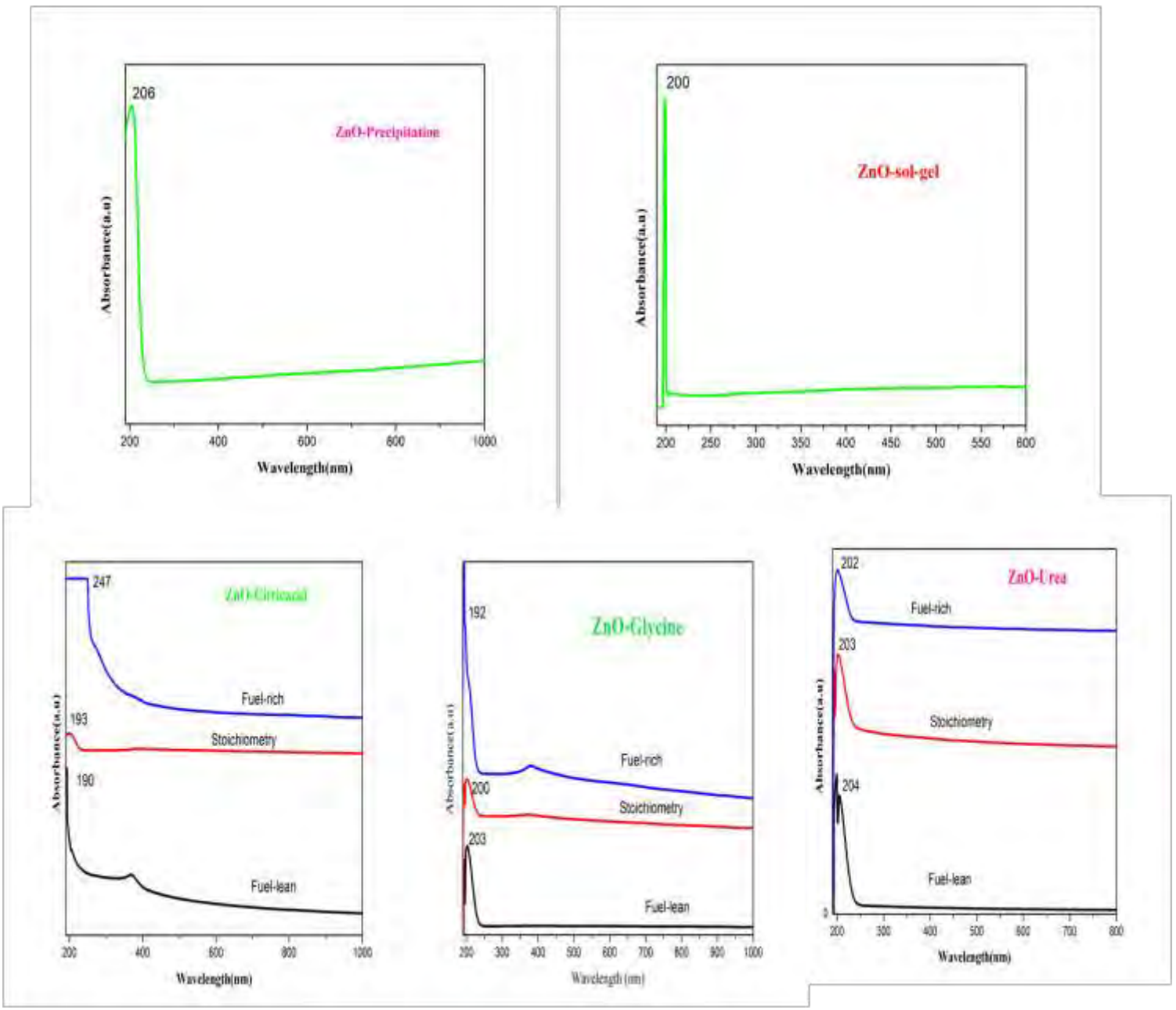


Fig (3) shows UV-Vis Spectrum of ZnO nanoparticles

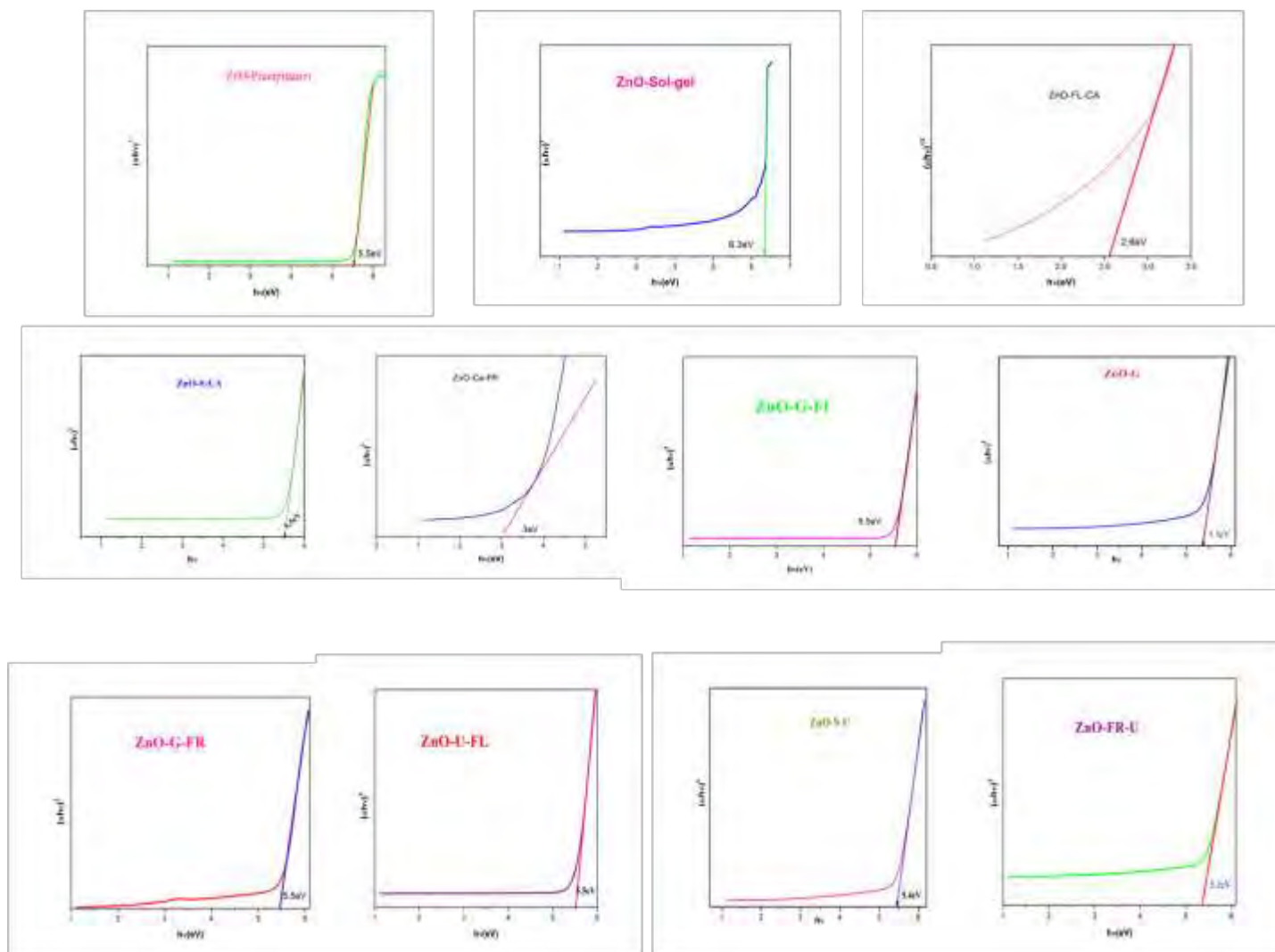


Fig (3) Touch plot of ZnO nanoparticles

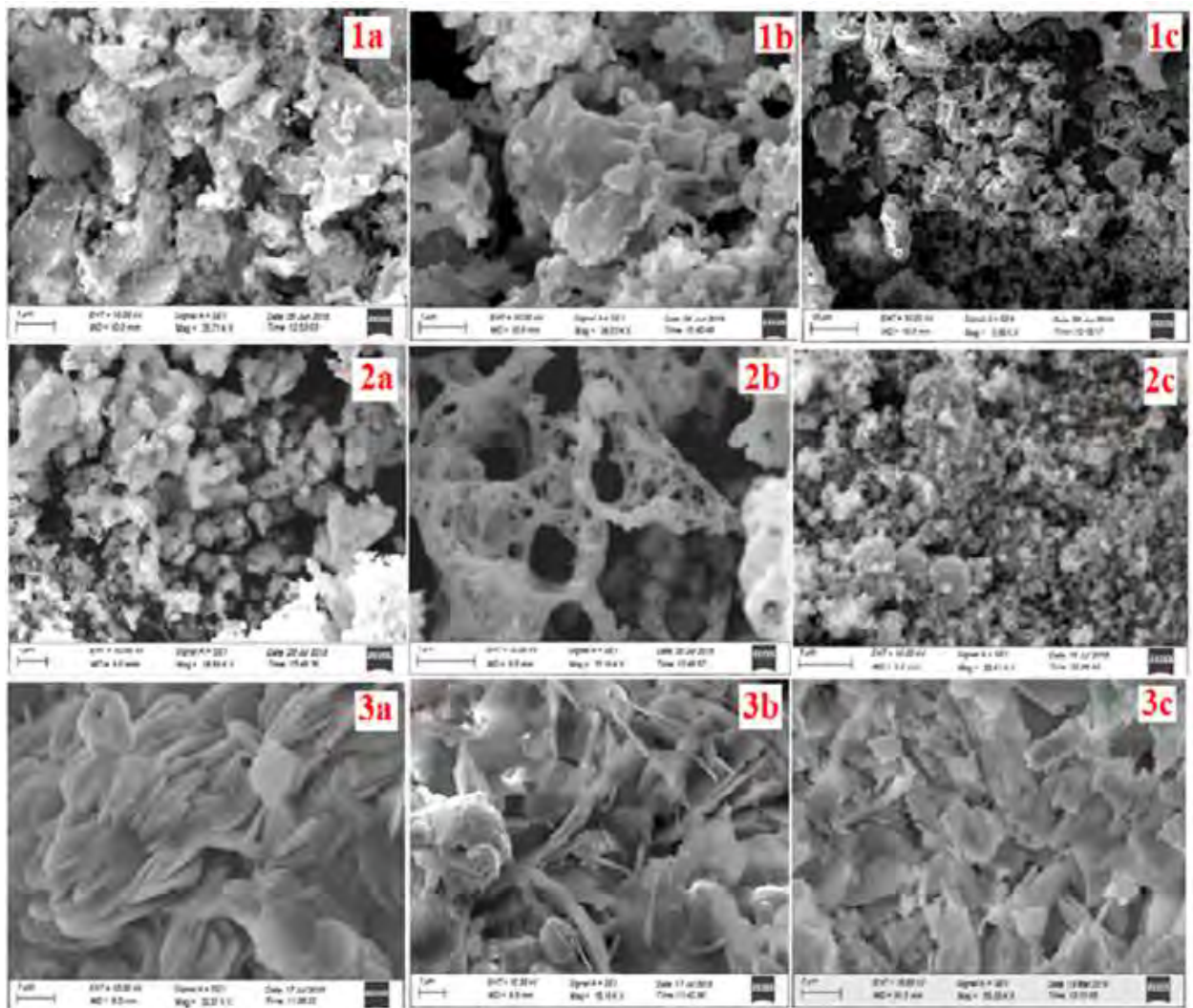


Fig (4) Shows SEM Spectrum of ZnO nanoparticles

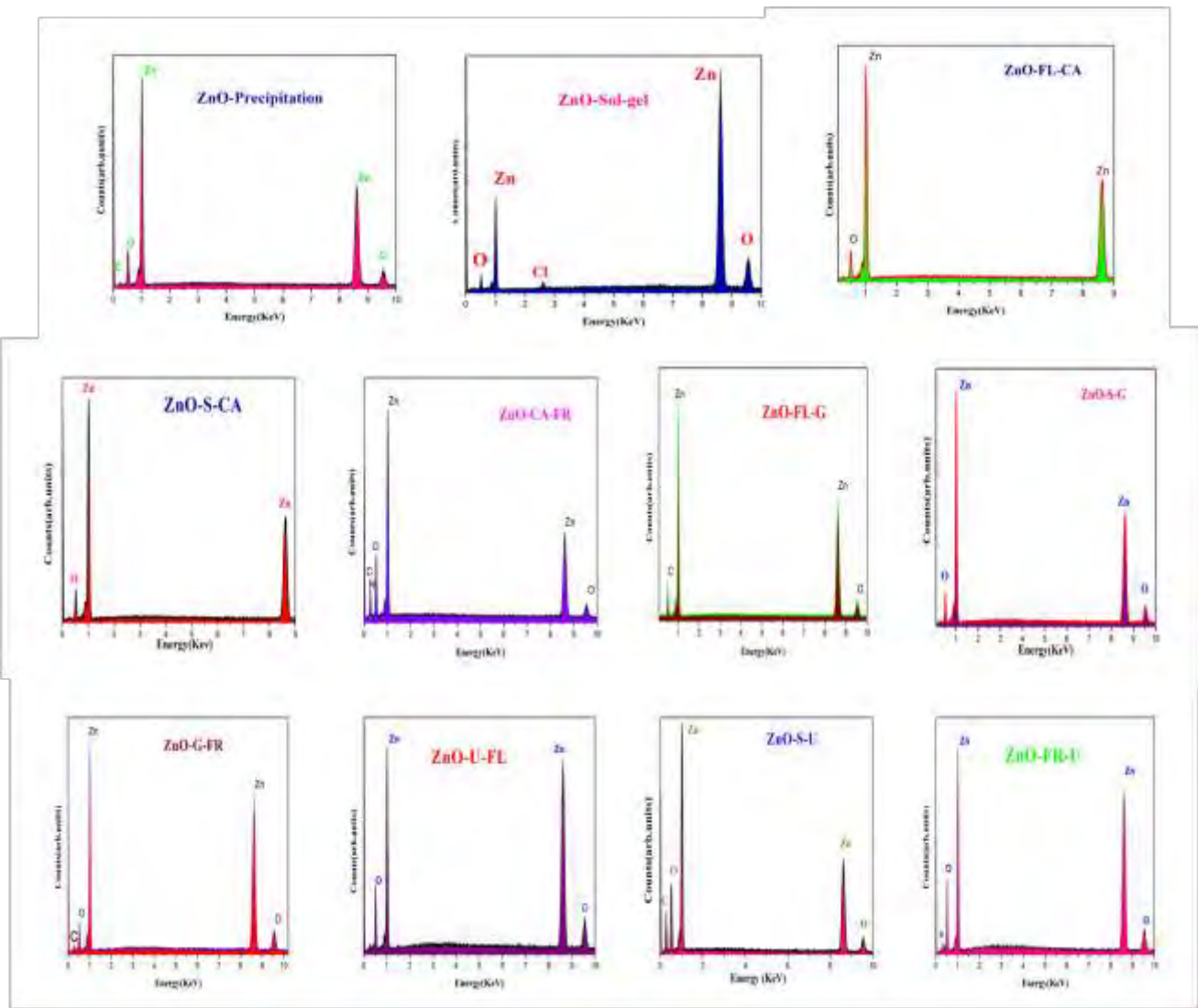


Fig (5) EDX Spectrum of ZnO nanoparticles

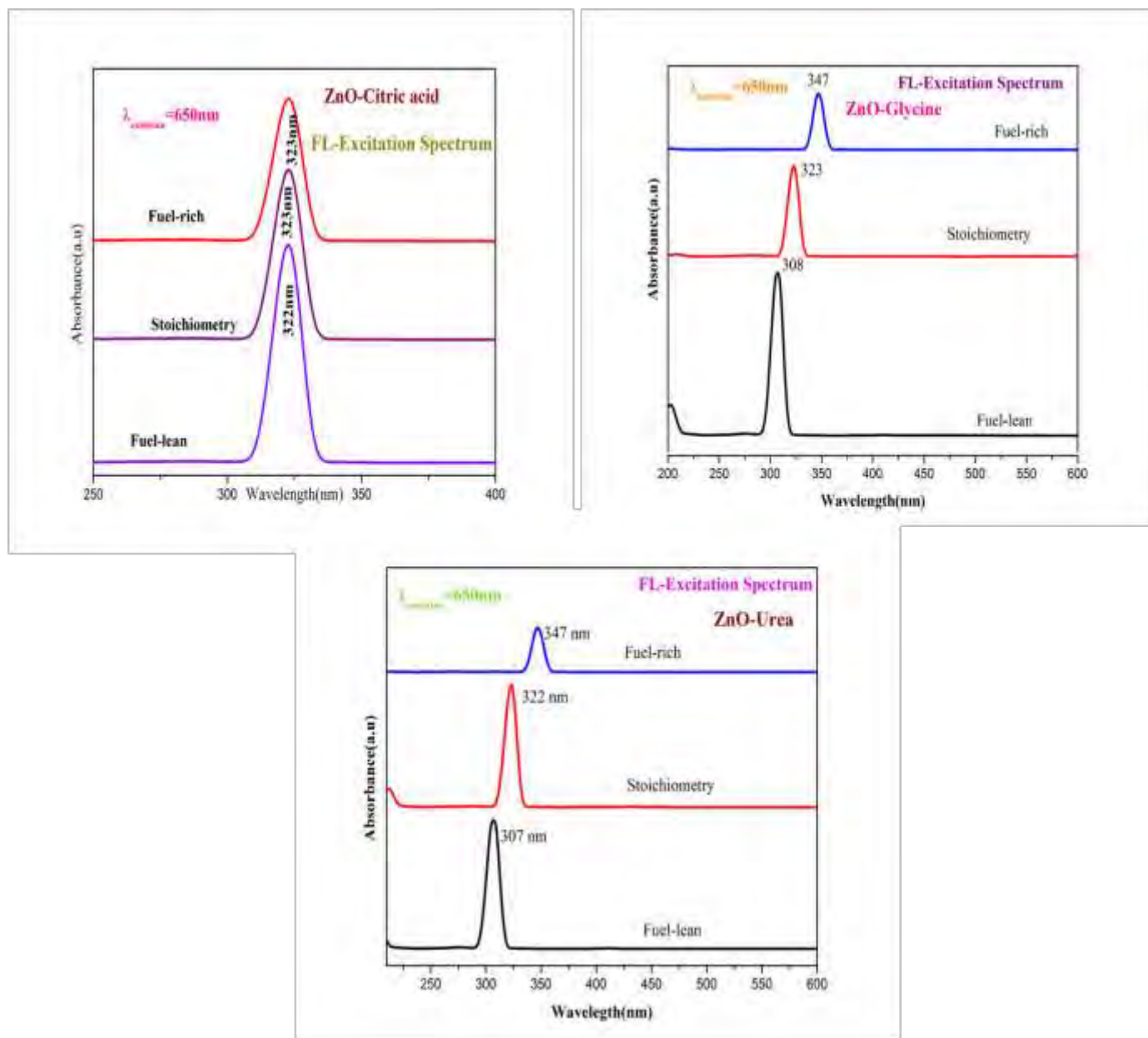


Fig (6) Shows FL- excitation Spectra

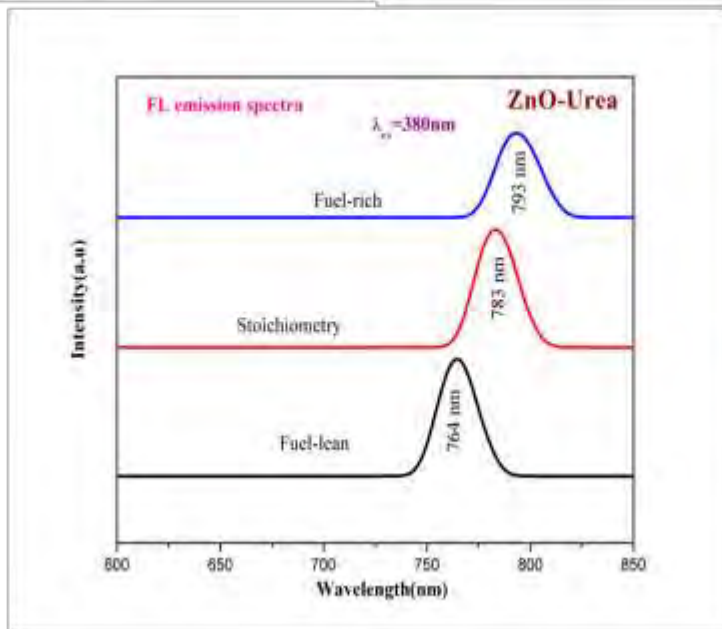
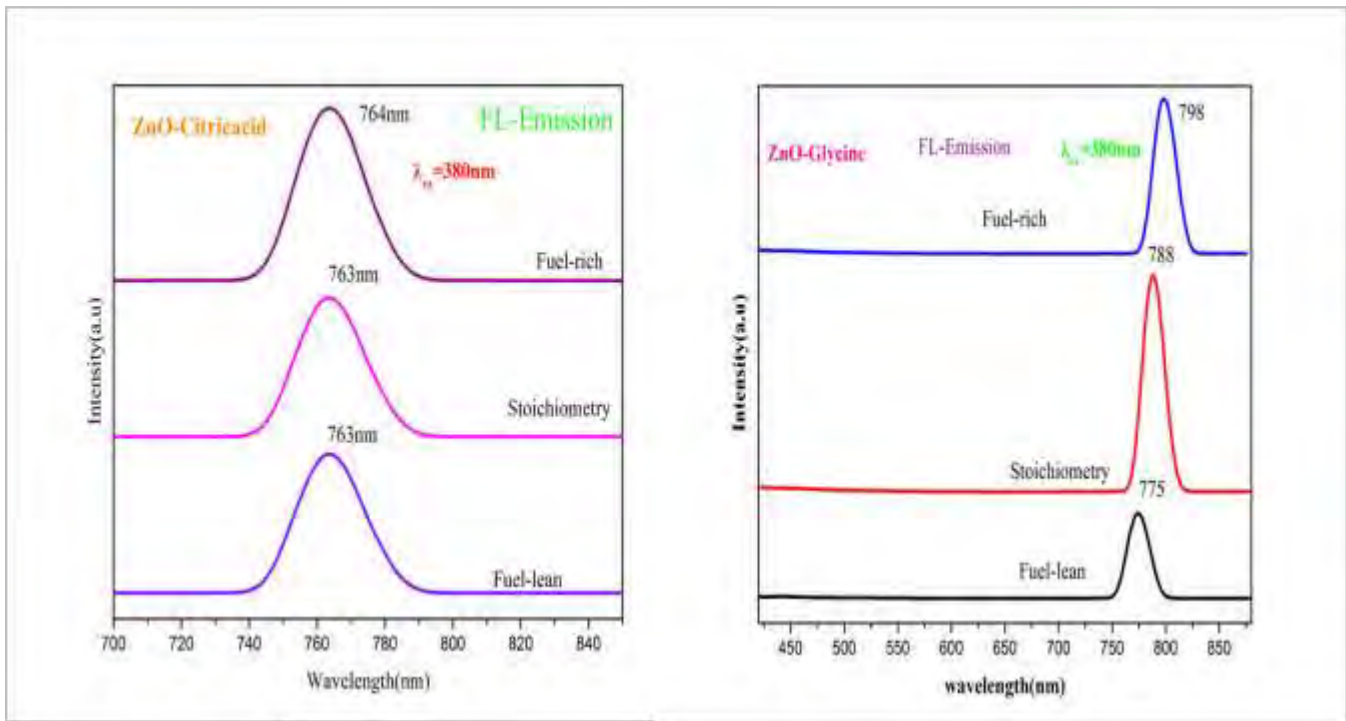


Fig (6) Shows FL- emission Spectra

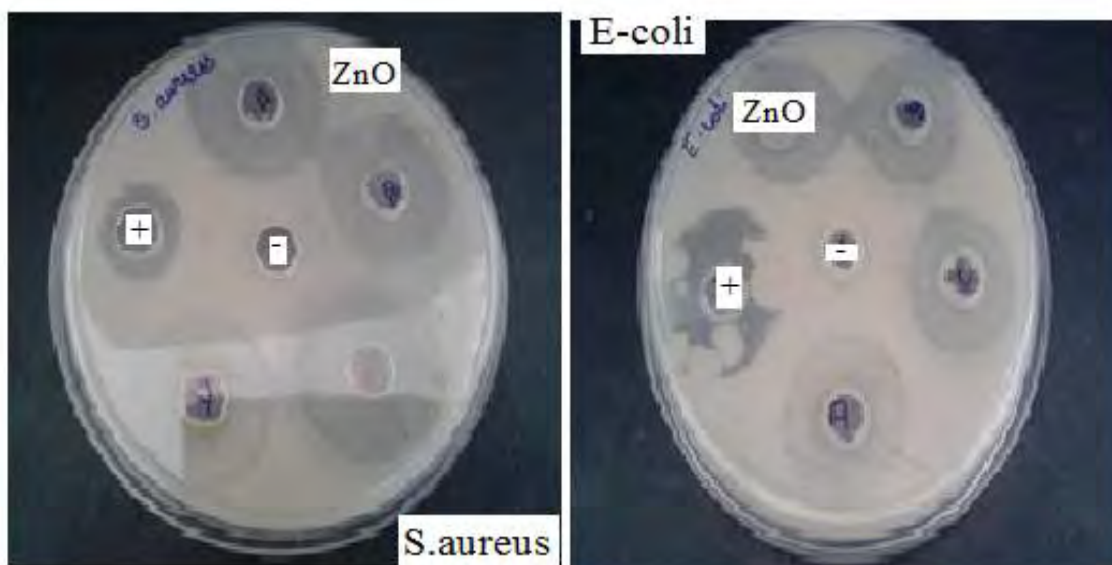


Fig (7) Shows anti-bacterial activity of ZO nanoparticles

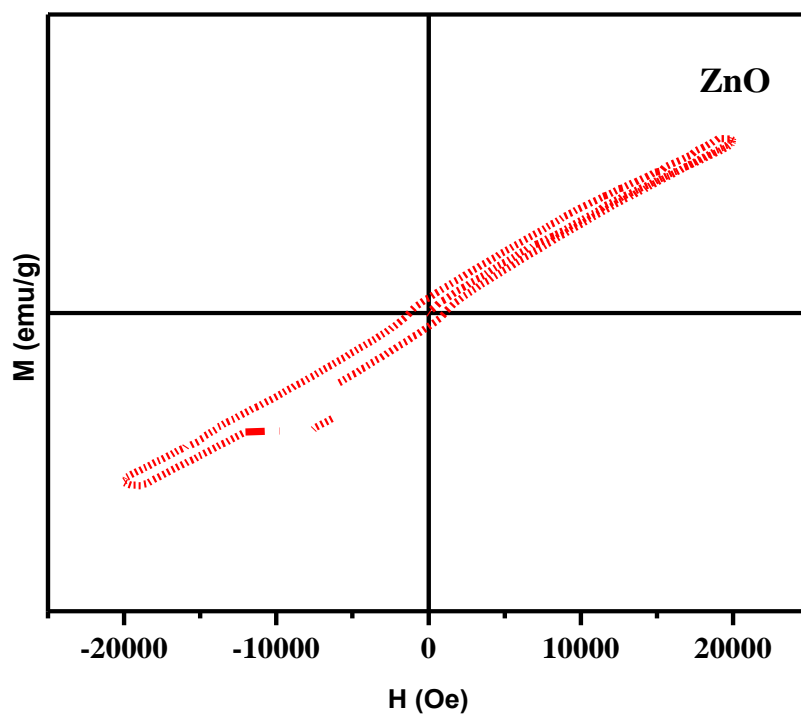


Fig (8) VSM Spectrum of ZnO nanoparticles

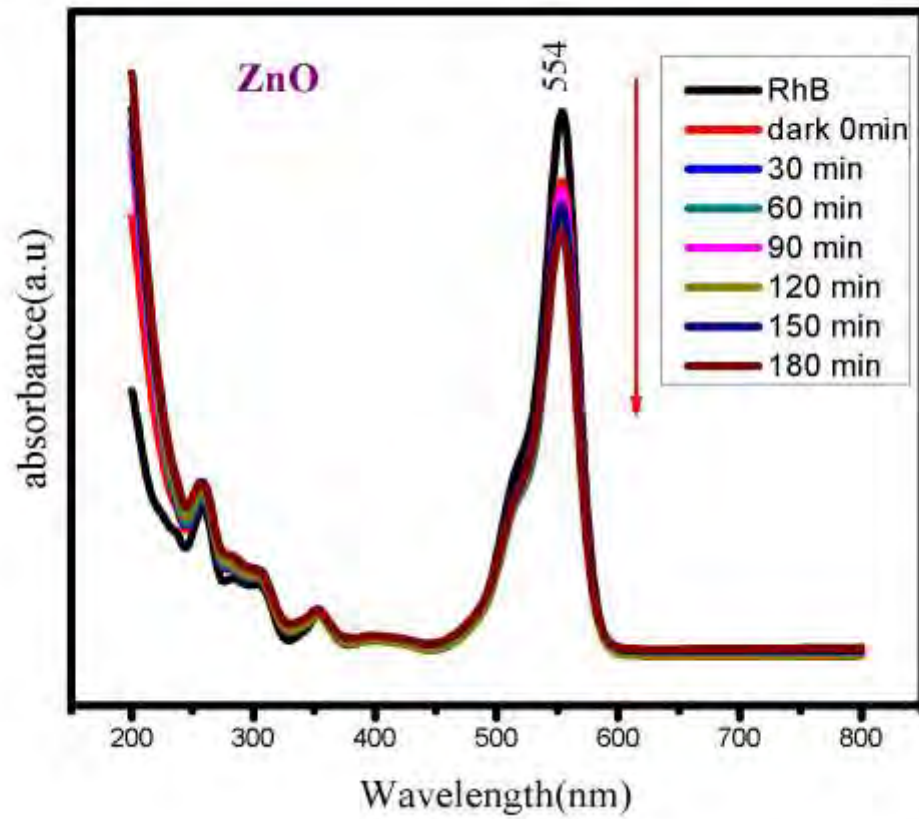


Fig (9) Photocatalytic activity of ZnO nanoparticles

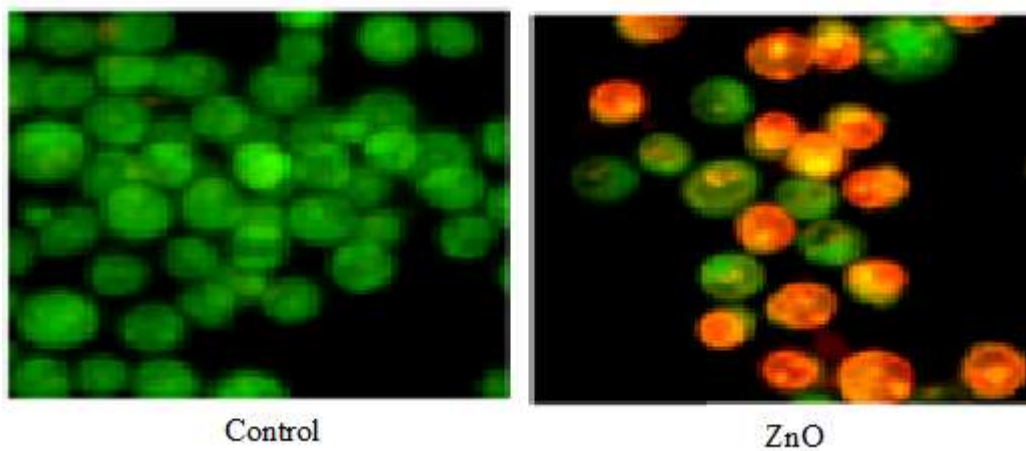


Fig (10) Shows Florescence imaging of ZnO nanoparticles

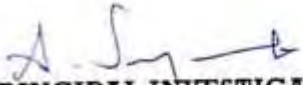
CONCLUSION OF THE PROJECT


- ❖ Copper oxide nanoparticles (CuO NPs) were synthesized by solution combustion technique using copper nitrate as an oxidizer and malic acid, oxalic acid and starch as a fuel for fuel rich, stoichiometric, and fuel lean conditions. The band gap was calculated from UV-Vis spectra and it was in the range of 3.23 to 3.28 eV for all the samples. The average particle size calculated from XRD spectra was around in the range of 14 to 20 nm for all the samples. The SEM images revealed that the prepared CuO NPs exhibit different structural morphology for different fuel ratios. The change in fuel ratios plays a vital role in tailoring the surface morphology of CuO NPs and it is studied in detail.
- ❖ The Magnesium Oxide (MgO) nanoparticles synthesized via combustion method, characterized by spectroscopic and microscopic analysis. X-ray diffraction illustrated that the MgO nanoparticles were crystalline in nature with a face centred cubic structure. UV-Vis spectrums of the MgO nanoparticles have a sharp absorption peak around 260 nm. The presence of Magnesium and Oxygen is confirmed by EDX spectrum. FTIR analysis showed the presence of M-O stretching vibration for the synthesis of MgO nanoparticles. The aim of present study is to determine antibacterial activity of MgO nanoparticles against gram-negative and gram-positive bacteria. *Escherichia coli* (*E. coli*) – gram negative and *Staphylococcus aureus* (*S. aureus*)-gram-positive were used as test organism. The effect of concentration on the antibacterial activity of MgO nanoparticles was studied using well diffusion agar methods for minimum bacterial concentration. The inhibitory concentration of MgO nanoparticles 20, 15, 10 and 5 $\mu\text{g}/\mu\text{l}$. The results showed that MgO nanoparticles have antibacterial inhibition average zone of 11 mm and 14 mm at the concentration of 10 $\mu\text{g}/\mu\text{l}$ against *E. coli* and *S. aureus* respectively. Photocatalytic activity of MgO nanoparticles witnessed by the quick

degradation of the organic dye RhB exposure visible light irradiation. .

- ❖ Using nickel nitrate as an oxidizer and starch, oxalic acid and malic acid as fuel, the solution combustion method was used to synthesize nickel oxide (NiO) nanoparticles (NPs). The X-ray diffraction (XRD) has a cubic structure and confirmed the presence of NiO NPs (JCPDS: 78-0429). The average size of crystallite for S1, S2, and S3 are around 42,34 and 36 nm. FTIR spectra showed the band in the 400-550 cm^{-1} range, corresponding to stretching vibration mode, which confirms the presence of NiO NPs. The optical absorption spectra confirmed the presence NiO nanoparticles. The NiO NPs exhibit cubic structure and rod-like structure, inferred from FESEM and High-Resolution Electron Microscopy Transmission (HRTEM). The samples S1 and S3 are exhibiting effective bacterial resistance against gram-positive and gram-negative bacteria. S2 is not showing any antimicrobial activity and can be explained under the surface roughness factor. The NPs, which is having rough surface exhibit greater antimicrobial activity than the smooth surface one. photocatalytic activity of the prepared NiO NPs is evaluated using Methylene Orange and revealed effective degradation.
- ❖ $\alpha\text{-Fe}_2\text{O}_3$ nanoparticles have been prepared by combustion method by using urea. Completion of reaction was followed by Fourier transform infrared spectroscopy (FT-IR) and X-ray diffraction (XRD). The obtained powder was further characterized by energy dispersive spectroscopy (EDS), and scanning electron microscopy (SEM). Their magnetic properties were done by vibrating sample magnetometer (VSM). Urea fuel has reflected morphology of crystallites as well as on their magnetic properties. This results show the finest crystallite size and also high level of magnetic properties. The Fe_2O_3 nanoparticles showed very good antibacterial activity. The Photocatalytic activity of Fe_2O_3 nanoparticles were also evaluated and were found that the prepared Fe_2O_3 nanoparticles enhance the photocatalytic degradation.
- ❖ The hexagonal Zinc Oxide Nanoparticles prepared by various methods. The ZnO were characterized by using XRD, FTIR, UV, FL, SEM, EDX, VSM, antibacterial & anticancer activity. The XRD results show hexagonal structure and the particle size of ZnO around 90 nm and lattice parameters $a=3.254\text{\AA}$, $c=5.122\text{\AA}$. With matches

to JCPDS card number 76-0704. The functional groups were identified by using FTIR. The optical properties were studied using UV- Vis Spectrum & FL Spectrum. The band gap energy of the material found using UV-Vis Spectrum. The emission peak of Fluorescence Spectrum at room temperature. The prepared sample ZnO was found to have a ferromagnetic material using VSM. The morphology of the SEM images. The elemental spectroscopy found using EDX Spectroscopy. The Photocatalytic activity shows excitation wavelength at 554nm under the degradation of RhB. The anticancer activity (MTT- assay) shows ZnO has a good anticancer agent.


PRINCIPAL INVESTIGATOR
D. A. MEETHA CHRISTY,
Associate Professor & Lecturer
Department of Chemistry
College of Women,
Periyakulam
PERIYAKULAM-625 601.


PRINCIPAL
Jayaram Annapackiam College
for Women (Autonomous)
Thamaraikulam, Periyakulam-625 601.
Theni District Tamilnadu.

UNIVERSITY GRANTS COMMISSION

BAHADUR SHAH ZAFAR MARG

NEW DELHI – 110 002

**PROFORMA FOR SUBMISSION OF INFORMATION AT THE TIME OF
SENDING THE FINAL REPORT OF THE WORK DONE ON THE PROJECT**

1. Title of the Project: **Tailoring the surface morphology of metal oxide nanoparticles and its influence on dye effluent treatment**
2. NAME AND ADDRESS OF THE PRINCIPAL INVESTIGATOR: **Dr. A. Jegatha Christy, Assistant Proferssor of Physics, Jayaraj Annapackiam College for Women, Periyakulam- 625601, Theni Dist**
3. NAME AND ADDRESS OF THE INSTITUTION **Jayaraj Annapackiam College for Women, Periyakulam- 625601, Theni Dist**
4. UGC APPROVAL LETTER NO. AND DATE : **F MRP-6823/16 (SERO/UGC) , 30 June 2107**
5. DATE OF IMPLEMENTATION **30 June 2107**
6. TENURE OF THE PROJECT **2 years**
7. TOTAL GRANT ALLOCATED **Rs. 4,90,000**
8. TOTAL GRANT RECEIVED **Rs. 4,90,000**
9. FINAL EXPENDITURE **Rs. 4,90,000**
10. TITLE OF THE PROJECT **Tailoring the surface morphology of metal oxide nanoparticles and its influence on dye effluent treatment**
11. NAME AND ADDRESS OF THE PRINCIPAL INVESTIGATOR: **Dr. A. Jegatha Christy, Assistant Proferssor of Physics, Jayaraj Annapackiam College for Women, Periyakulam- 625601, Theni Dist**

12. OBJECTIVES OF THE PROJECT

The objectives of the projects are

- To synthesize photoactive and bioactive semiconductor nanoparticles like Iron oxide, Titanium oxide, Zinc oxide, Aluminium oxide etc of various shapes by combustion method.
- To study the physico-chemical properties like UV- vis spectroscopy, XRD, BET, HRTEM, FESEM, XPS, Laser Raman, Photoluminescence of the prepared nano powders.
- To study the photocatalytic and antimicrobial activity of the prepared nanoparticles.
- To apply the synthesized nanoparticles for dye effluent treatment by Advanced Oxidation Processes (AOP) - Photocatalytic Degradation MONPs/UV and to study in detail.
- To study effect of the surface morphology on dye effluent treatment.
- To collaborate with local companies that will support the study of effluent in reusable/drinkable water.

13. WHETHER OBJECTIVES WERE ACHIEVED (GIVE DETAILS)

- photoactive and bioactive semiconductor nanoparticles like Iron oxide, Nickel Oxide, Copper oxide, Zinc oxide, Magnesium oxide of various shapes were synthesized by solution combustion method.
- UV- vis spectroscopy, XRD, BET, HRTEM, FESEM, XPS, Laser Raman, Photoluminescence characterizations were done for the prepared nano powders.
- photocatalytic and antimicrobial activity of the prepared nanoparticles were studied.
- Advanced Oxidation Processes (AOP) - Photocatalytic Degradation MONPs/UV is applied in the synthesized nanoparticles for dye effluent treatment by and studied in detail.
- Effect of the surface morphology on dye effluent treatment is studied.

The work is completed as per plan the results are achieved accordingly. The steps were taken to collaborate with nearby agencies but the progress was not successful.

14. ACHIEVEMENTS FROM THE PROJECT

- ✓ photoactive and bioactive semiconductor nanoparticles like Iron oxide, Nickel Oxide, Copper oxide, Zinc oxide, Magnesium oxide of various shapes were synthesized by solution combustion method.
- ✓ UV- vis spectroscopy, XRD, BET, HRTEM, FESEM, XPS, Laser Raman, Photoluminescence characterizations were done for the prepared nano powders.
- ✓ photocatalytic and antimicrobial activity of the prepared nanoparticles were studied.
- ✓ Advanced Oxidation Processes (AOP) - Photocatalytic Degradation MONPs/UV is applied in the synthesized nanoparticles for dye effluent treatment by and studied in detail.
- ✓ Effect of the surface morphology on dye effluent treatment is studied.

15. SUMMARY OF THE FINDINGS (IN 500 WORDS)

- ✓ Copper oxide nanoparticles (CuO NPs) were synthesized by solution combustion technique using copper nitrate as an oxidizer and malic acid, oxalic acid and starch as a fuel for fuel rich, stoichiometric, and fuel lean conditions. The band gap was calculated from UV-Vis spectra and it was in the range of 3.23 to 3.28 eV for all the samples. The average particle size calculated from XRD spectra was around in the range of 14 to 20 nm for all the samples. The SEM images revealed that the prepared CuO NPs exhibit different structural morphology for different fuel ratios. The change in fuel ratios plays a vital role in tailoring the surface morphology of CuO NPs and it is studied in detail.
- ✓ The Magnesium Oxide (MgO) nanoparticles synthesized via combustion method, characterized by spectroscopic and microscopic analysis. X-ray diffraction illustrated that the MgO nanoparticles were crystalline in nature with a face centred cubic structure. UV-Vis spectrums of the MgO nanoparticles have a sharp absorption peak around 260 nm. The presence of Magnesium and Oxygen is confirmed by EDX spectrum. FTIR analysis showed the presence of M-O stretching vibration for the synthesis of MgO nanoparticles. The aim of present

study is to determine antibacterial activity of MgO nanoparticles against gram-negative and gram-positive bacteria. Escherichia coli (E. coli) – gram negative and Staphylococcus aureus (S. aureus)-gram-positive were used as test organism. The effect of concentration on the antibacterial activity of MgO nanoparticles was studied using well diffusion agar methods for minimum bacterial concentration. The inhibitory concentration of MgO nanoparticles 20, 15, 10 and 5 $\mu\text{g}/\mu\text{l}$. The results showed that MgO nanoparticles have antibacterial inhibition average zone of 11 mm and 14 mm at the concentration of 10 $\mu\text{g}/\mu\text{l}$ against E. coli and S. aureus respectively. Photocatalytic activity of MgO nanoparticles witnessed by the quick degradation of the organic dye RhB exposure visible light irradiation. .

- ✓ Using nickel nitrate as an oxidizer and starch, oxalic acid and malic acid as fuel, the solution combustion method was used to synthesize nickel oxide (NiO) nanoparticles (NPs). The X-ray diffraction (XRD) has a cubic structure and confirmed the presence of NiO NPs (JCPDS: 78-0429). The average size of crystallite for S1, S2, and S3 are around 42,34 and 36 nm. FTIR spectra showed the band in the 400-550 cm^{-1} range, corresponding to stretching vibration mode, which confirms the presence of NiO NPs. The optical absorption spectra confirmed the presence NiO nanoparticles. The NiO NPs exhibit cubic structure and rod-like structure, inferred from FESEM and High-Resolution Electron Microscopy Transmission (HRTEM). The samples S1 and S3 are exhibiting effective bacterial resistance against gram-positive and gram-negative bacteria. S2 is not showing any antimicrobial activity and can be explained under the surface roughness factor. The NPs, which is having rough surface exhibit greater antimicrobial activity than the smooth surface one. photocatalytic activity of the prepared NiO NPs is evaluated using Methylene Orange and revealed effective degradation.
- ✓ $\alpha\text{-Fe}_2\text{O}_3$ nanoparticles have been prepared by combustion method by using urea. Completion of reaction was followed by Fourier transform infrared spectroscopy (FT-IR) and X-ray diffraction (XRD). The obtained powder was further characterized by energy dispersive spectroscopy (EDS), and scanning electron microscopy (SEM). Their magnetic properties were done by vibrating

sample magnetometer (VSM). Urea fuel has reflected morphology of crystallites as well as on their magnetic properties. This results show the finest crystallite size and also high level of magnetic properties. The Fe₂O₃ nanoparticles showed very good antibacterial activity. The Photocatalytic activity of Fe₂O₃ nanoparticles were also evaluated and were found that the prepared Fe₂O₃ nanoparticles enhance the photocatalytic degradation.

- ✓ The hexagonal Zinc Oxide Nanoparticles prepared by various methods. The ZnO were characterized by using XRD, FTIR, UV, FL, SEM, EDX, VSM, antibacterial & anticancer activity. The XRD results show hexagonal structure and the particle size of ZnO around 90 nm and lattice parameters $a=3.254\text{\AA}$, $c=5.122\text{\AA}$. With matches to JCPDS card number 76-0704. The functional groups were identified by using FTIR. The optical properties were studied using UV- Vis Spectrum & FL Spectrum. The band gap energy of the material found using UV-Vis Spectrum. The emission peak of Fluorescence Spectrum at room temperature. The prepared sample ZnO was found to have a ferromagnetic material using VSM. The morphology of the SEM images. The elemental spectroscopy found using EDX Spectroscopy. The Photocatalytic activity shows excitation wavelength at 554nm under the degradation of RhB. The anticancer activity (MTT- assay) shows ZnO has a good anticancer agent.

16. CONTRIBUTION TO THE SOCIETY

The dye industry presents a global pollution problem owing to the dumping or accidental discharge of dye effluent into waterways, which is having a major impact on the quality and aesthetics of water resources. MONPs like titanium dioxide usually exhibit notable photocatalytic and antimicrobial behavior. These unique nanoparticles exhibit considerable changes and their photocatalytic activity used to destroy industrial solvents, dyes and germs too and will help for the degradation of dyes.

In this project, Bio and Photo active nanomaterials were synthesized and characterized. The prepared nanoparticles exhibited very effective photocatalytic and antimicrobial activities. A novel, feasible and cost effective process of fabricating MONPs is successfully demonstrated, which would be very

promising and implementing method for dye effluent in large or small scale. It shall pave the way for an easy, economic way of effluent treatment involving the industrial dyes.

17. WHETHER ANY PH.D. ENROLLED/PRODUCED OUT OF THE PROJECT **NO**

18. NO. OF PUBLICATIONS OUT OF THE PROJECT

Papers published in international journal: 3

Book Chapter :1

Papers communicated : 4

PUBLICATIONS RESULTING FROM WORK

PAPER PUBLISHED

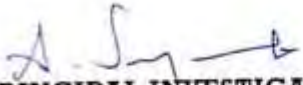
- 1. Rapid solution combustion synthesis of NiO Nanostructures: Characterization and Evaluation of antibacterial activity, International Research Journal of Engineering and Technology e-ISSN: 2395-0056, Volume 04, Special Issue: 09, Sep 2017**
- 2. Visible light active photocatalyst: Hydrothermal green synthesized TiO₂NPs for degradation of picric acid, Materials Letters (Elsevier)222 (2018) 45–49. Impact Factor: 3.019**
- 3. Nickel oxide nanosheets for enhanced antibacterial and photocatalytic applications, Materials Express, American Scientific Publishers (Accepted) 2020, Impact Factor: 1.597**


BOOK CHAPTER PUBLISHED:

Chapter 16: “Metal oxides powder technology in membranes” in the book “Metal oxide powder technologies: Fundamentals, Processing Methods and Applications”, Elsevier Publications, 2020

PAPERS COMMUNICATED:

1. Effect of fuel ratios in tailoring the surface morphology of copper oxide nanoparticles – Materials letters- Elsevier
2. Properties of magnesium oxide nanoparticles and their activity on gram-positive and gram-negative bacteria via combustion method- Applied nanoscience- Springer
3. Effect of urea on the structural and magnetic properties of Fe_2O_3 and its antimicrobial and photocatalytic activities- Spectro chimica Acta part A- Elsevier
4. Photocatalytic ,antimicrobial and anticancer activities of ZnO nanoparticles – Materials letters – Elsevier


PRINCIPAL INVESTIGATOR
D. A. MEETHA CHRISTY,
Associate Professor & Lecturer
Department of Chemistry
College for Women,
Periyakulam
PERIYAKULAM-625 601.


PRINCIPAL
Jayaram Annapackiam College
for Women (Autonomous)
Thamarakulam, Periyakulam-625 601.
Theni District Tamilnadu.

Rapid solution combustion synthesis of NiO Nanostructures: Characterization and Evaluation of antibacterial activity

R. Jamuna A.Jegatha Christy *

PG & Research Centre of Physics, Jayaraj Annapackiam College for Women (Autonomous),
Periyakulam-625 601, and Theni district, Tamilnadu.

E-mail id: jegathachristy@gmail.com

Abstract: Nickel oxide (NiO) NPs were synthesized by solution combustion method using Nickel nitrate as an oxidizer and starch as fuel. The X-Ray Diffraction (XRD) exhibit cubic structure and confirmed the presences of NiO NPs (JCPDS: 65-2901). The morphology of the NiO nanoparticles was investigated by means of SEM and confirms the nanostructure. It is possible to suggest that the organic fuel starch is responsible for the formation of nanostructure due to the easier complex formation. The chemical composition of NiO NPs was investigated by Energy Dispersive Spectroscopy (EDAX). It confirms the presence of Nickel oxide nanoparticles. In the FTIR analysis, Ni-O stretching vibration mode is obtained in the region of 454.02 cm^{-1} . The prepared NiO NPs are very effective to gram positive strains than the gram negative strains. Gram positive and gram negative bacteria have differences in their membrane structure, the most distinctive of which is the thickness of the peptidoglycan layer.

Key words: Nickel oxide NPs, Solution Combustion method, XRD, SEM & EDAX, UV, FT-IR, Antibacterial activity.

1. INTRODUCTION

Nickel oxide (NiO) is a significant transition metal oxide that has garnered attention as a strong candidate for many fields including super paramagnetic devices, photovoltaic devices, electrochemical super capacitors, magnetic materials, catalysis, smart windows, fuel cell, and photovoltaic devices [1]. These nanostructured particles are regarded as a p-type semiconductor having large exciton binding energy with stable wide band gap (3.6–4.0 eV). Bulk NiO is an antiferromagnetic insulator with a Neel temperature of 523K [2]. They exhibit many unique magnetic, optical, electronic, and chemical properties that are significantly different than those of bulk-sized NiO particles due to their quantum size and surface effects [3]. Some of these techniques suffer from the difficulty in size homogeneity and dispersion of NiO nanoparticles (NPs). Generally, most techniques aim to reduce the costs of chemical synthesis and to produce materials for technological applications [4]. These materials like copper, zinc, nickel, silver present high antibacterial activity, low toxicity, chemical stability, long lasting action period and thermal resistance compared to organic antibacterial agents [5]. In the present study, NiO nanostructures were synthesized by solution combustion method using starch as fuel. The antibacterial activities of the prepared NiO nanostructure were investigated.

2. MATERIALS AND METHODS

2.1 Synthesis of NiO NPs

For the preparation of NiO NPs, nickel nitrate, starch was taken as starting materials. The stoichiometric composition of solution components fuel and oxidizer was calculated according to the principle of chemistry keeping the oxidizer (metal nitrate) to fuel (starch) ratio unity. Stoichiometric amount of Nickel (II) nitrate and starch were dissolved in de-ionized water separately. The solution was mixed vigorously until the homogenous solution was obtained and then the solution was kept the furnace at 300°C. The solution boils and undergoes dehydration, then the solution reaches the point of combustion, it began to burn released a lot of heat as fumes and vaporizing all the solution. As a result, NiO product and gases of H₂O, N₂ can be formed directly from the reaction between fuel and oxidizer without necessary of getting oxygen from outside. The process was completed in 20 minutes and fine black colour powder was obtained as a result.

One Day International Seminar on Materials Science & Technology (ISMST 2017)4th August 2017

Organized by

Department of Physics, Mother Teresa Women's University, Kodaikanal, Tamilnadu, India

2.2 Characterizations

The Shimadzu IR affinity-1 Fourier Transform Infrared spectrometer was used to carry out vibrational studies. The X-ray diffraction patterns were recorded on PANalytical X-ray Diffractometer using Cu K α radiation ($\lambda=0.1542\text{nm}$) operated at 50kV and 100mA. The experiments were performed in the diffraction angle range of 2θ . Energy Dispersive Spectroscopy was carried out by BRUKER instrument. Scanning Electron Microscopy images were obtained by an instrument VEGA3 LMU.

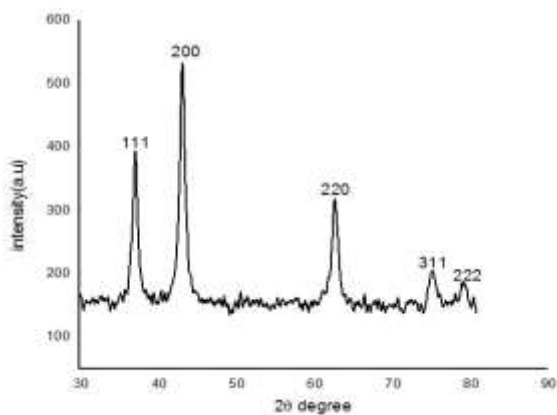
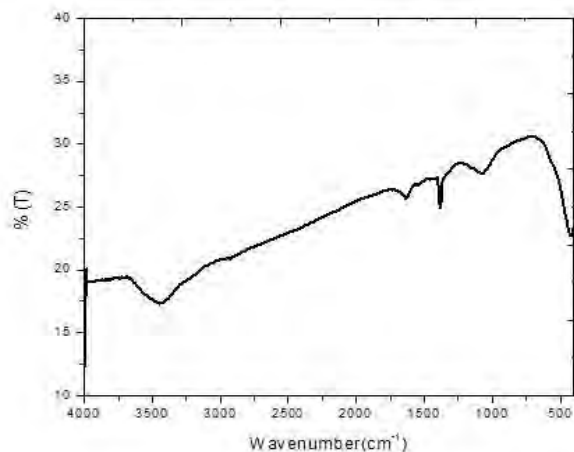
2.3 Assay for antimicrobial activity of NiO NPs against microorganism

The antibacterial activity of NiO NPs was evaluated against gram positive Bacillus cereus, Entero coccus, and Staph aureus, gram negative bacteria Escherichia coli, Klebsiella pneumonia and Pseudomonas aeruginosa. Exactly 0.2 ml of fresh cultures of each organism was inoculated into 5 ml of sterile nutrient broth and incubated for 3-5 h to standardize the culture to McFarland standards (106 CFC/ml). Three replicates of respective microorganism were prepared by spreading 100 μl of the revived culture on MHA (Mueller Hinton Agar-Hi Media) with the help of spreader. The well was made having a diameter of about 7 mm and 50 μl samples of NiO were added in one well and 50 μl of distilled water as control. The petri plates were kept at 37 $^{\circ}\text{C}$ for 24 h in incubator for bacteria during which its antibacterial activity was evidenced by presence of a zone of inhibition (mm) surrounding the well.

3. RESULTS AND DISCUSSION

3.1 X-ray diffraction spectroscopy (XRD)

XRD is a popular technique for determining phase purity of the materials. The width of the diffraction lines is closely related to the size distribution defects and strain in NPs. Fig.1 shows the XRD spectra of NiO NPs. The purity and crystalline of the synthesized NiO NPs were examined by using powder X-ray diffraction (XRD). The five diffraction peaks of the XRD pattern of NiO NPs were observed at 37.23 $^{\circ}$, 43.19 $^{\circ}$, 62.72 $^{\circ}$, 75.28 $^{\circ}$, 79.31 $^{\circ}$ which correspond to (111), (200), (220), (311), and (222) diffraction planes respectively (JCPDS, NO: 65-2901). All diffraction peaks of NiO correspond to the cubic structure and the volume of the cell was 49.97 (A°)³. The average particle size of the NiO NPs was calculated using the Debye scherrer equation [6]. The lattice constant value is calculated as 4.194 A° . The average particle size found to be around 18 nm. Fig.2 shows the FTIR spectra of combustion product of NiO NPs. The FTIR spectrum was observed over the frequency range 400-4000 cm^{-1} .

**Fig.1** XRD spectra for NiO NPs**Fig.2.** FTIR spectra of NiO NPs

One Day International Seminar on Materials Science & Technology (ISMST 2017)

4th August 2017

Organized by

Department of Physics, Mother Teresa Women's University, Kodaikanal, Tamilnadu, India

The broad band in the region of 454 cm^{-1} is assigned to Ni-O stretching vibration mode. The FTIR band seen around 3500 cm^{-1} was attributed to O-H stretching of hydrogen bonded water on the surface of NPs and the band at 1634 cm^{-1} is assigned to H-O-H bending vibrations mode presented due to the adsorption of water in air during the preparation of FTIR sample disks in an open air atmosphere. The band at 1385 cm^{-1} is attributed to O-C=O symmetric and asymmetric stretching vibrations. The moderate peak at 1071 cm^{-1} may be due to single C-O band stretching mode [7].

3.2 Scanning electron microscopy (SEM)

Fig.3 shows that the SEM image of NiO NPs. Studying, the growth mechanism of NiO NPs, it is possible to suggest that the organic fuel starch is responsible for the formation of the NiO nanostructure due to the easier complex formation [8]. When starch is employed, the heat released in combustion is more and as a result which is responsible for the growth of the sample and complete combustion reaction with more crystalline phase. So the result indicates that the presence of starch has a significant effect on the morphology of the sample. Fig.4 shows that the chemical composition of NiO NPs which was investigated by Energy Dispersive Spectroscopy (EDAX). It confirms the presence of NiO NPs.

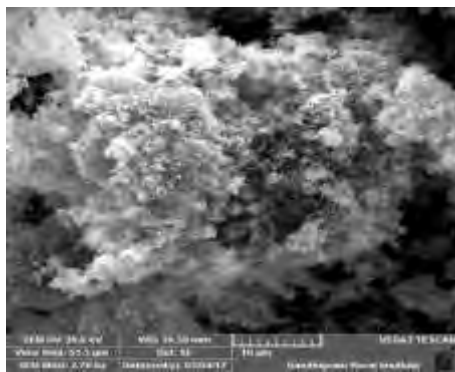


Fig.3. SEM image of NiO NPs

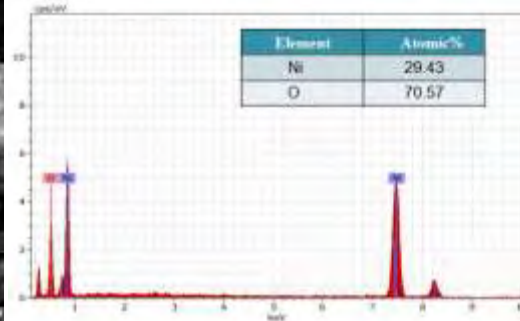


Fig.4. EDAX for NiO NP

3.3 Antibacterial activity

In this study, to evaluate the antibacterial effects against various microorganisms (gram positive and gram negative), Staphylococcus aureus, Enterococcus, Bacillus cereus, E.coli, Klebsilla pneumonia, Pseudomonas aeruginosa were used. Antibacterial activity done for synthesized NiO NPs using Kirby-Bauer method on both Gram-negative and Gram positive bacteria. Fig.5, 6, shows the antibacterial activity of NiO nanostructure on the corresponding microorganisms.

Gram-negative bacteria



Fig.5. (a), (b), (c) *E.coli*, *Klesilla pneumonia*, *Pseudomonas aeruginosa* negative bacteria

Gram-positive bacteria



Fig.6. (a), (b), (c) Entero coccus, Bacillus cereus, Staph aureus, positive bacteria

Table1. Antibacterial efficacy results of NiO NpS.

Microorganisms	Zone of inhibition (mm)
<i>E. coli</i>	23
<i>K. pneumonia</i>	22
<i>P. aeruginosa</i>	19
<i>S. aureus</i>	26
<i>E. coccus</i>	17
<i>B. cereus</i>	29

The diameter of inhibition zones (in mm) produced by NiO NpS against these test strains are shown in Table1. The prepared NiO NPs is effective to Gram positive strains than the Gram negative strains. Gram positive and Gram negative bacteria have differences in their membrane structure, the most distinctive of which is the thickness of the peptidoglycan layer. The lower efficacy of the NiO NPs against *Entero coccus*, *Pseudomonas aruginosa* may derive from the difference as a point of membrane structure [9]. The growth inhibition of bacterial cells may be due to distractions of cell membrane by NiO NPs which results in breakdown of cell enzyme.

4. CONCLUSION

The NiO NPs were synthesized by using solution combustion method. The XRD confirms the NiO NPs and the average crystalline size of the NiO NPs were found to be about 18 nm and exhibits cubic structure. The morphology of the NiO nanoparticles was investigated by means of the SEM and confirms the nanostructure. It is possible to suggest that the organic fuel starch is responsible for the formation of nanostructure due to the easier complex formation. The EDAX is confirms the presence of NiO NPs. It confirms the presence of Nickel oxide nanoparticles. In the FTIR analysis, Ni-O stretching vibration mode is obtained in the region of 454.02cm^{-1} . As prepared NiO NPs are very effective to gram positive strains than the gram negative strains. Gram positive and gram negative bacteria have differences in their membrane structure, the most distinctive of which is the thickness of the peptidoglycan layer.

ACKNOWLEDGEMENT

The Author Dr. A. Jegatha Christy is grateful to the UGC SERO for the financial Assistance

REFERENCES

[1]. H.T. Rahal, R. Awad, A.M. Abdel-Gaber and D. El-Said Bakeer, "Synthesis, characterization and magnetic properties of pure and EDTA-Capped NiO Nanoparticles", Journal of Nanomaterials, 2017, pp-9.

One Day International Seminar on Materials Science & Technology (ISMST 2017)**4th August 2017****Organized by****Department of Physics, Mother Teresa Women's University, Kodaikanal, Tamilnadu, India**

- [2]. Marin Tadic, Dobrica Nikolic, Matjaz panjan, Graeme R. Blake, "Magnetic properties of NiO Nanoparticles: Blocking temperature and Neel temperature", *Journal of Alloys and Compounds* 647, 2015, 1061-1068.
- [3]. M. Salavati-Niasari, F. Mohandes, F. Davar, M. Mazaheri, M. Monemzadesh, and N. Yavarinia, "Preparation of NiO Nanoparticles via a solid state decomposition route", *Inorganica Chimia Acta*, vol.362, No. 10, 2009. pp. 3691-3697.
- [4].B. Kavitha, M. Nirmala, A. Pavithra, "Annealing effect on NiO Nanoparticles synthesized by Sol-gel method", *World scientific news* 52, 2016, 118-129.
- [5]. S. Mohseni meybodi, S.A. Hosseini, M. Rezaee, S.K. Sadrnezhaad, D. Mohammadyani, "Synthesis of wide band gap nanocrystalline NiO powder via a sonochemical method" *ultrasonics sonochemistry* 19, 2012, pp. 841- 845.
- [6]. Assem Barakat, Mousa Al-Noaimi, Mohammed Suleiman, Abdullah S. Aldwayyan, Belkheir Hammouti, Taibi Ben Hadda, Salim F.Haddad, Ahmed Boshala and Ismail Warad, "One step synthesis of NiO Nanoparticles via solid state thermal decomposition at low-temperature of novel Aqua Nickel complex". *Int. J. Mol. Sci.*, 2013- 2014, pp. 23941-23954.
- [7]. S. Suresh, S. Karthikeyan, P. Saravanan, K. Jayamoorthy, "Comparision of antibacterial and antifungal activities of 5-amino- 2-mercaptobenzimidazole and functionalized NiO Nanoparticles" *Karbal international journal of morden science* 2, 2016, 188-195
- [8]. A. Jegatha Christy, L.C. Nehru, M. Umadevi, "A novel combustion method to prepare CuO nanorods and Its antimicrobial and photo catalytic activities" *Powder Technology* 235, 2013, 783-786.
- [9]. A. Jegatha Christy, L.C. Nehru, M. Umadevi, "Optical, structure and morphological properties of silver nanoparticles and their antimicrobial activity" *International journal of ChemTech Research*, vol. 7, No.3, 2014-2015, pp 1191-1197.

See discussions, stats, and author profiles for this publication at: <https://www.researchgate.net/publication/323850613>

Visible Light Active Photocatalyst: Hydrothermal Green Synthesized TiO₂ NPs for Degradation of Picric Acid

Article in *Materials Letters* · March 2018

DOI: 10.1016/j.matlet.2018.03.109

CITATIONS

7

READS

361

4 authors, including:



D. Hariharan

Bharathidasan University

5 PUBLICATIONS 15 CITATIONS

[SEE PROFILE](#)



Jegatha Jehinder

Jayaraj Annapackiam College for Women, periyakulam

14 PUBLICATIONS 182 CITATIONS

[SEE PROFILE](#)



Jeyanthinath Mayandi

Madurai Kamaraj University

72 PUBLICATIONS 444 CITATIONS

[SEE PROFILE](#)

Some of the authors of this publication are also working on these related projects:



An experimental study on effect of thermal properties of PVDF polymer SIMS Study of 30keV H⁺ Ion-Implanted n-GaAs [View project](#)



Biomaterials [View project](#)



Visible light active photocatalyst: Hydrothermal green synthesized TiO₂ NPs for degradation of picric acid



D. Hariharan^a, A. Jegatha Christy^b, Jeyanthinath Mayandi^c, L.C. Nehru^{a,*}

^a Department of Medical Physics, School of Physics, Bharathidasan University, Tiruchirappalli, Tamilnadu, India

^b PG & Research Center of Physics, Jayaraj Annapackiam College for Women, Periyakulam, Tamilnadu, India

^c Department of Materials Science, Madurai Kamaraj University, Madurai, Tamilnadu, India

ARTICLE INFO

Article history:

Received 17 January 2018

Received in revised form 14 March 2018

Accepted 17 March 2018

Available online 19 March 2018

Keywords:

Green synthesis

Picric acid

Aloe Vera

Photocatalysis

ABSTRACT

Recent research on photocatalytic activities has been investigated using visible light region rather consuming ultraviolet region. In this Paper, a facile and eco-friendly method was developed to the synthesis of TiO₂ NPs using Aloe Vera gel (AV-TiO₂). The synthesized nanoparticles were characterized using XRD, XPS, HRTEM, EDAX and Raman spectroscopy. The sharp peaks by XRD pattern show the crystallinity and purity of titanium dioxide nanoparticles. The shape and morphology were studied by HR-TEM images and confirms the NPs size which falls in the range from 6 to 13 nm. Raman spectrum and XPS shows the energy modes and oxidation state of synthesized TiO₂ NPs. TiO₂-mediated photo-degradation of trinitrophenol (Picric acid- PA) irradiated by visible light source has also been investigated.

© 2018 Published by Elsevier B.V.

1. Introduction

The metal oxide nanoparticles play a very important role in the synthesis of materials, preserving the environment, production, and conservation of energy. Titanium dioxides (TiO₂) possess the strong medical applications among all the nanoparticles, because of its strong oxidation power, non-toxicity, and chemical stability [1]. TiO₂ has its applications in the areas of solar energy cells, environmental purification, electronic devices, gas sensors, photo-electrodes and photo-catalysts [2]. Titanium dioxide has emerged because of the properties like photo induced super-hydrophobicity and antifogging effect, hence it is helpful in the environmental purification by removing bacteria and harmful organic materials from water and air [3,4]. In the recent years, a number of physical and chemical methods were reported for the synthesis of nanostructures which are less eco-friendly and cost-effective. The chemical synthesis of nanoparticles produces a lot of toxic substances where the green synthesis of nanoparticles is easy, efficient, and eco-friendly. The biomolecules present in plants act as capping and reducing agents by stopping the agglomeration of nanostructures and promote their stability [5]. *Aloe barbandensis miller*, commonly known as aloe Vera is a very succulent plant species and had been used only as an herbal medicine in the past.

Tanaka K et al. [6], reported the photocatalytic degradation of picric acid using TiO₂ in the ultraviolet region. Umabala AM et al. [7], reported visible light active photocatalytic degradation of picric acid within 3 to 4 h using BiVo₄ + H₂O₂. Visible light active degradation of Methylene blue using green synthesized TiO₂ nanoparticles reported by Muniandy SS [8]. Also, Picric Acid (PA) is a strong irritant, allergen and environmentally pollutant [9]. In this paper, we have reported the synthesis of TiO₂ nanoparticles using Aloe Vera gel and studied the degradation efficiency of PA in the visible region. To our knowledge, it is the first report for explosive compound degradation in visible region using green synthesized TiO₂ nanoparticle.

2. Materials and methods

2.1. Hydrothermal synthesis of TiO₂ nanoparticles

Aloe Vera skin was peeled and the gel was washed seven times in the running water. 10 mL of Aloe Vera gel was added into 100 mL of deionized water and stirred for one hour. To this aqueous solution, 0.1 M of titanium (IV) isopropoxide was added drop by drop wise. The reaction mixture was stirred continuously for one hour at 20 °C. The solution was kept in an autoclave at 180 °C for 4 h. Then the prepared solution was heated on a hot plate at 80 °C. The obtained product was pounded finely and then calcinated in a muffle furnace at 500 °C for 5 h. Finally, Aloe Vera mediated TiO₂ nanoparticles (AV-TiO₂) was obtained.

* Corresponding author.

E-mail address: lcnehru@bdu.ac.in (L.C. Nehru).

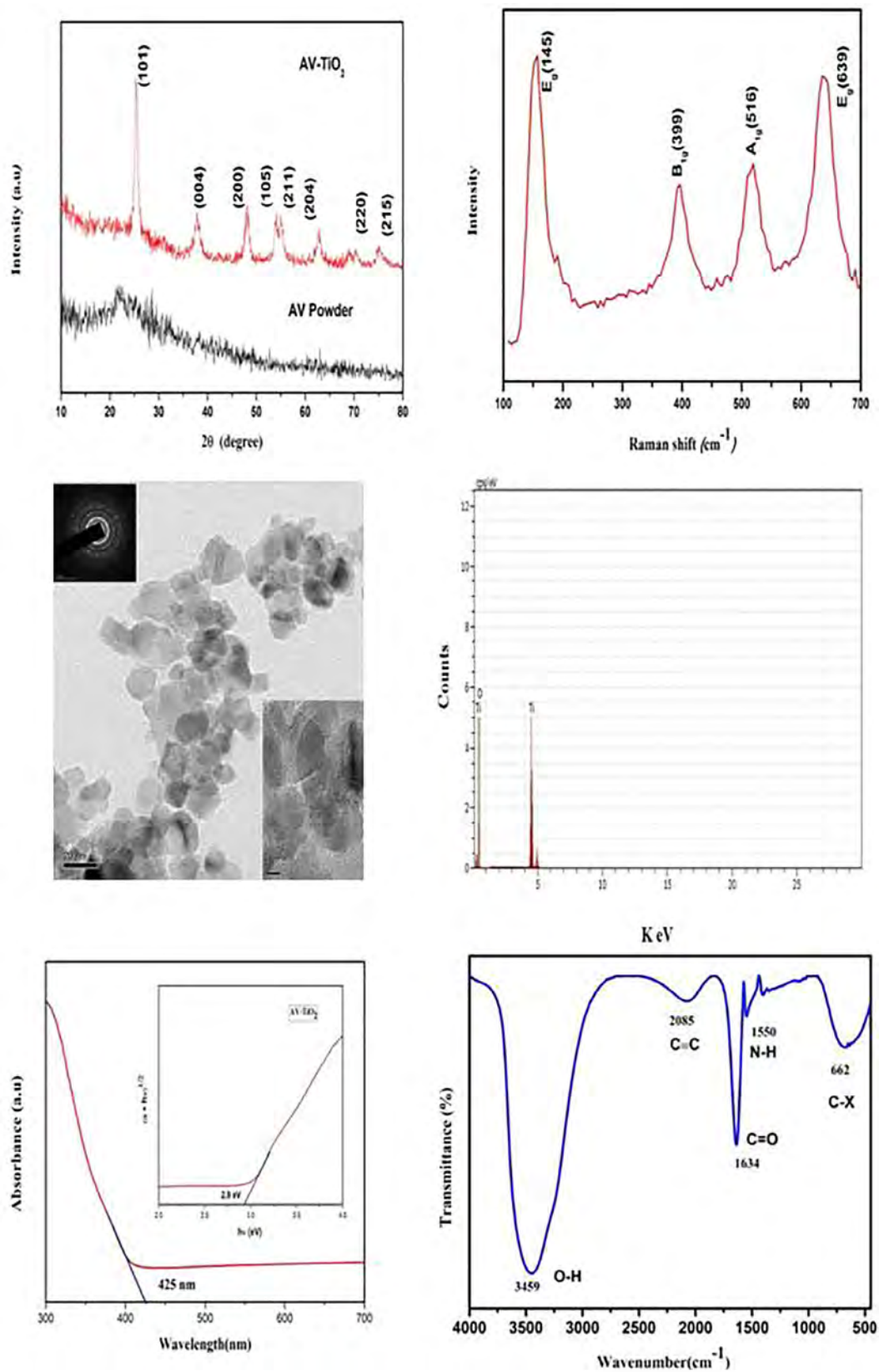


Fig. 1. (A) XRD spectra (B) Raman spectrum (C) HR-TEM image and (D) EDAX spectrum for the green synthesized AV-TiO₂. (E) UV-Vis spectrum for green synthesized TiO₂ NPs (F) FT-IR spectrum of 500 °C calcined Aloe Vera gel.

2.2. Characterization of TiO₂ nanoparticles

XRD analysis was performed using XPERT – PRO equipped with CuK α radiation. The structural property was also investigated using Raman spectroscopy, in the range of 100–700 cm⁻¹ using Renishaw equipment. High-Resolution Transmission Electron Microscopy (HRTEM) and Selected Area Electron Diffraction (SAED) images we obtained using JEM-2100F field emission TEM. Energy dispersive X-ray spectrometry (EDS) was performed with a spectroscope attached to TEM.

2.3. Photocatalytic experiments

Photocatalytic activities of the AV-TiO₂ were evaluated by the degradation of PA. In each experiment, 20 mg of TiO₂ catalyst was added in 100 mL of PA solution (500 mg/L) to obtain the catalyst at 200 mg/L. The experiments were carried out in a Pyrex beaker illuminated with a 15 W high-pressure mercury lamp emitting visible light (543 nm). The distance between the lamp and the pyrex beaker is about 12 cm. Prior to visible light irradiation, the suspension was stirred for 30 min in dark to reach the adsorption-desorption equilibrium. The solution was continuously stirred during the experiments. At given irradiation time intervals, 5 mL of the suspension was collected. The PA concentration was evaluated by UV–visible spectra monitoring the absorption maximum. A calibration plot based on Beer–Lambert's law was estab-

lished by relating the absorbance to the concentration. In each case, blank experiments were also conducted with the catalysts in the absence of light and without the catalysts when the solution containing the dissolved picric acid was illuminated. Moreover, Photocatalytic experiments were performed only under the visible region by using UV cut-off filter and in the same conditions with different milligram (10–50) of AV-TiO₂ catalyst were studied.

3. Results and discussion

The X-Ray diffraction patterns of the AV-TiO₂ are shown in the Fig. 1. The XRD pattern agrees with the JCPDS card No 89 – 4921 (anataseTiO₂). The XRD peaks 25.3°, 37.8°, 48.0°, 53.9°, 55.1°, 62.7°, 68.8°, 70.3° and 75.1° can be attributed to the respective 'hkl' planes of the crystalline structure of the AV-TiO₂. The crystalline size of the AV-TiO₂ can be calculated using the Scherer's formula and found to be 9 nm. In Fig. 1(A), no diffraction pattern absorbed for Aloe Vera powder, because of its amorphous nature.

The morphological information and particles size are determined using HR-TEM. Fig. 1(C) exhibits the tetragonal shape. The particle size range is 6 nm–13 nm with moderate variations in size. The Dotted rings in Selected Area Electron Diffraction are well matched to the XRD 'hkl' miller indices. The lattice springe's is indicating AV-TiO₂ nanoparticles is crystalline in nature. In green synthesized TiO₂ nanoparticles, Ti percentage is 52 and O percentage is 48.

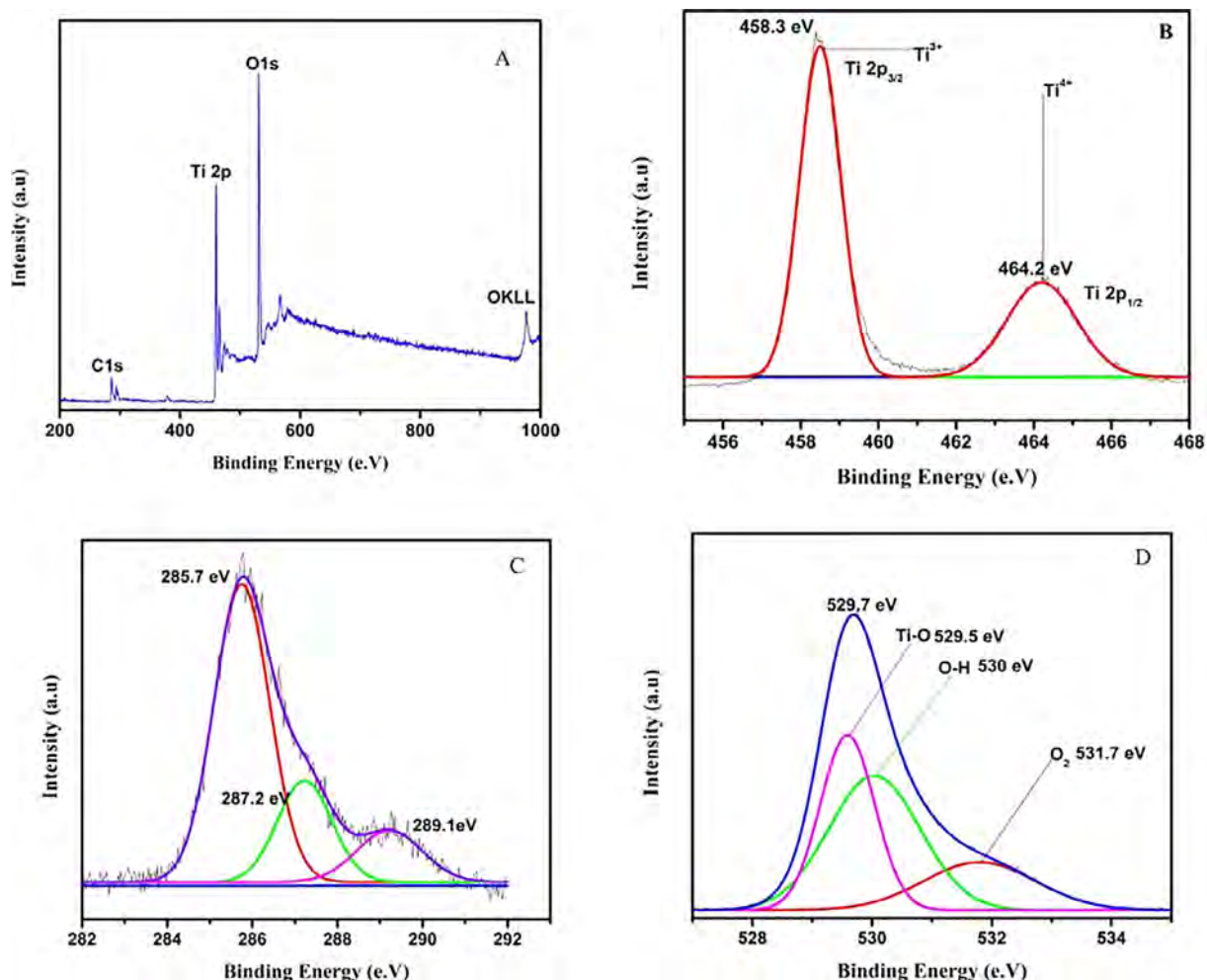


Fig. 2. XPS spectra of TiO₂ samples: (A) survey spectra of TiO₂; (B) Ti2p state; (C) C1s (D) O1s.

AV-TiO₂ absorption spectra (425 nm) shows a shift towards the visible region (Fig. 1E), so band gap energy (2.9 eV) is reduced compared to pure anatase TiO₂ (3.2 eV). This indicates the electron holes pairs are generated during visible light irradiation, which may contribute to the significant improvement in the photocatalytic activity in the visible light region. More importantly, the presence of Ti³⁺ sites with narrow band gap is identified by XPS, which is also a vital factor in improving the response of TiO₂ to the visible region.

Fig. 1F shows FTIR spectrum of Aloe Vera gel after calcination 500 °C in which the peaks at 3459 cm⁻¹ and 2085.8 cm⁻¹, in the spectra, are due to stretching of the O–H (Alcohol) and C≡C (Alkyne) group. The peaks corresponding to 1634 cm⁻¹, 1550 cm⁻¹, and 662 cm⁻¹ were indicated as the functional groups of C=O (carbonyl, stretching), N–H (amide, bending), and C–X (Halogen). The obtained products are the result of the organic compounds like are enzymes, vitamins, lignin's, monosaccharide, polysaccharides, salicylic acids, amino acids and sterols present in the leaf extract of Aloe Vera. It is well matched to XPS carbon spectra.

XPS explains about the elemental composition of AV-TiO₂. The survey spectra (Fig. 2A) show that the Ti, C, and O elements exist on the surface of the AV-TiO₂ sample. The TiO₂ sample was carbon

element can be ascribed to the adventitious carbon-based contaminant. Fig. 2B shows the peaks at 458.3 and 464.2 eV, which correspond to Ti 2p_{3/2} and Ti 2p_{1/2}, respectively. The peak position between Ti 2p_{3/2} and Ti 2p_{1/2} lines at 5.7 eV, suggest the existence of the Ti⁴⁺ oxidation state [10]. The peak at 464.2 eV, attributed to Ti⁴⁺ species, and the other centered on 458.3 eV corresponding to Ti³⁺ species [11]. Certainly, the presence of Ti³⁺ oxide with narrow band gap may be advantageous to the higher photocatalytic activity of the AV-TiO₂ nanostructures driven by visible light [12]. Fig. 2C C1s peak at 285.7 eV BE (major peak), which corresponds to the carbon atoms within the amino acids, vitamins, lignin, monosaccharide, anthraquinones, enzymes, minerals, salicylic acids, polysaccharides, saponins and sterols of Aloe Vera gel binding energy peaks at 287.2 and 289.1 eV were observed. The higher binding energy peak at 289.1 eV was attributed to electron emission from carbons in carbonyl groups [13]. (Carbonyl carbons of the polysaccharides or proteins-enzymes). The lower peak at 287.2 eV binding energy was most likely from carbons to the carbonyl carbons. XPS spectra of O1s in the AV-TiO₂ samples (Fig. 2d). The wide and asymmetric O1s spectra indicate that there would be three components, which can be further fitted into three peaks of oxygen (O_{Ti-O} at 529.5 eV), hydroxyl groups (O_{O-H} at 530 eV) [14], and adsorbed O₂ (at 531.7 eV) [15].

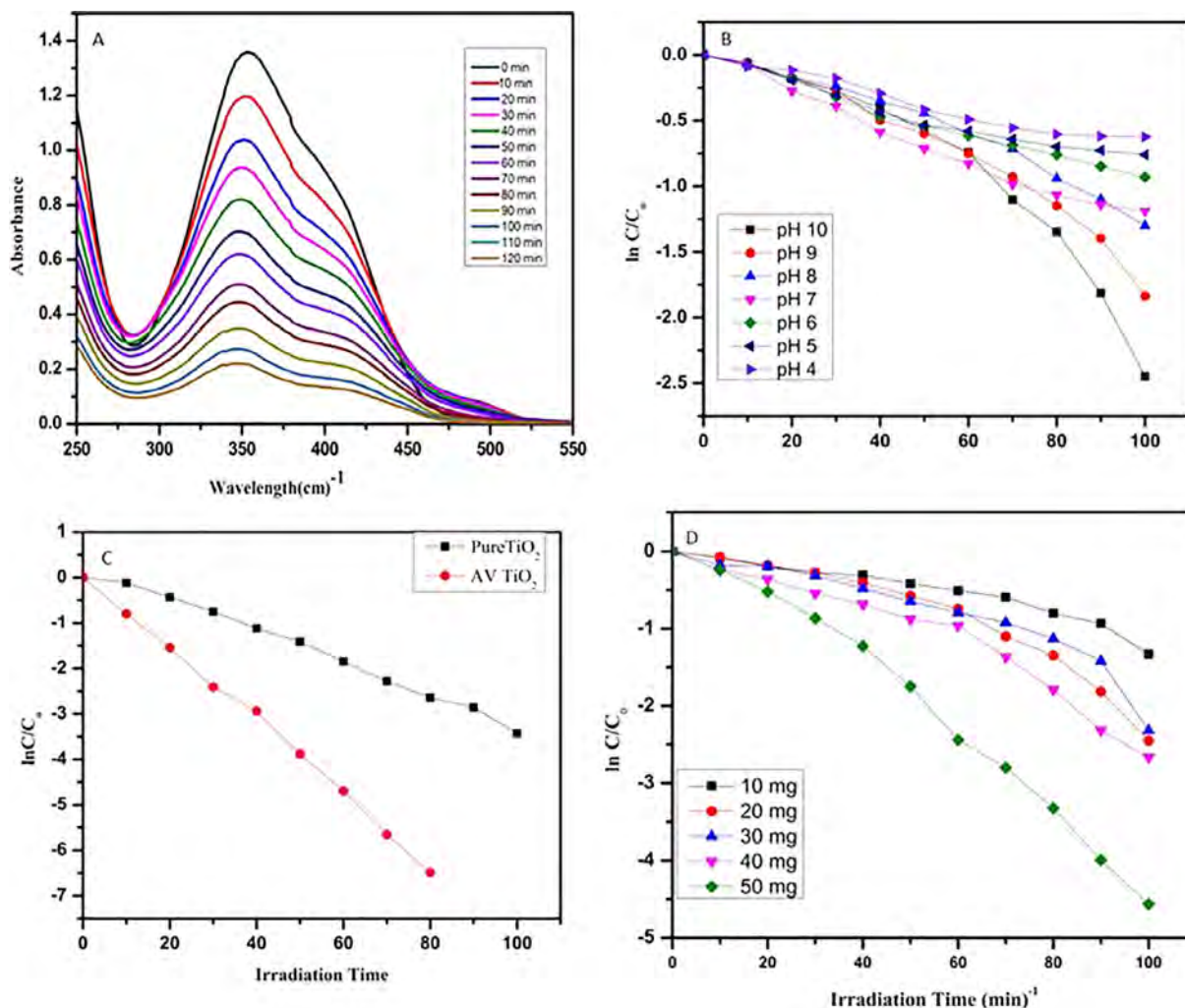


Fig. 3. (A) UV-Vis (DRS) absorption spectra for degradation of picric acid AV-TiO₂ kinetic linear simulation curves of PA photocatalytic degradation with (B) pH variation (C) Catalyst variation (D) Mg Variation.

3.1. Photocatalytic studies

From Fig. 3, as expected the AV-TiO₂ samples exhibit remarkable improvement in photocatalytic activity compared to that of the pure TiO₂. In Fig. 3a, 10 mg AV-TiO₂ catalyst treated PA absorbance spectra is observed in 0 min. After a time interval of each 10 min, the absorbance spectrum is decreased. The total absorbance spectrum of PA is decreased within 120 min. Fig. 3b explains, Acid is not degraded in acidic nature which is degraded in base condition, so pH value is increased, the Picric acid degradation rate is increased. In our experiment, PA is degraded in base condition (pH = 10). AV-TiO₂ concentration is increased, PA degradation rate is also increased (Fig. 3d), that indicates AV-TiO₂ concentration amount is increased, more free radicals are produced. The degradation order of photocatalytic activity for the samples can be summarized as follows: AV-TiO₂ > Pure TiO₂ (Fig. 3c).

The photocatalytic reaction can be considered as the process of generation, transfer, and consumption of the photo-generated carriers [16]. First, the photo catalyst absorbs the incident photons with energy above the semiconductor's band gap, generating electrons and the same amount holes. The holes abstract electrons from absorbed pollutants or react with H₂O to form hydroxyl radicals. However, the conduction band electrons reduce absorbed oxygen to form superoxide anions which can further disproportionate to form hydroxyl radicals via chain reactions. In addition, the electrons could react directly with the pollutant.

During visible light irradiation, the equilibrated Fermi level electrons were injected rapidly into the TiO₂ conduction band via a Surface Phonon Resonance (SPR) mechanism, and the injected electrons were trapped by dissolved oxygen molecules in water to yield high oxidative species, such as superoxide radical anions ([•]O₂⁻) and hydroxyl radicals (HO[•]) [17]. The TiO₂ facilitates electron-hole separation and subsequently helps in the formation of hydroxyl radicals. The superoxide radical anions ([•]O₂⁻) and hydroxyl radicals (HO[•]) produced under visible light irradiation might be responsible for mineralization of the organic pollutants [18]. The photocatalytic activity has a positive correlation with the formation rate of reactive radicals, i.e., faster formation radicals leading to a higher photocatalytic activity of the catalyst [19]. Overall, these results suggest that TiO₂ will help increase the rate of forma-

tion of [•]O₂⁻ and HO[•] reactive radicals due to AV-TiO₂ stimulate excess electrons ejection, and simultaneously facilitate the degradation of organic pollutants. The total amount of PA is degraded within 120 min when AV-TiO₂ is acting as a catalyst. As the concentration of AV-TiO₂ and pH level is increased, PA degradation is increased.

4. Conclusion

The AV-TiO₂ was synthesized successfully with Aloe Vera gel in a very simple and eco-friendly way. The physico-chemical properties of synthesized TiO₂ nanoparticles were investigated by XRD, XPS, HRTEM, EDAX and Raman spectroscopy analysis indicating that the synthesized TiO₂ nanoparticles are crystalline in the anatase phase with smaller size range and high surface area. AV-TiO₂ has enhanced photocatalytic activity for the degradation of picric acid in 120 min.

References

- [1] Kazuhito Hashimoto, Hiroshi Irie, Akira Fujishima, *Appl. Phys.* 44 (12R) (2005) 8269.
- [2] A. Karami, *Iran. Chem. Soc.* 7 (2) (2010) 154–S160.
- [3] Fujishima, Akira, and Kenichi Honda *nature*, 238, 5358, 1972, pp. 37–38.
- [4] Sachiko Tojo, *Phys. Chem. C* 112 (38) (2008) 14948–14954.
- [5] Makarov, V. V, *Acta Nat.* 6 1 (20) (2014).
- [6] Tanaka, Luesaiwong, Hisanaga *Mol. Cat. A Chem.* 18, 122, 1997, pp. 67–74.
- [7] A.M. Umabala, P. Suresh, A.P. Rao, *Der Pharma Chem.* 8 (6) (2016) 228–236.
- [8] Muniandy, Kaus, Jiang, Altarawneh, Lee, *RSC Adv.* 7, 76, 2017, pp. 48083–48094.
- [9] Gang He, *Mater. Chem.* 19 (39) (2009) 7347–7353.
- [10] Chen, Hua Wei, Young Ku, and Yu-Lin Kuo, *Chem. Eng. Technol.* 30, 9, 2007, pp. 1242–1247.
- [11] Chunyan Su, *CrystEngComm* 14 (11) (2012) 3989–3999.
- [12] Xiaoye Applied Xin, *Catal. B Environ.* 176 (2015) 354–362.
- [13] S. Li, Y. Shen, A. Xie, X. Yu, L. Qiu, Li Zhang, Q Zhang, *Green Chem.* 9 (2007) 852–858.
- [14] G.B. Hoflund, Z.F. Hazos, *Phys. Rev. B* 62 (2000) 11126–11133.
- [15] X.J. Quan, Q.H. Zhao, H.Q. Tan, X.M. Sang, F.P. Wang, Y. Dai, *Mater. Chem. Phys.* 114 (2009) 90–98.
- [16] Zhao, Jincai, Chuncheng Chen, and Wanhong Ma *Topics Catalysis*, 35, 3, 2005, pp. 269–278.
- [17] Liqiang Jing et al., *Chem. Soc. Rev.* 42 (2013) 249509–249549.
- [18] Peng Wang, *Phys. Chem. Chem. Phys.* 14 (28) (2012) 9813–9825.
- [19] Jing Liqiang, *Solar Energy Mater. Solar Cells* 90 (12) (2006) 1773–1787.